TU Delft

Delft University of Technology

Electrochemical recovery of rare earth metals in molten salts

Abbasalizadeh, Aida

DOI
10.4233/uuid:4977c439-9925-4907-8350-6b3fd50e72fa

Publication date
2018

Document Version
Final published version

Citation (APA)
Abbasalizadeh, A. (2018). *Electrochemical recovery of rare earth metals in molten salts*. [Dissertation (TU Delft), Delft University of Technology]. https://doi.org/10.4233/uuid:4977c439-9925-4907-8350-6b3fd50e72fa

Important note
To cite this publication, please use the final published version (if applicable).
Please check the document version above.

Copyright
Other than for strictly personal use, it is not permitted to download, forward or distribute the text or part of it, without the consent of the author(s) and/or copyright holder(s), unless the work is under an open content license such as Creative Commons.

Takedown policy
Please contact us and provide details if you believe this document breaches copyrights.
We will remove access to the work immediately and investigate your claim.

This work is downloaded from Delft University of Technology.
For technical reasons the number of authors shown on this cover page is limited to a maximum of 10.

Electrochemical recovery of rare earth metals in molten salts

Dissertation

For the purpose of obtaining the degree of doctor

at Delft University of Technology,

by the authority of the Rector Magnificus prof.dr.ir. T.H.J.J. van der Hagen,

chair of the Board for Doctorates,

to be defended publicly on

Thursday 29 November at 10:00

by

AIDA ABBASALIZADEH

Master of Science in Materials Science and Engineering, Royal Institute of Technology, Sweden

born in Tehran, Iran.

This dissertation has been approved by the promotors:

Dr. Y. Yang

Prof. dr. ir. J. Sietsma

Composition of the doctoral committee:

Rector Magnificus	chairperson
Dr. Y. Yang	Delft University of Technology, promotor
Prof. dr. ir. J. Sietsma	Delft University of Technology, promotor

Independent members:

Prof. dr. B. Friedrich	RWTH Aachen, Germany
Prof. dr. G.M. Haarberg	NTNU, Norway
Prof. dr. B. Blanpain	KU Leuven, Belgium
Prof. dr. ir. J.M.C. Mol	TUDelft, The Netherlands
Prof.dr. I.M. Richardson	TUDelft, The Netherlands

Other member:

Prof.dr. S. Seetharaman	KTH, Sweden

This research was funded by the European Community's Seventh Framework Programme (FP7).

ISBN: 978-94-6186-987-6
Publisher: GVO Printers and Designers BV

Copyright © 2018 Aida Abbasalizadeh

To Ahed Tamimi

and all the brave hearts behind the walls

Propositions accompanying the thesis

"Electrochemical recovery of rare earth metals in molten salts"

Aida Abbasalizadeh, 29 November 2018

1- Massive and complex problems like climate change, waste management etc cannot be solved through competitive free market. They require decisive regulations, collective ownership and partnerships beyond borders.
2- Rare earth affinity to oxygen makes it difficult to calculate the yield of the recycling process in lab scale (This thesis).
3- In order to prevent CO, CO_2, CF_4 and CF_6 gas evolution in electrochemical metal extraction processes, the conventional graphite anode should be substituted by reactive anodes (This thesis).
4- FeF_3 is the best option for the fluoridising treatment since the contribution of FeF_3 in the electrochemical process leads to Nd-Fe alloy formation, which can be used as the master alloy for NdFeB magnet production (This thesis).
5- Combining fluoridising treatment with use of iron as reactive anode made it possible to generate in situ and consume FeF_3 in one set-up (This thesis).
6- The way we relate to the people at work, the capacity for autonomy and care, the freedom of thinking and the material conditions of our work are the elements which qualify as work.
7- Educational institutions should take a side between sustainability and weapon engineering, as having them both is a big contradiction. For every weapon that is made one life is destroyed.
8- The ultimate function of every educational entity should be practicing the ability to question everything.
9- As the consequence of neoliberal system, we are living in atomized human societies with enforced competition, insecurity and precarity. In order to experience our being as social animals, we should recognize our collective human power and practice solidarity together.
10- Annex to proposition 9: Monthly borrel in the faculty is not considered as a collective practice. Yet it is highly appreciated.

These propositions are regarded as opposable and defendable and have been approved by the supervisors dr. Y. Yang and prof. dr. ir. J. Sitesma.

Table of contents

Chapter 1 Introduction

1.1 Background

Rare earth (RE) elements are seventeen elements in the periodic table including fifteen lanthanides, scandium and yttrium. These elements are characterized by similar chemical properties. RE elements play a key role in the advancement of green, sustainable and low-carbon technologies as well as in military technologies. These elements are used in applications such as wind turbines, electric vehicles and ultra-efficient lighting [1]. The most important application of the RE elements is in NdFeB permanent magnet materials, containing Nd, Dy and Pr, which have excellent magnetic and conductive properties. Current annual consumption rate of RE elements is reported to be 130 kt and is expected to increase significantly with the expansion of RE elements market in the coming decade [2].

The United States was the leader in global rare earth production from the 1960s to the 1980s, but due to the lower labour cost and lower environmental restrictions, RE production has been shifted almost entirely to China. At present China produces more than 90% of the global rare earth output and is the largest producer of these elements in the world.

In 2011 China tightened the export restriction for these elements which highlighted the supply risk of RE metals for governments as well as businesses [3]. Despite the fact that China ended this quota at the beginning of 2015, concern on supply shortages of rare earth elements have raised over past years due to the uncertainty of the RE market and increasing global demand for these elements [4].

Different strategies have been proposed in order to alleviate the RE element supply risk. Substituting critical rare earth elements by other elements, investing in primary mining resources outside China and recycling of RE metal scrap are the main approaches to tackle this challenge [5].

Substitution can be used as a strategy to mitigate the RE elements shortage problem. However, some of the RE elements remain the first choice for many applications such as electric motors and turbines. In view of primary mining, some old mines are reopened and mining companies are performing research in search of new exploitable RE metal resources [6].

Recycling is the most reliable solution for the problem of RE metals supply crisis since most developed countries do not possess primary resources and hence they need to import their RE requirements [7]. Moreover, recycling has many advantages over primary production, such as cheaper material resources (end-of-life products or industrial waste residue), smaller environmental footprints and establishing the

resources loop. It is also more beneficial in view of the so-called “balance problem”. For example, neodymium always coexists with other RE metals in natural ores (bastnasite and monazite). In primary mining of RE ores, more abundant RE elements such as cerium and lanthanum are extracted along with neodymium and dysprosium, hence generating an excess of cerium that does not necessarily match the market requirement [3].

Despite extensive research and developments on recycling of RE elements, only less than 1% of the end-of-life products containing RE elements were recycled before 2011. The greatest challenge in RE metals recycling is collection and disassembly of the end-of-life products. This is mainly due to the diversity of component design and material composition of RE containing commodities in different applications. For instance, NdFeB magnets used in electronic devices and household electrical appliances mainly end up in the ferrous metal waste or scrap.

Environmental issues due to the RE metals recycling technologies form another challenge. Primary RE metal production as well as RE recycling processes have environmental issues due to halogen, fluorocarbon, carbon monoxide or carbon dioxide gas generation. Therefore, an effective and a clean process for the recovery of RE metals from RE oxide and RE magnets is an absolute necessity which is investigated in this thesis.

1.2 Research aim

Electrochemical extraction (molten salt electrolysis) in molten fluorides is the dominant industrial method for extraction of RE metals from their oxides [6–8]. Lithium fluoride (LiF) is the main component as electrolyte in the RE oxide electrolysis process. The solubility of the RE oxides in LiF is an important factor in this process.

Two major challenges pertaining to RE metals recycling using this technology are a) low solubility of RE oxides in molten salts and b) the possibility of anodic halogen or fluorocarbon gas evolution (if electrolysis rate exceeds oxide feed of neodymium [8]) or carbon monoxide or dioxide gas generation. Therefore, a high yield halogen and carbon-free recycling route for recovery of rare earth elements from RE scrap needs to be designed.

By RE scrap we do not mean only the end-of-life products. The products that contain more sludge powder than the standard capacity after the machining step and also ‘off-spec’ products which have higher oxygen impurity than the required specification are disposed as scrap during the manufacturing [9]. Thus, about 50% of the charged neodymium during the manufacturing process of the neodymium (NdFeB) magnets is disposed as scrap.

As was mentioned earlier, current technology of RE metals recycling deals with environmental issues due the carbon monoxide, carbon dioxide and even halogen or

fluorocarbon gas generation during the electrochemical processes. An alternative method is needed for carbon-free generation of pure RE metals as well as RE alloys.

Hence the main questions to be answered in this project are first, how to increase the RE metal extraction yield from RE oxide by increasing the RE oxide solubility in the molten salt and second, how to prevent halogen, fluorocarbon or carbon monoxide or dioxide gas generation in the RE metal production from RE oxide and RE magnet in molten salt electrolysis process.

1.3 Research methodology

In this research new methods for the direct electrochemical reduction of RE oxides and NdFeB magnets materials into RE metals and RE-based alloys are investigated. The first challenge to be solved is the low solubility of RE oxides in molten fluorides. A two-fold approach is adopted to address this issue. First, a treatment is proposed to convert the RE oxides into RE fluorides using effective fluorinating agents. Zinc fluoride (ZnF_2), aluminium fluoride (AlF_3), iron fluoride (FeF_3) and cryolite (Na_3AlF_6) have been examined as fluorinating agents.

Secondly, the same approach is investigated for the NdFeB magnet scrap. The results show the feasibility of the conversion of the RE in the magnet to RE fluoride in molten salts. Once RE fluoride is formed, it can subsequently be electrolyzed and extracted on the cathode. However, this conversion introduces a new obstacle in the electrochemical extraction part for both RE oxide and NdFeB magnet, which is the fluorine or fluorocarbon gas evolution as the anodic reaction.

To prevent fluorine or fluorocarbon gas evolution on the anode, a reactive anode is employed. Iron is anodically dissolved, re-generating the fluorinating agent FeF_3 *in situ* in the electrochemical reactor. The RE fluoride thus formed is subsequently processed through the electrolysis route in the same reactor to extract RE metal as the cathodic deposit in the form of Fe-Nd alloy. The design of the reactor should be such that formed non-RE oxide as the result of conversion reaction can be collected and removed at the bottom of the cell.

1.4 Research outline

After the introduction in **Chapter 1**, **Chapter 2** of this thesis gives an overview of the studies on electrochemical extraction of rare earth oxides and NdFeB magnets containing dysprosium both in molten chlorides and fluorides.

Chapter 3 investigates the low solubility of the rare earth oxides in the molten fluorides. In this chapter conversion of rare earth oxides to rare earth fluorides using fluorinating agents is studied. Zinc fluoride (ZnF_2), aluminium fluoride (AlF_3), iron fluoride (FeF_3) and cryolite (Na_3AlF_6) are used as fluorinating agents. The feasibility of this conversion is studied from thermodynamic point of view using FactSage software

as well as with laboratory experiments. In **Chapter 4** we investigate the conversion method for NdFeB magnets using the same research approach and the same fluorinating agents.

Once the conversion step is examined, the subsequent topic of the study is avoiding fluorine or fluorocarbon gas generation as the anodic product during the electrolysis of rare earth fluoride. **Chapter 5** studies the use of a novel anode as a substitute for the graphite anode in the industrial processes. In the electrolysis process, iron is used as a reactive anode, promoting electrochemical dissolution of iron into the melt, thus preventing fluorine gas evolution at the anode. Therefore, the fluorinating agent is constantly generated *in situ* which enables the continuous conversion of neodymium oxide feed. In this chapter the electrochemical behaviour of different fluoride salt systems is studied using cyclic voltammetry, chronopotentiometry and square wave voltammetry techniques.

In the absence of information on thermodynamic data and phase equilibria in the literature and considering the importance of these data for optimal design of molten fluorides electrolysis processes, thermodynamic modelling of LiF-DyF_3-NdF_3 system is carried out. In **Chapter 6** we study the thermodynamic modelling of LiF-DyF_3-NdF_3 system using the CALPHAD approach. Gibbs free energy modelling for LiF-NdF_3 and LiF-DyF_3 systems is carried out using the constitutional data from literature. Moreover, *ab initio* calculations were used to obtain enthalpy of formation of $LiDyF_4$, an intermediate phase that is found to exist in the LiF-DyF_3 system. Experiments of thermal analysis are carried out for four compositions within the NdF_3-DyF_3 system. Subsequently, liquidus and solidus temperatures at these compositions are measured using differential thermal analysis (DTA). Scanning electron microscopy (SEM) and energy-dispersive X-ray spectroscopy (EDS) are employed to confirm the nature of the solid phases. The obtained Gibbs energy functions for limiting binaries determined in this work along with DTA analysis for LiF-NdF_3-DyF_3 system are used for modelling Gibbs free energy functions of equilibrium phases in the ternary system.

The conclusions of the proposed methods in this thesis are summarized in **Chapter 7**. In this chapter some avenues for further research are also presented.

1.5 References

[1] Yang, Y., Walton, A., Sheridan, R., Güth, K., Gauß, R., Gutfleisch, O., Buchert, M., Steenari, B.-M., Van Gerven, T., Jones, P. T., and Binnemans, K., 2017, "REE Recovery from End-of-Life NdFeB Permanent Magnet Scrap: A Critical Review," Journal of Sustainable Metallurgy, 3(1), pp. 122-149.

[2] Bauer, D., Diamond, D., Li, J., Sandalow, D., Telleen, P., and Wanner, B., 2010, "Critical Materials Strategy," U.S. Department of Energy Critical Materials Strategy.

[3] Binnemans, K., Jones, P. T., Blanpain, B., Van Gerven, T., Yang, Y., Walton, A., and Buchert, M., 2013, "Recycling of rare earths: a critical review," Journal of Cleaner Production, 51(0), pp. 1-22.

[4] Alonso, E., Sherman, A. M., Wallington, T. J., Everson, M. P., Field, F. R., Roth, R., and Kirchain, R. E., 2012, "Evaluating Rare Earth Element Availability: A Case with Revolutionary Demand from Clean Technologies," Environmental Science & Technology, 46(6), pp. 3406-3414.

[5] Kooroshy, J. G. T. A. T. A. W., 2015, "Strenthening the European rare earths supply-chain: challenges and policy Options," ERECON.

[6] Habib, K., and Wenzel, H., 2014, "Exploring rare earths supply constraints for the emerging clean energy technologies and the role of recycling," Journal of Cleaner Production, 84, pp. 348-359.

[7] Okabe, T. H., Takeda, O., Fukuda, K., and Umetsu, Y., 2003, "Direct Extraction and Recovery of Neodymium Metal from Magnet Scrap," Materials Transactions, 44(4), pp. 798-801.

[8] Kaneko, A., Yamamoto, Y., and Okada, C., 1993, "Proceedings of the International Conference, Rare Earths '92 Electrochemistry of rare earth fluoride molten salts," Journal of Alloys and Compounds, 193(1), pp. 44-46.

[9] Abbasalizadeh, A., Teng, L., Sridhar, S., and Seetharaman, S., 2015, "Neodymium extraction using salt extraction process," Mineral Processing and Extractive Metallurgy, 124(4), pp. 191-198.

Chapter 2 Chlorinating treatment of NdFeB magnets and study on fluorinating

Abstract

In the present research, the feasibility of the recovery of neodymium and dysprosium from end-of-life Nd-Fe-B magnets (~6 wt% Dy) is investigated by using molten salt processes. The salt bath consisted of eutectic composition of NaCl-KCl-LiCl mixture. In order to enable efficient dissolution of the metals into the molten salt phase, $AlCl_3$ is used as a chlorinating agent. Iron-free electrodeposition is carried out. Energy Dispersive Spectroscopy (EDS) analysis of the electrodeposit revealed that co-deposition of the dysprosium occurs along with neodymium at the cathode. The process shows that this method is well-suited for recovering rare earth metals from the magnetic scrap containing these metals.

Furthermore the set-up design for recovery of neodymium and dysprosium from their oxides is investigated. Stability of different fluorides and chlorides salts is studied by means of thermodynamic calculations. AlF_3 based molten salt systems are studied in detail as the electrolyte for electrochemical extraction of rare earth (RE) oxides into RE-Al alloys.

Keywords: rare earth, electrodeposition, molten salts, neodymium magnet, rare earth oxides.

Chapter 2 is based on the published book chapter:

A. Abbasalizadeh, L. Teng, S. Seetharaman, J. Sietsma and Y. Yang, Rare Earths Industry, D. Lima, I. Borges and W.L. Filho, 2015, Elsevier, 357

2.1 Introduction

International concerns have been raised on the supply shortages of rare earth elements since China, the largest producer of rare earths, reduced the export of these elements, while, on the other hand, global demand has increased over last years.

Among the rare earth elements, neodymium is extensively applied for production of permanent magnets. These magnets are used in different applications, such as computer hard disk drives, generators in wind turbines, magnetic resonance imaging sources, because of their superior magnetic properties. Dysprosium is often used as additive element in neodymium magnets in order to retain the magnetic properties at high temperatures. An effective recovery method for Dy and Nd is needed, since REs in magnets are not recovered after being used [1].

Electrochemical deposition is one of the methods for the recovery of rare earth elements. However, electrochemical deposition in aqueous solutions is not a feasible method since rare earth elements have highly negative electrode potentials and also they react with water and oxygen. Therefore, molten salt electrolytes are selected for electrowinning of rare earths [2]. In this work we use molten chloride salt in order to electro-reduce the rare earth elements from NdFeB magnets.

The other important issue which has been discussed in the recent years is the recovery of rare earths from rare earth oxides (REOs). Different methods were used in order to remove the oxygen from rare earth oxides: direct electrochemical deoxidation process [3], solid state electrotransport [4-6], oxyhalide formation [7] and calcium-halide deoxidation [8], which was further combined with electrolysis in order to balance the CaO activity in the molten salt [3]. Yet the strong affinity of rare earth metals to oxygen [9] has made it difficult to industrialize any of these methods except molten salt electrolysis. Nowadays the main technology for producing pure rare earth metals and rare earth master alloys is the rare earth oxide electrolysis in fluoride molten salts [10]. In general, because of the higher efficiency, lower energy consumption, no limitation due to H_2 evolution and higher purity of the deposits, a number of reactive metals such as aluminium, magnesium, sodium and potassium are produced by molten salt reduction or electrolysis [11]. Metal chlorides are mostly used for different applications since, as compared to fluorides, they are less expensive, less corrosive and also have lower melting temperatures [12]. However, fluorides have higher stability, higher conductivity and in particular higher solubility of oxides, compared to chloride salts.

In this chapter we discuss the possibility of using aluminium chloride as the chlorinating agent in LiCl-KCl-NaCl ternary electrolyte for reduction of Nd and Dy from NdFeB magnets. Using eutectic composition of LiCl-KCl-NaCl electrolyte (eutectic point at 354 °C) made it possible to perform the experiments at lower temperatures compared to fluoride salts. However, due to the low solubility of metal oxides in molten chlorides salts and low stability of these salts, it was decided to use the fluoride salts for electrochemical reduction of rare earth metals from rare earth oxides. Hence thermodynamic calculations are performed in order to study the aluminium fluoride as

a fluxing agent in the molten fluorides to react with rare earth oxide and form rare earth fluoride which can be further subjected to electrolysis under the applied voltage.

2.2 Thermodynamic considerations

2.2.1 Electrochemical reduction of NdFeB magnets containing Dy

Efficient dissolution of metal in the molten salts depends on the choice of the additives. Earlier studies on the extraction of Fe, Cr and Nd from industrial electric arc furnace slag (EAF), chromite ore [13] and spent neodymium magnets [14], have proven that $AlCl_3$ can act as a powerful chlorinating agent. The reaction between the NdFeB magnet and $AlCl_3$ leads to the selective metal chloride formation. The formed metal chloride will be subjected to electrolysis and will be reduced on the cathode.

The standard Gibbs energy for formation of different metal chlorides (for the metals present in the magnets), using $AlCl_3$ as the chlorinating agent, is calculated by using the FactSage software (FactSage 6.3). The results show that Nd and Dy trichlorides are more stable than $AlCl_3$, while the formation of $FeCl_3$, $FeCl_2$ and BCl_3 is not favoured. The Gibbs free energies ΔG^0 and enthalpies ΔH^0 of the corresponding reactions are listed in Table 2.1.

Table 2.1– Gibbs free energy and enthalpy values of the reaction of $AlCl_3$ with the different metals in the system.

Chlorination Reactions	ΔG^o[kJ/mol]	ΔH^o[kJ/mol]	ΔG^o[kJ/mol]	ΔH^o[kJ/mol]
	at 800 °C		at 25 °C	
$AlCl_3$(salt)+Dy(s) ⇄ $DyCl_3$+Al(liq.)	-206.2	-353.5	-291.2	-293.9
$AlCl_3$(salt)+Nd(s) ⇄ $NdCl_3$+Al(liq.)	-247.8	-368.0	-331.4	-330.2
$AlCl_3$(salt)+Fe(s) ⇄ $FeCl_3$ +Al(liq.)	296.7	337.7	296.4	306.6
$AlCl_3$(salt)+3/2Fe(s) ⇄3/2$FeCl_2$+Al(liq.)	207.0	165.1	176.8	193.2
$AlCl_3$(salt)+B(s) ⇄ BCl_3 +Al(liq.)	180.2	195.3	242.4	303.0

From the Gibbs energy values given in Table 2.1, it can be concluded that Nd and Dy react with $AlCl_3$ and as a result, $NdCl_3$ and $DyCl_3$ are formed in the salt bath. These can be further electrolyzed under the applied voltage. Iron (II, III) chloride as well as boron chloride will not form in the system due to their positive Gibbs energy value. Selective chlorination of the rare earth elements by aluminium chlorides is very important since it separates the rare earth elements from iron and boron in the magnet. It should be noted that these calculations are based on the pure substances at their standard state at 800 °C, whereas the activity of Nd and Dy in the magnet as well as the activity of the chlorides will change after the dissolution in the salt bath.

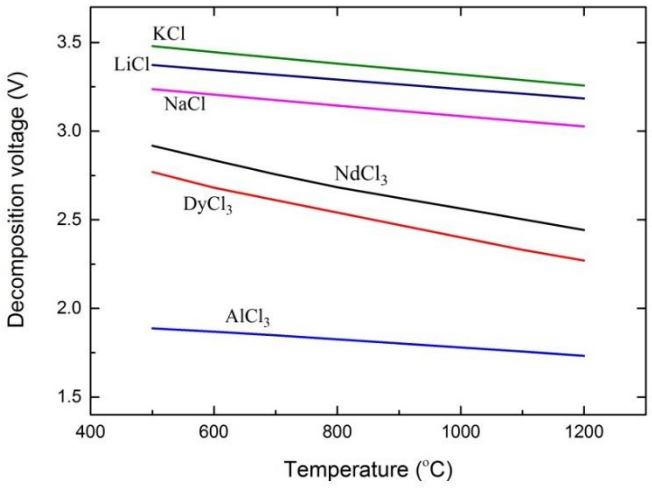

Figure 2.1– Calculated standard decomposition voltage as a function of temperature for the chlorides formed in LiCl–KCl–NaCl–$AlCl_3$ molten salt bath.

The formed rare earth chloride can be decomposed according to the reaction under external voltage in the molten electrolytes:

$$RECl_3 \rightarrow RE^{3+} + 3Cl^- \quad (2.1)$$

The decomposition voltages of the different metal chlorides and alkali chlorides are calculated using FactSage software and the results are presented in Figure 2.1.

An over-potential of 0.8 V is suggested for the decomposition of $NdCl_3$ [14]. Considering that Nd and Dy possess similar properties and also based on the decomposition voltage of $DyCl_3$ shown in Figure 2.1 (2.6 V at 800 °C), a voltage of 3.4 V was applied for the electro-decomposition of $DyCl_3$.

2.2.2 Electrochemical reduction of rare earth oxides for Nd-Al alloy production

For the electrochemical reduction of REOs, the first step is the electrolyte selection. The reduction potential of the electrolyte should be more negative than the reduction potential of the rare earth oxides, meaning that the molten salt electrolyte has to be more stable than the rare earth compounds in the system. In order to compare the stability of different chloride and fluoride electrolyte systems, thermodynamic studies are performed on these salt components as well as on the oxides. The decomposition voltages of the neodymium oxides, neodymium fluoride and the most common molten salts, calculated using FactSage, are compared in Figure 2.2. Due to the similarity of the chemical behaviour of the rare earth elements, the thermodynamic calculation has been done only for neodymium compounds, as the representative for other rare earth elements.

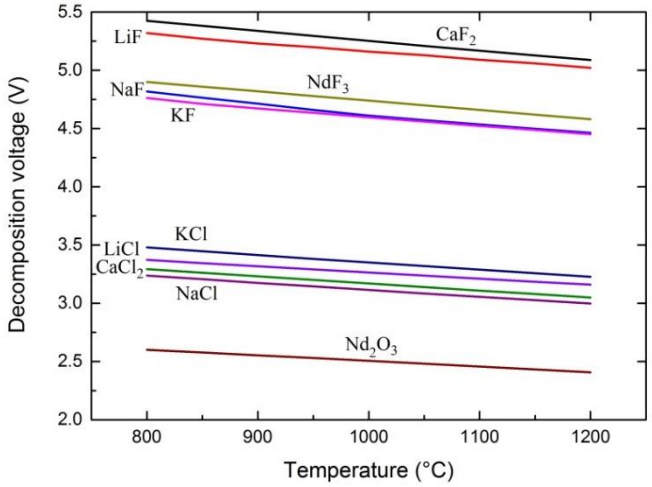

Figure 2.2– Calculated comparison of decomposition voltages of different salts and oxides at different temperatures.

Figure 2.2 exhibits that fluorides have higher decomposition voltages comparing to the chlorides, since they are more stable. However, the solubility of REOs in chloride salts is lower compared to fluoride salts. Among chlorides, KCl is the most stable one and NaCl has the lowest stability. From the thermodynamic results, it can also be seen that between CaF_2, LiF, KF and NaF at different temperatures, the most stable fluoride is CaF_2. Hence the relative stability of these metal fluorides is: CaF_2>LiF>NaF>KF. Comparing the decomposition voltage of rare earth fluorides and the alkali fluorides and chlorides, it can be seen that only CaF_2 and LiF are more stable than NdF_3. In other words, in the case of using NaF, NaCl, KF, KCl, $CaCl_2$ and LiCl, we can expect that Na, K, Ca and Li will be reduced on the cathode from their corresponding halides before the reduction of neodymium from neodymium fluoride. Therefore, for the electrochemical decomposition of rare earth fluorides, the most suitable electrolytes among fluorides are CaF_2 and LiF. In China since 1990s fluorides are substituted for chloride salts in rare earth metals production. LiF-REF_3-REO (RE = La, Nd, Dy, Ce, Pr and rare earth master alloys) is the main electrolyte system in the rare earth electrochemical production industry [10]. Considering the high melting point of calcium fluoride (1418°C), the eutectic composition of LiF-CaF_2 (79-21 mol%, reducing the melting temperature to 768 °C, shown in Figure 2.3), is a suitable option to be used as the molten salt electrolyte for the electrochemical reduction of the rare earth oxides.

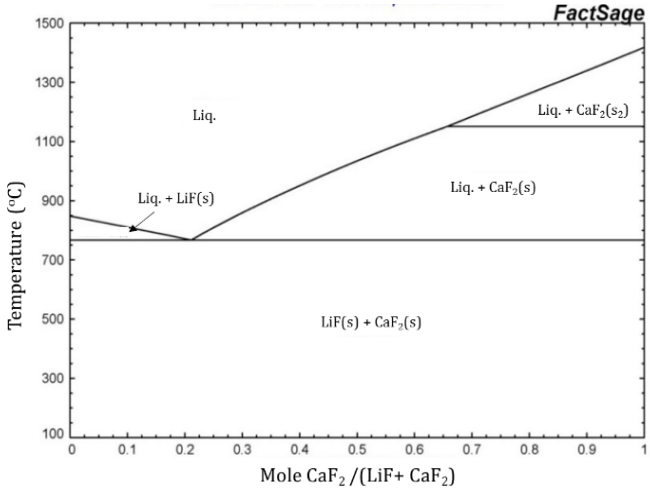

Figure 2.3– LiF-CaF_2 phase diagram from FactSage software package [15]

The experimental results of Hamel et al. [16] support the thermodynamic results in the present study. These authors have measured the standard potential of different fluoride electrolytes in order to find the most suitable electrolyte for reduction of Nd. Their results show that in LiF-NaF and LiF-KF systems, no electrochemical reduction of Nd is observed.

In the present work AlF_3 is suggested for electrochemical reduction of neodymium from neodymium oxide, while $AlCl_3$ is used for Nd and Dy extraction from neodymium magnets. Comparing the relative advantages of AlF_3 to $AlCl_3$, experiments with $AlCl_3$ indicated the loss of some of the aluminium chloride added to the vapour phase from the molten chloride bath before being dissolved in the molten salt due to the high vapour pressure of chloride salts [14]. AlF_3 on the other hand, is found in the present work as a suitable fluorinating agent for the electrolysis of rare earth oxides in molten fluorides. From the negative Gibbs energy value of the reaction

$$Nd_2O_3 + 2AlF_3 \rightarrow Al_2O_3 + 2NdF_3 \quad \Delta G^o(\text{at } T = 900°C) = -183 \text{ kJ/mol} \qquad (2.2)$$

it is seen that aluminium fluoride can react with rare earth oxides forming rare earth fluorides, which can be further reduced at the cathode. *In situ* formation of REF_3 is very important since the solubility of REOs is very low in the molten fluorides, which is the main challenge for the current industrial operation. Moreover REOs form rare earth oxyfluoride in molten fluorides according to the reaction [17]

$$Nd_2O_3 + NdF_3 + 3(x-1)LiF \rightleftarrows 3NdOF_x^{(x-1)-} + 3(x-1)Li^+ \qquad (2.3)$$

The preliminary experiments in our laboratory show the formation of oxyfluoride in a LiF-NdF_3-Nd_2O_3 system.

Figure 2.4 shows the EDS line scan of the sample cross-section after 3 hours at 900 °C. The changes of oxygen and fluorine exhibit the same trend, showing the formation of oxyfluoride compounds in this system. It is not possible to determine Li changes using EDS line scan since lithium is a light element.

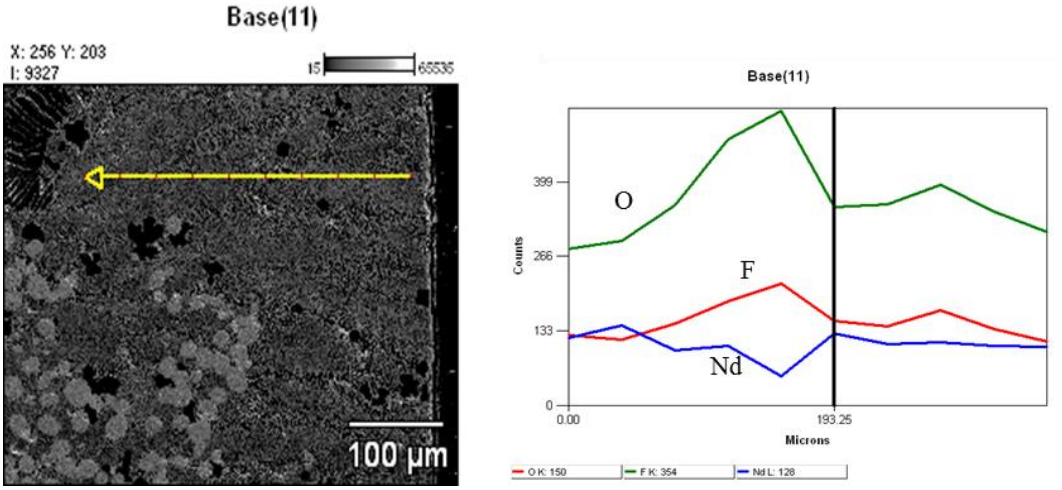

Figure 2.4– Line scan graph of the quenched LiF- NdF_3-Nd_2O_3 sample after 3 hours at 900°C shows the same trends in the concentrations of oxygen and fluorine, indicating the formation of oxyfluoride compound.

Stefanidaki et al. [17] have studied the oxide solubility and Raman spectra of Nd_2O_3 in the alkali fluorides. They have reported that the NdF_6^{3-} anion is the dominant complex in the eutectic NdF_3-LiF melt system and when Nd_2O_3 is added, $NdOF_5^{4-}$ complex might form in the melt. They have found that the solubility of Nd_2O_3 varies from 0.15 to 0.38 mol% when the NdF_3 concentration changes from 15 to 30 mol% at 900°C. This is in support of the earlier results that rare earth oxide solubility in electrolyte is enhanced by the presence of rare earth fluoride salt [17].

Contradictory results have been reported on the electrochemical reduction of rare earth oxyfluorides in the molten salts, which shows that further investigation is needed. According to Taxil et al. [18], Ln fluorides in the presence of the metal oxides will form lanthanum oxyfluoride, which is an insoluble product. Stefanidaki et al. [19] have shown that the neodymium oxyfluoride is not reduced to neodymium metal. In the voltammetric characterization of LiF-NdF_3-Nd_2O_3 system, they have observed the same voltammogram as the one for LiF-NdF_3 system. They have concluded that neodymium is reduced on the tungsten cathode by electroreduction of neodymium fluorides (present in the form of $[NdF_6]^{3-}$), while oxygen is generated on the glassy carbon anode by oxidation of neodymium oxyfluorides (present in the form of $[NdOF_5]^{4-}$), producing CO and CO_2 gasses. They proposed that electrochemical production of neodymium in an oxyfluoride melt is possible at low voltage electrolysis, in which fluorocarbon compounds are not formed. Thudum et al. [20] have shown that neodymium in LiF-CaF_2-NdF_3-Nd_2O_3 and LiF-CaF_2-LaF_3-Nd_2O_3 systems can be reduced both from neodymium oxyfluorides and neodymium fluoride ions, depending on the molar ratio of neodymium oxyfluorides to neodymium fluoride ions (OF/F). At low OF/F ratios, $[NdF_6]^{3-}$ is reduced to neodymium. Meanwhile above a critical Nd_2O_3 concentration, $[NdOF_5]^{4-}$ are cathodically active ions and are reduced on the cathode. Kaneto et al. [21]

have suggested that in the oxyfluoride system, oxygen is generated on the anode, while fluorine can be produced at the anode at higher cell voltage.

Role of AlF_3: Based on the Gibbs energy value of reaction (2.2), rare earth fluoride formation is possible at 900°C. One important advantage of in-situ formation of REF_3 as the result of reaction of REO with aluminium fluoride is that the formation of rare earth oxyfluoride might be avoided. Based on reaction (2.2) aluminium oxide is also formed in the system. We should consider whether the aluminium oxide participates in electrochemical reactions or not. There would be two scenarios after aluminium oxide formation in the system: either it is dissolved in the molten fluorides or it remains undissolved in the molten salt. The density of aluminium oxide at 950°C is 3.95 g/cm^3. An estimation based on the density of the LiF containing different contents of NdF_3 [22], shown in Table 2.2, shows that the density of lithium fluoride containing 5 mol% neodymium fluoride is about 4 g/cm^3. This means that the critical composition in which the aluminium oxide starts to float is LiF-5 mol% NdF_3. For higher solubility of neodymium oxide in molten salt, more than 5 mol% neodymium fluoride is added to the electrolyte. Moreover, based on reaction (2.2), neodymium fluoride is also formed in the salt as the result of the reaction between aluminium fluoride and neodymium oxide. Thus, we expect that the undissolved aluminium oxide will float on top of the salt. In this case, Al_2O_3 can be removed from the salt. In the case that the formed aluminium oxide is not dissolved in the molten fluoride salt, an alternative is the addition of cryolite (Na_3AlF_6) to the system. Cryolite is used in aluminium production industry as the solvent for aluminium oxide.

Electrochemical decomposition voltages of aluminium oxide, neodymium oxide and neodymium fluoride are calculated and compared in Figure 2.5.

Table 2.2 – Density of LiF at different NdF_3 content at 950°C [22].

NdF_3 contents (mol.%)	0	25	30	35	40	45	50
Density (g/cm^3) at 950 °C	1.541	4.451	4.618	4.763	4.856	4.952	5.031

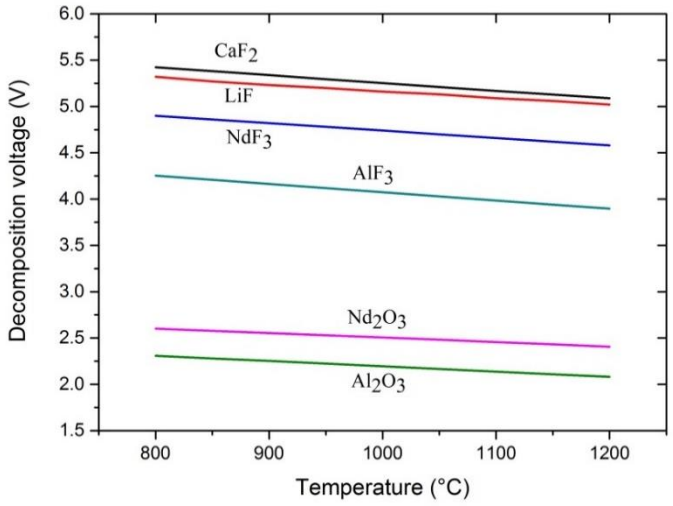

Figure 2.5– Decomposition voltages of different components in the system.

From Figure 2.5 it is seen that aluminium fluoride (AlF_3) that is used as additive to LiF-CaF_2-NdF_3 electrolyte system and the aluminium oxide (Al_2O_3), which is formed in the system as the result of chemical reaction between the aluminium fluoride and neodymium oxide, have lower decomposition voltages than neodymium fluoride (NdF_3) and neodymium oxide (Nd_2O_3). This means that when the voltage for electrolysis of neodymium fluoride is applied to the system, the formed Al_2O_3 and the remaining AlF_3 in the system will go through the electrolysis process as well. Hence the co-deposition of aluminium along with neodymium will occur. In this case anodic and cathodic reactions at the cell voltage higher than 4.8 V (neodymium fluoride decomposition voltage at 900°C) are

Cathodic reactions:

$$Nd^{3+} + 3e^- \rightarrow Nd \quad (2.4)$$

$$Al^{3+} + 3e^- \rightarrow Al \quad (2.5)$$

Anodic reactions (on graphite anode):

$$O^{2-}\,(salt) + C\,(anode) \rightarrow CO\,(g) + 2e^- \quad (2.6)$$

$$2O^{2-}\,(salt) + C\,(anode) \rightarrow CO_2\,(g) + 4e^- \quad (2.7)$$

According to Al-Nd phase diagram, shown in Figure 2.6, formation of six different intermetallics is possible on the cathode. It is possible to control the alloy formation by adjusting the voltage of the system. More investigation on the electrochemical behaviour of LiF-CaF_2-NdF_3-Al_2O_3 is necessary. A cyclic voltammetry analysis of the system can give us a better insight in this regard. The results of electrochemical behaviour studies of these systems are presented in chapter 5.

Nd-Al co-deposition is beneficial since it would cause the potential that is needed for the neodymium ions reduction on the cathode to move to more positive values, based on the "depolarization effect" [23]. The depolarization effect is expected in the case of binary systems which form intermetallic compounds. In the Nd-Al binary system, neodymium reduces at lower potential since the activity of neodymium is decreased in the intermetallic compound. This phenomenon would increase the extraction efficiency of neodymium. Nd-Al alloy, which is formed on the cathode, can be used as the master alloy for the NdFeAl bulk amorphous alloys which are attractive because of their glass-forming ability and also their ferromagnetic properties at room temperature [24].

As was discussed earlier, in-situ formation of NdF_3 might reduce the problem of low solubility of REOs in molten fluorides. Moreover, the alloy formation would increase the rare earth extraction efficiency due to lower activity of the metal in the alloy, which decreases the reduction potential of the rare earth. A suited Al-Nd alloy with industrial applications should be explored as the target cathodic product.

2.3 Experiments

The ternary eutectic composition of LiCl-KCl-NaCl salt (55 mol% LiCl, 35 mol% KCl and 10 mol% NaCl) was dried at 200 ^{o}C for 24 hours. High purity aluminium chloride (99%) was added as the chlorinating agent. Neodymium magnets containing approximately 6 wt% dysprosium were crushed into small particles (about 1 mm). According to the results from scanning electron microscopy (SEM) equipped with an energy dispersive spectroscopy probe (EDS) analysis, the chemical composition of the magnet is $Fe_{14}Nd_{1.4}Dy_{0.6}$, in which boron, being a light element, remains undetermined in EDS analysis).

Experiments on the reduction of Nd and Dy from scrap magnets in molten chlorides were performed at 800 ^{o}C for 6 hours. The flux/neodymium and flux/salt ratios were

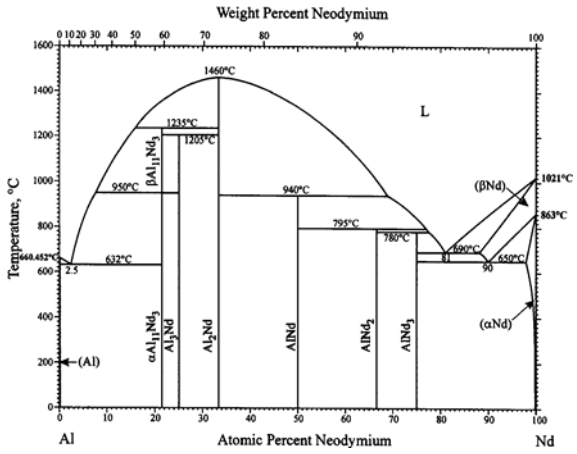

Figure 2.6– Nd-Al phase diagram [25].

Table 2.3 – Fractions of different components used in the electrolysis experiment (wt%).

Composition	$AlCl_3$	$Nd_2Fe_{14}B$	NaCl	KCl	LiCl
(wt%)	3.14	9.18	1.59	7.48	6.63

chosen as 2 (molar fraction) and 20 wt% respectively. Table 2.3 shows the fractions of different components used in the experiments.

Salt mixture, flux and magnets are heated up to 800 ^oC in an alumina crucible in a vertical furnace. Inert atmosphere, containing argon gas, is used which was dehydrated by passing through silica gel. Graphite rods are chosen as anode and cathode in view of their additional advantage as oxygen getters. The mixture is kept at 800 ^oC for 3 hours, so the neodymium chloride is formed and subsequently dissolves in the molten fluoride electrolyte. Then the electrolysis is started by dipping the electrodes into the salt bath and a constant voltage of 3.4 V is applied between anode and cathode by a DC power supply (HP, Hewlett, 6632A) based on the decomposition voltage of the $DyCl_3$ at 800 ^oC. Figure 2.7(a) shows the schematic diagram of the set-up. After 6 hours electrolysis, the crucible is cooled down under argon gas. The deposited layer on the graphite cathode, shown in Figure 2.7(b), is separated and washed with distilled water in order to dissolve the salts. After removing the salts, the deposited powder is dried and prepared for analysis. To investigate the morphology and composition of the deposited product, SEM/EDS analysis is carried out.

2.4 Results

The microstructures of the cathode samples were analysed by SEM and are presented in Figure 2.8. The phase with bright contrast in this image, indicated by A, is confirmed to be a metallic phase with dysprosium and neodymium as the main elements. The phase with dark contrast indicated by B is aluminium-oxide and the remaining salt. The composition of the metallic phase on cathode samples, analysed by EDS, is presented in Figure 2.9. The data from EDS point analysis show the presence of neodymium and dysprosium in the deposited product to be dominant in comparison to other elements. It should be noted that oxygen detection with EDS is not reliable.

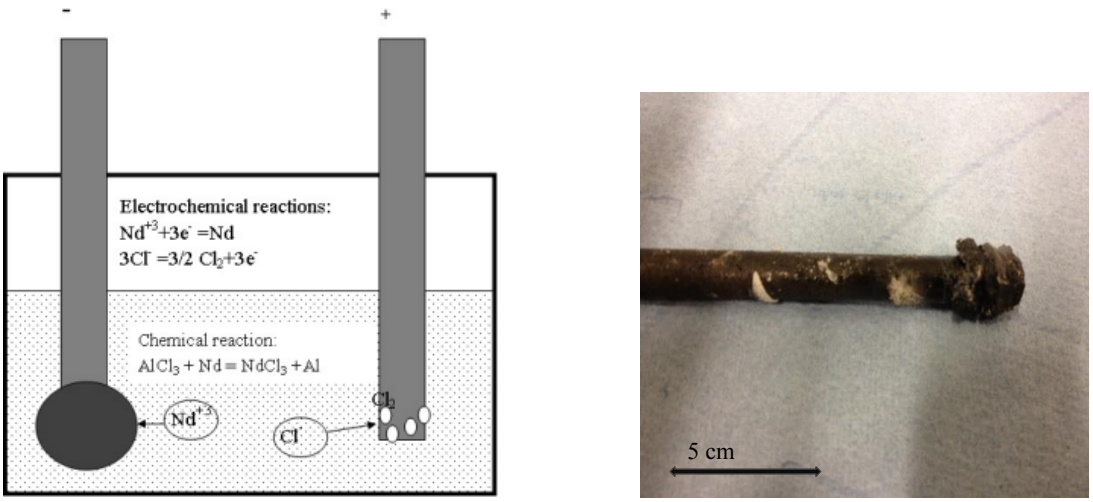

(a) (b)

Figure 2.7– (a) Schematic diagram of the set-up (b) Image taken from graphite cathode after electrolysis at 800°C for 6 hours in argon atmosphere.

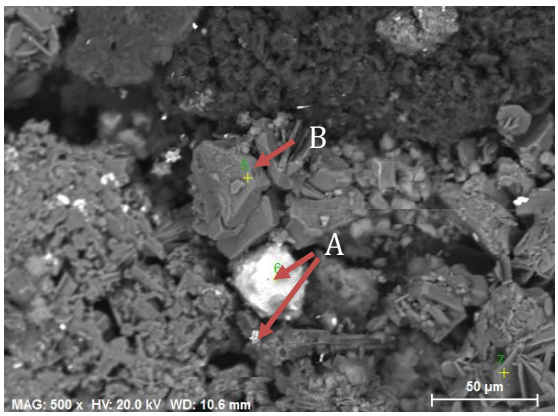

Figure 2.8– SEM image of cathode deposition after electrolysis of magnet, using $AlCl_3$ as flux, at V=3.4 V and T=800°C during 6 hours. A is the metallic phase (Dy-Nd), B is the oxide phase.

The formation of Dy-Nd metallic phase on the cathode was also investigated by EDS mapping analysis on the same region of the sample, shown in Figure 2.10. The intensity of the colour in the image related to neodymium is very low, however it can be seen that dysprosium and neodymium are distributed in the same areas, confirming the formation of metallic phase, since these regions are poor in oxygen. Dysprosium deposition along with neodymium was confirmed using molten salt electro-deposition method. It can be also seen that aluminium and oxygen are distributed in the same areas, which shows the presence of aluminium oxide phase.

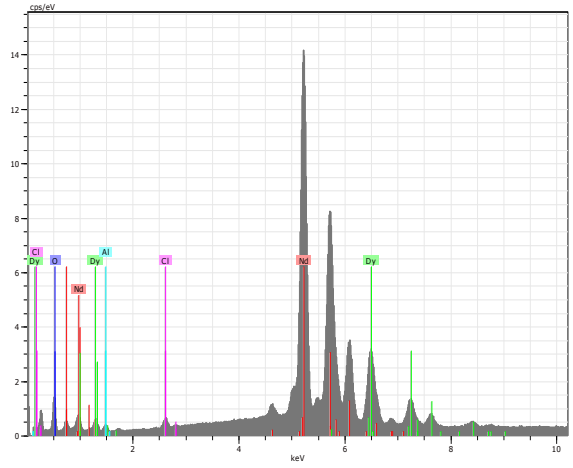

Figure 2.9– EDS pattern of Dy-Nd deposit on graphite cathode in LiCl-KCl-NaCl molten salt at 800°C.

It is not possible to detect boron in the EDS analysis due to it being a light element. In the earlier studies on the electrochemical reduction of neodymium from Nd magnet scraps [26], the results from wavelength dispersive spectroscopy (WDS) showed that boron remains in the bulk salt bath, and the intensity of the boron peak in the cathode sample was lower than the detection limit, shown in Figure 2.11. Detection limit is usually defined as three times the background intensity.

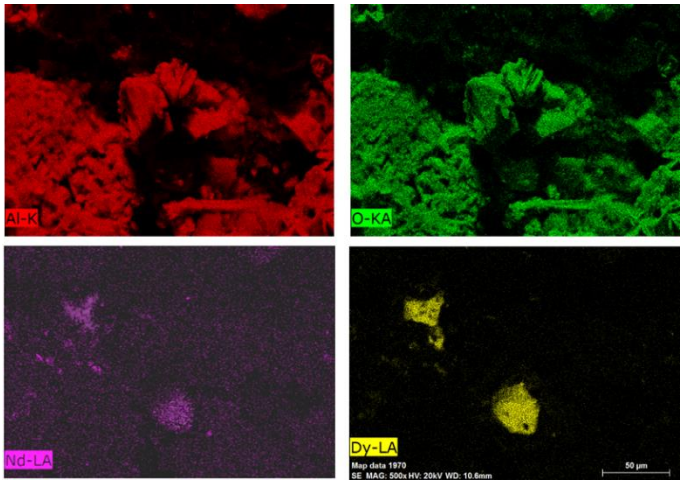

Figure 2.10– Mapping images of Dy-Nd-Al-O deposit on graphite electrode in LiCl-KCl-NaCl molten salt at 800 °C.

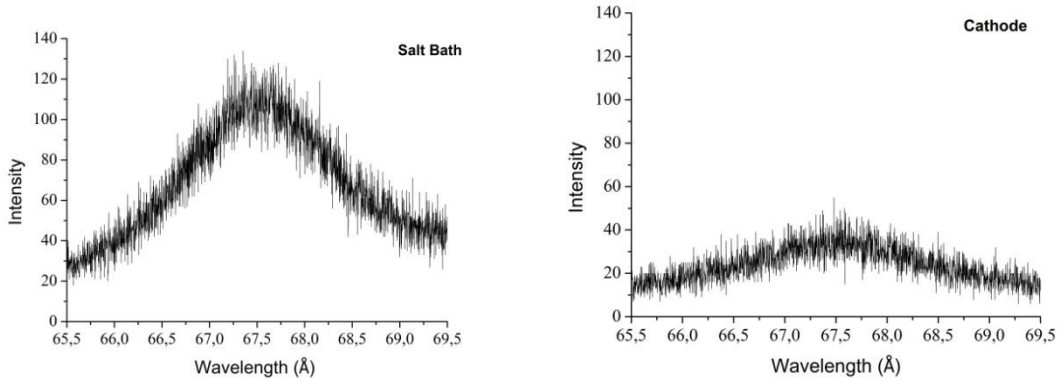

Figure 2.11– Intensity scan over the boron peak position in the salt bath sample and cathode sample from the earlier study [26].

2.5 Discussion

The eutectic composition of LiCl-NaCl-KCl ternary mixture was used as electrolyte for the electrochemical decomposition of NdFeB magnets containing dysprosium. Aluminium chloride was used as the chlorinating agent in order to selectively react with the rare earth metals in the neodymium magnet. It was shown by Licham and Osteryoung [27] that aluminium chlorides exist in the form of $AlCl^{4-}$ ionic species in the alkali chlorides solvents, which results in the formation of a pseudo–binary solution.

The results from SEM/EDS show the presence of Nd-Dy metallic phase in the deposited material. This is explained by the proximity of their electrode potentials. It can be concluded that neodymium and dysprosium have been dissolved in the alkali chloride melt, forming $RECl_3$. In fact, the results from Raman spectrometry have confirmed that neodymium(III) exists as $NdCl_6^{3-}$ complex with octahedral symmetry in the molten alkali chlorides [28]. Thus, in the chloride melt, the rare earth elements dissolve according to [29]

$$RE^{3+} + 6Cl^- \rightarrow RECl_6^{3-} \quad (2.8)$$

Considering the cathodic and anodic electrochemical reactions, these can be represented as

$$\text{Anodic reaction} \quad 3Cl^- \rightarrow \frac{3}{2}Cl_2 + 3e^- \quad (2.9)$$

$$\text{Cathodic reactions} \quad Nd^{3+} + 3e^- \rightarrow Nd$$

$$Dy^{3+} + 3e^- \rightarrow Dy \quad (2.10)$$

RE^{3+} is the most stable state of the rare earth elements in the molten salts [30]. It has been reported that most of the rare earth elements (La, Ce, Pr, Y) have a single decomposition signal in the molten chlorides, however Nd reduction in chloride salts occurs in two steps [29]. The formation of divalent rare earth metal ions in the chlorides melt is most likely one of the reasons for the low current efficiency in RE reduction

processes, which would be caused by two-step reduction of the rare earth metals according to

$$RE^{3+} + e^{-} \rightarrow RE^{2+} \quad (2.11)$$

$$RE^{2+} + 2e^{-} \rightarrow RE \quad (2.12)$$

Contradictory results have been reported on the electrochemical mechanism of neodymium and dysprosium reduction in molten salts. It has been reported that the reduction process of $NdCl_3$ to Nd metal in LiF–$CaCl_2$ melts [16], LiF [19], LiF–CaF_2 [23] and LiCl-KCl [31] is a one-step mechanism. However, De Córdoba et al. [32] and Masset et al. [33] have confirmed that the reduction of $NdCl_3$ takes place in two steps.

The electrode material is one of the factors that can influence the electrochemical reduction behaviour of the rare earth elements in molten salts. Castrillejo et al. [34] have observed that their cyclic voltammogram results exhibit different behaviour of dysprosium on the W and Al wire electrodes. They have observed that, on the W electrode, which is used as inert cathode, Dy is reduced in two steps, *viz.* Dy(III) → Dy(II) → Dy(0), while on the Al electrode the electrochemical reaction would be [Stefanidaki, 19] :

$$Dy^{3+} + 3Al + 3e^{-} \rightarrow DyAl_3 \quad (2.13)$$

in which Dy is reduced at more positive potentials compared to those on an inert W cathode, due to the lower activity of dysprosium in the formed $DyAl_3$ intermetallic.

The study of the electrochemical reduction of Nd and Dy from neodymium magnets containing dysprosium is based on a new process line for the electrolytic recovery of rare earth elements [35]. In the proposed molten salt process the rare earth compounds, which can be magnet scrap or rare earth oxide, are mixed with the molten salts and are heated to the specific temperature.

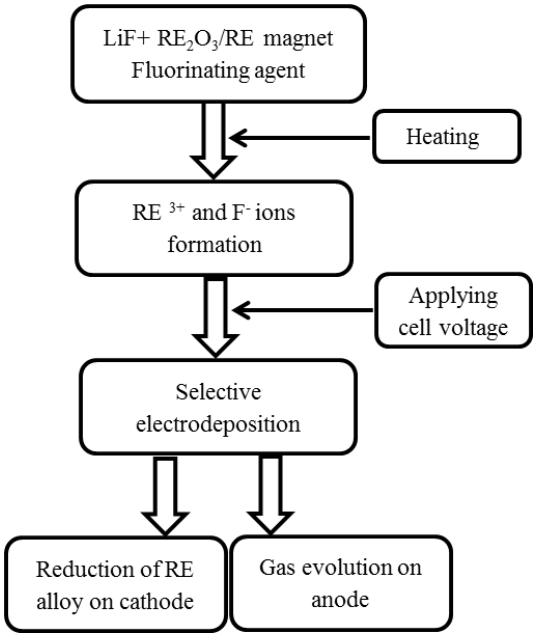

Figure 2.12– Schematic diagram of the salt extraction process.

The working temperature depends on the salt system and the state in which the rare earth elements are reduced on the cathode. The mixture is kept at this temperature for a certain time (about 3 hours), so that the magnet or REOs are dissolved in the electrolyte and the metal ions are formed in the salt. Subsequently, based on the rare earth metal which will get deposited on the cathode, a specific voltage is applied to the cell, and the pure RE metal or the alloy is reduced on the cathode. The process steps are shown in Figure 2.12.

2.6 Conclusion

Feasibility of neodymium and dysprosium extraction from $Nd_2Fe_{14}B$ magnets containing 6% dysprosium was investigated using a combined method of molten salt extraction and electrolysis. LiCl-NaCl-KCl ternary composition was used as electrolyte. Aluminium chloride was proven to be a strong chlorinating agent which reacted with neodymium and dysprosium in the magnet and as the result $NdCl_3$ and $DyCl_3$ were formed. On the other hand, the formation of iron chloride and barium chloride was not feasible, which makes the selective extraction of Nd and Dy possible. The formed rare earth chlorides were subsequently subjected to electrolysis, hence neodymium and dysprosium were reduced on the cathode. In the present approach it was shown that neodymium and dysprosium recovery from magnetic scrap enables a direct separation of these metals from iron, eliminating the oxide or halide conversion steps. The simplicity of this method, due to the single step recovery of the RE metals from the magnet scrap, makes this process attractive from the industrial point of view. This process has the advantage of being environmental-friendly since the salt bath can be reutilized without contaminating the environment.

Further, based on thermodynamic calculations, it was shown that the strong tendency for AlF_3 towards reaction with Nd_2O_3 and Dy_2O_3 would enhance the *in-situ* formation of rare earth fluorides in the salt bath and thereby increase the solubility of REOs in the molten fluorides. Hence AlF_3 can act as an efficient flux agent in the fluorides melt for recovery of rare earth metals from their oxides. In such a system, RE-Al alloy will be produced on the cathode. The use of AlF_3 will be experimentally explored in the forthcoming chapters.

2.7 References

[1] Kurachi, A., Matsumiya, M., Tsunashima, K., and Kodama, S., 2012, "Electrochemical behavior and electrodeposition of dysprosium in ionic liquids based on phosphonium cations," Journal of Applied Electrochemistry, 42(11), pp. 961-968.

[2] Lodermeyer, J., Multerer, M., Zistler, M., Jordan, S., Gores, H. J., Kipferl, W., Diaconu, E., Sperl, M., and Bayreuther, G., 2006, "Electroplating of Dysprosium, Electrochemical Investigations, and Study of Magnetic Properties," Journal of The Electrochemical Society, 153(4), pp. 242-248.

[3] Hirota, K., Okabe, T. H., Saito, F., Waseda, Y., and Jacob, K. T., 1999, "Electrochemical deoxidation of RE–O (RE=Gd, Tb, Dy, Er) solid solutions," Journal of Alloys and Compounds, 282(1–2), pp. 101-108.

[4] Fort, D., Beaudry, B. J., and Gschneidner Jr, K. A., 1987, "The ultrapurification of rare earth metals: Gadolinium and neodymium," Journal of the Less Common Metals, 134(1), pp. 27-44.

[5] Fort, D., Pecharsky, V. K., and Gschneidner Jr, K. A., 1995, "Solid state electrotransport purification of dysprosium," Journal of Alloys and Compounds, 226(1–2), pp. 190-196.

[6] Jordan, R. G., Jones, D. W., and Hems, V. J., 1975, "The purification of the rare earth metals: II. Solid state electrotransport processing of Terbium," Journal of the Less Common Metals, 42(1), pp. 101-110.

[7] Corbett, J. D., Smith, J. D., and Garcia, E., 1986, "The selective removal of oxygen from rare earth and thorium metals through oxyhalide formation," Journal of the Less Common Metals, 115(2), pp. 343-355.

[8] Okabe, T. H., Hirota, K., Kasai, E., Saito, F., Waseda, Y., and Jacob, K. T., 1998, "Thermodynamic properties of oxygen in RE–O (RE=Gd, Tb, Dy, Er) solid solutions," Journal of Alloys and Compounds, 279(2), pp. 184-191.

[9] Carlson, O. N., Lichtenberg, R. R., and Warner, J. C., 1974, "Solid solubilities of oxygen, carbon and nitrogen in yttrium," Journal of the Less Common Metals, 35(2), pp. 275-284.

[10] Siming, P., Shihong, Y., Zongan, L., Dehon, C., Liha, X., and Bin, Z., 2011, "Development on Molten Salt Electrolytic Methods and Technology for Preparing Rare Earth Metals and Alloys in China," Chinese Journal of Rare Metals, 35(3), pp. 440-450.

[11] Mishra, B., and Olson, D. L., 2005, "Molten salt applications in materials processing," Journal of Physics and Chemistry of Solids, 66(2–4), pp. 396-401.

[12] Han, W., Chen, Q., Sun, Y., Jiang, T., and Zhang, M., 2011, "Electrodeposition of Mg-Li-Al-La Alloys on Inert Cathode in Molten LiCl-KCl Eutectic Salt," Metallurgical and Materials Transactions B, 42(6), pp. 1367-1375.

[13] Ge, X. L., Grinder, O., and Seetharaman, S., 2010, "The salt extraction process: a novel route for metal extraction Part I – Cr, Fe recovery from EAF slags and low grade chromite ores," Mineral Processing and Extractive Metallurgy, 119(1), pp. 27-32.

[14] Abbasalizadeh, A., Seetharaman, S., Teng, L., Sridhar, S., Grinder, O., Izumi, Y., and Barati, M., 2013, "Highlights of the Salt Extraction Process," Journal Of Materials, 65(11), pp. 1552-1558.

[15] Bale, C., Pelton, A., Thompson, W., Eriksson, G., Hack, K., Chartrand, P., Decterov, S., Jung, I., Melançon, J., and Peterson, S., 2012, "FactSage™ 6.3. 1," Thermfact and GTT-Technologies, CRCT, Montreal, Canada.

[16] Hamel, C., Chamelot, P., and Taxil, P., 2004, "Neodymium(III) cathodic processes in molten fluorides," Electrochimica Acta, 49(25), pp. 4467-4476.

[17] Stefanidaki, E., Photiadis, G. M., Kontoyannis, C. G., Vik, A. F., and Østvold, T., 2002, "Oxide solubility and Raman spectra of NdF_3-LiF-KF-MgF_2-Nd_2O_3 melts," Journal of the Chemical Society, Dalton Transactions(11), pp. 2302-2307.

[18] Taxil, P., Massot, L., Nourry, C., Gibilaro, M., Chamelot, P., and Cassayre, L., 2009, "Lanthanides extraction processes in molten fluoride media: Application to nuclear spent fuel reprocessing," Journal of Fluorine Chemistry, 130(1), pp. 94-101.

[19] Stefanidaki, E., Hasiotis, C., and Kontoyannis, C., 2001, "Electrodeposition of neodymium from LiF-NdF_3-Nd_2O_3 melts," Electrochimica Acta, 46(17), pp. 2665-2670.

[20] Thudum, R., Srivastava, A., Nandi, S., Nagaraj, A., and Shekhar, R., 2010, "Molten salt electrolysis of neodymium: electrolyte selection and deposition mechanism," Mineral Processing and Extractive Metallurgy, 119(2), pp. 88-92.

[21] Kaneko, A., Yamamoto, Y., and Okada, C., 1993, "Electrochemistry of rare earth fluoride molten salts," Journal of Alloys and Compounds, 193, pp. 44-46.

[22] Hu X., Wang Z., Gao B., Shi Z. , Liu F. , and Cao X., 2010, "Density and ionic structure of NdF3-LiF melts," Journal of Rare Earths, 28(4), pp. 587-590.

[23] Nourry, C., Massot, L., Chamelot, P., and Taxil, P., 2009, "Electrochemical reduction of Gd(III) and Nd(III) on reactive cathode material in molten fluoride media," Journal of Applied Electrochemistry, 39(6), pp. 927-933.

[24] Inoue, A., Zhang, T., and Takeuchi, A., 1996, "Bulk Nd-Fe-Al amorphous alloys with hard magnetic properties," Materials Transactions, 37(2), pp. 99-108.

[25] Okamoto, H., 2000, Desk handbook: phase diagrams for binary alloys, ASM international.

[26] Abbasalizadeh, A., Teng, L., Sridhar, S., and Seetharaman, S., 2014, "Neodymium extraction using salt extraction process," Mineral Processing and Extractive Metallurgy.

[27] Lichum, H., and Osteryoung, R. A., 1981, "Chemical and electrochemical studies in room temperature aluminium halide containing melts in Ionic Liquids," Plenum press, Edited by D. G. Lovering.

[28] Barbanel, Y., Kolin, V., Kotlin, V., and Lumpov, A., 1990, "Coordination chemistry of actinides in molten salts," J Radioanal Nucl Chem, 143(1), pp. 167-179.

[29] Castrillejo, Y., Bermejo, M. R., Barrado, E., Martinez, A. M., and Diaz Arocas, P., 2003, "Solubilization of rare earth oxides in the eutectic LiCl-KCl mixture at 450°C and in the equimolar CaCl2-NaCl melt at 550°C," Journal of Electroanalytical Chemistry, 545, pp. 141-157.

[30] Zhu, H., 2014, "Rare Earth Metal Production by Molten Salt Electrolysis," Encyclopedia of Applied Electrochemistry, G. Kreysa, K. Ota, and R. Savinell, eds., Springer New York, pp. 1765-1772.

[31] Serp, J., Allibert, M., Terrier, A. L., Malmbeck, R., Ougier, M., Rebizant, J., and Glatz, J.-P., 2005, "Electroseparation of Actinides from Lanthanides on Solid Aluminum Electrode in LiCl-KCl Eutectic Melts," Journal of The Electrochemical Society, 152(3), pp. C167-C172.

[32] De Córdoba, G., Laplace, A., Conocar, O., Lacquement, J., and Caravaca, C., 2008, "Determination of the activity coefficient of neodymium in liquid aluminium by potentiometric methods," Electrochimica Acta, 54(2), pp. 280-288.

[33] Masset, P., Konings, R. J. M., Malmbeck, R., Serp, J., and Glatz, J.-P., 2005, "Thermochemical properties of lanthanides (Ln=La, Nd) and actinides (An=U, Np, Pu, Am) in the molten LiCl–KCl eutectic," Journal of Nuclear Materials, 344(1–3), pp. 173-179.

[34] Castrillejo, Y., Bermejo, M. R., Barrado, A. I., Pardo, R., Barrado, E., and Martinez, A. M., 2005, "Electrochemical behaviour of dysprosium in the eutectic LiCl-KCl at W and Al electrodes," Electrochimica Acta, 50(10), pp. 2047-2057.

[35] Seetharaman, S., and Grinder, O., 2010, US patent application nr. 12/991128, ref. no.: 12057

Chapter 3 Fluorinating treatment of NdFeB magnets

Abstract

In the present work, selective extraction of rare earth (RE) metals from NdFeB magnets is investigated by studying the effects of various fluxes, *viz.* AlF_3, ZnF_2, FeF_3 and Na_3AlF_6 in the LiF-NdFeB system. The aim is to convert RE elements from NdFeB magnet into the fluoride salt melt. The results show the complete selective separation of neodymium (also dysprosium) from the magnet and the formation of rare earth fluoride, leaving iron and boron unreacted. The formed rare earth fluoride can subsequently be processed in the same reactor through an electrolysis route in which RE metal can be deposited as a cathode product. The results of X-Ray Diffraction (XRD) and Electron Probe MicroAnalysis (EPMA) analysis of the reacted samples indicate that AlF_3, ZnF_2 and FeF_3 can act as strong fluorinating agents for extraction of rare earth elements from NdFeB magnet, converting the RE to REF_3. The results confirm the feasibility of the rare earth metals recovery from scrap NdFeB magnet as raw material. The fluoride conversion-electrolysis route suggested in the present work enables the extraction of rare earth metals in a single step using the above-mentioned fluxes.

Keywords: rare earth, recycling, rare earth magnet, fluorination

---

Chapter 3 is based on the published scientific paper:

A. Abbasalizadeh, A. Malfliet, S. Seetharaman, J. Sietsma and Y. Yang, J. Mat. Trans, 2017, *58*(3)-400

3.1 Introduction

In view of the issues of supply and demand of the rare earth metals due to the uneven distribution of these metals, there is a strong demand for recycling waste products, for example, rare earth magnets. Due to the lack of technologically and economically feasible recycling methods, only less than 1% of the rare earth elements were recycled until 2011 [1]. An effective process for the recycling of rare earth containing scrap is a major concern since most developed countries import their required rare earth elements [2].

Hydrometallurgical and pyro-metallurgical process routes have been the subject of investigation by a number of researchers [3-7]. However, the drawbacks of hydrometallurgy processes are the low reaction rates and the serious environmental problems arising from the huge amounts of waste water generated in the process, which, in turn, need further processing. Alternatively, molten salt processing routes offer a more attractive flow sheet in view of the lower energy consumption, higher efficiency and higher purity of the deposits [8-10]. The molten salt process is currently used in the production of reactive metals such as aluminium, magnesium, sodium, potassium and also in general for the production or separation of lanthanides from actinides [11].

Based on the *Salt Extraction Process* [12, 13] and for recovery of metal in the molten salt systems [14], the feasibility of the neodymium extraction from NdFeB magnet in chloride salt electrodeposition method has been investigated [15]. A new approach involving molten fluoride bath has been proposed in chapter 2 of this thesis for solving the problem of low solubility and oxyfluoride formation of rare earth oxides (REOs) in molten fluorides. In this approach, AlF_3 was used as fluorinating agents in the LiF-Nd_2O_3 system. The rare earth oxide is converted into rare earth fluoride, which can subsequently be processed in the electrolysis route in which rare earth metal is electrochemically extracted as the deposition on the cathode. Complete conversion of REO in molten fluorides can circumvent the problem of the low solubility of REOs in the molten fluorides. The objective of the present work is to examine the applicability of this process concept for the extraction of neodymium and other rare earth elements from NdFeB magnets, using AlF_3, ZnF_2, FeF_3 and Na_3AlF_6 as addition to the LiF-NdFeB system. It is interesting to examine the possibility of selective extraction of the rare earth metal from Nd magnet by fluorination. The REF_3 which is formed as the result of the chemical reaction between the additives and the RE-containing components of the magnet, will be subjected to electrolysis to extract the RE metal as the cathodic product. To overcome fluorocarbon formation on the anode a reactive anode is employed instead of the conventionally used graphite anode. This reactive anode is anodically dissolved to re-generate the fluorinating agent *in situ* in the electrochemical reactor. This method provides a one-step process for direct recycling of rare earth metal from neodymium magnet scrap by molten fluoride salt extraction and electrolysis.

3.2 Thermodynamic evaluations

Thermodynamic calculations in chapter 2 confirm the feasibility of the conversion of neodymium oxide to neodymium fluoride using AlF_3 (ZnF_2 and FeF_3 in chapter 4) as fluorinating agents, and experimental results will be discussed in Chapter 4. These fluorides are used in the present work for the rare earth extraction from neodymium magnet (NdFeB). Due to the high price of AlF_3 compared to cryolite, the use of Na_3AlF_6 as a substitute for AlF_3 is also studied. Hence the LiF-NdFeB-Na_3AlF_6 system is also investigated as part of the present work.

Thermodynamic calculations on the pure components show that AlF_3, ZnF_2, FeF_3 and Na_3AlF_6 act as the fluorinating agents, leading to formation of REF_3 (RE=Nd, Dy), while Fe from the magnet remains unreacted in the molten fluorides. The standard Gibbs free energies ΔG^0 of the binary reactions of the four systems were calculated using FactSage (Tables 3.1 and 3.4).

Table 3.1 – Gibbs free energies of possible binary reactions for the formation of fluoride in the LiF-$Nd_2Fe_{14}B$-AlF_3 system at T = 950 °C.

Reaction	ΔG^o [kJ/mol]
$Nd + AlF_3 \rightleftarrows NdF_3 + Al$	-176
$Dy + AlF_3 \rightleftarrows DyF_3 + Al$	-199
$Fe + AlF_3 \rightleftarrows FeF_3 + Al$	411
$3Fe + 2AlF_3 \rightleftarrows 3FeF_2 + 2Al$	769
$B + AlF_3 \rightleftarrows BF_3 + Al$	130

Table 3.2 – Gibbs free energies of possible binary reactions for the formation of fluoride in the LiF-$Nd_2Fe_{14}B$-ZnF_2 system at T = 950 °C.

Reaction	ΔG^o [kJ/mol]
$2Nd + 3ZnF_2 \rightleftarrows 2NdF_3 + 3Zn$	-1076
$2Dy + 3ZnF_2 \rightleftarrows 2DyF_3 + 3Zn$	-1121
$2Fe + 3ZnF_2 \rightleftarrows 2FeF_3 + 3Zn$	99
$Fe + ZnF_2 \rightleftarrows FeF_2 + Zn$	15
$2B + 3ZnF_2 \rightleftarrows 2BF_3 + 3Zn$	-462

Table 3.3 – Gibbs free energies of possible binary reactions for the formation of fluoride in the LiF-$Nd_2Fe_{14}B$-FeF_3 system at T = 950 °C.

Reaction	ΔG^o [kJ/mol]
$Nd + FeF_3 \rightleftarrows NdF_3 + Fe$	-588
$Dy + FeF_3 \rightleftarrows DyF_3 + Fe$	-610
$B + FeF_3 \rightleftarrows BF_3 + Fe$	-281

Table 3.4 – Gibbs free energies of possible binary reactions for the formation of fluoride in the LiF-NdFeB-Na_3AlF_6 system at T = 950 °C.

Reaction	ΔG^o [kJ/mol]
$Nd + Na_3AlF_6 \rightleftarrows NdF_3 + 3NaF + Al$	-67
$Dy + Na_3AlF_6 \rightleftarrows DyF_3 + 3NaF + Al$	-89
$Fe + Na_3AlF_6 \rightleftarrows FeF_3 + 3NaF + Al$	521
$3Fe + 2Na_3AlF_6 \rightleftarrows 3FeF_2 + 6NaF + Al$	989
$B + Na_3AlF_6 \rightleftarrows BF_3 + 3NaF + Al$	240

According to the standard Gibbs free energies of the reactions in Tables 3.1 and 3.4, aluminium fluoride reacts only with the RE elements in the magnet. The formation of FeF_3 and BF_3 are not thermodynamically feasible in the standard state. However, ZnF_2 and FeF_3 do not only react with REEs but also with B in the magnet (Tables 3.2 and 3.3), showing the feasibility of BF_3 formation in both cases. Yet, the formation of FeF_3 in the LiF-$Nd_2Fe_{14}B$-ZnF_2 and LiF-$Nd_2Fe_{14}B$-Na_3AlF_6 systems at T = 950 °C is not favoured. In the case of the presence of Dy in the magnet, DyF_3 would be formed in all systems. It is important to note that these reactions refer to the case of the reacting species at their standard state as pure substances. In the real salt systems, the activity of the components would be lower than unity. Due to the absence of thermodynamic data for the fluoride systems, it is not possible to calculate the equilibrium potential of the fluorides in a similar way as it has been calculated for chlorides [16]. Therefore, the ideal Temkin model is used in order to calculate the activities of the different fluorides in the system, assuming that the magnet is dissolved in the salt, thereby forming fluorides which are completely ionized in the salt melt. Hence, the system is a mixture of cations and fluorine ions. Based on this model, the activity a_j of a compound j, such as NdF_3, is calculated as:

$$a_{NdF_3} = (X_{Nd^{3+}})\,(X_{F^-})^3, \tag{3.1}$$

in which the *X*-parameter refers to the ionic fraction of cations and anions, according to

$$X_{Nd^{3+}} = n_{Nd^{3+}} / \sum n_{+} \quad \text{and} \quad X_{F^{-}} = n_{F^{-}} / \sum n_{-} \tag{3.2}$$

n_i is the number of moles of *i*-ions. Using these activities, the relative partial molar Gibbs free energies (chemical potentials) ΔG of the fluorides species in the LiF-NdFeB-AlF_3, LiF-NdFeB-ZnF_2, LiF-NdFeB-FeF_3 and LiF-NdFeB-Na_3AlF_6 systems are calculated using the expression:

$$\Delta \overline{G}_{NdF_3} = RT \ln a_{NdF_3} \tag{3.3}$$

where *R* is the universal gas constant (8.314 J.mol^{-1}.K^{-1}), *T* is the temperature in K and *a* is the activity.

The activities and relative partial molar Gibbs free energies of the fluorides are listed in Table 3.5. The relative partial molar Gibbs free energies of NdF_3 in all systems are lower than the corresponding values for FeF_3. Using a reactive iron anode in which FeF_3 is constantly generated in the system will generate sufficient FeF_3 that are instantly consumed in the fluorination of the magnet scrap. This should enable NdF_3 formation. The same approach can be used in the case of using molten aluminium or zinc as reactive anodes, in which ZnF_2 and AlF_3 are constantly being generated and consumed in the system.

The REF_3 formed in the system will dissolve in the LiF melt which will further participate in the electrolysis process. Based on the calculated Gibbs free energies for the formation of the pure substances (Tables 3.1 and 3.4), the decomposition voltage of NdF_3 at 950 ^{o}C for pure substances is about 4.7 V, not considering the over-potential which needs to be determined experimentally. This enables the extraction of Nd from the fluoride bath. In case of BF_3 formation, B can be co-deposited on the cathode with the RE elements, since it has a lower decomposition voltage than NdF_3. As the boron concentration in the magnet is however quite low (1 wt%), the B co-deposition on the cathode will be negligible. Using cryolite as the extracting agent, NaF will form in the molten salt, which has a lower decomposition voltage than NdF_3 (decomposition voltage of NaF at 950 ^{o}C considering calculation with pure substances is ~ 3.6 V). The cathodic reactions will be:

$$RE^{3+} + 3e^{-} \rightarrow RE \tag{3.4}$$

$$Na^{+} + e^{-} \rightarrow Na \tag{3.5}$$

Table 3.5 – Relative partial molar Gibbs energies and activities of the fluoride species in the systems with different fluorinating agents, assuming ideal Temkin behaviour of the systems at T = 950 °C.

System	LiF-NdFeB-AlF_3		LiF-NdFeB-ZnF_2		LiF-NdFeB-FeF_3		LiF-NdFeB-Na_3AlF_6	
	a	$\Delta\overline{G}$[kJ/mol]	a	$\Delta\overline{G}$[kJ/mol]	a	$\Delta\overline{G}$[kJ/mo]	a	$\Delta\overline{G}$[kJ/mol]
LiF	0.26	-13.6	0.237	-14.6	0.260	-13.6	0.211	-15.8
NdF_3	0.077	-25.9	0.071	-26.9	0.077	-25.9	0.063	-28
FeF_3	0.544	-6.1	0.496	-7.1	0.622	-4.8	0.441	-8.3
BF_3	0.039	-33	0.035	-33.9	0.039	-33	0.031	-35.1
ZnF_2			0.160	-18.6				
AlF_3	0.077	-25.9						
Na_3AlF_6							0.0004	-78.8

Reaction (3.5) will occur only in the case of using cryolite. The general anodic reaction using a reactive anode (M) is:

$$M\ (anode) + xF^-\ (salt) \rightarrow MF_x\ (salt) + xe^- \quad (3.6)$$

The formed metal fluoride (MF_x) would be ideally the fluorinating agent for the NdFeB magnet scrap. A schematic diagram of the salt extraction process, including the fluorinating step and the electrochemical extraction step is shown in Figure 3.1.

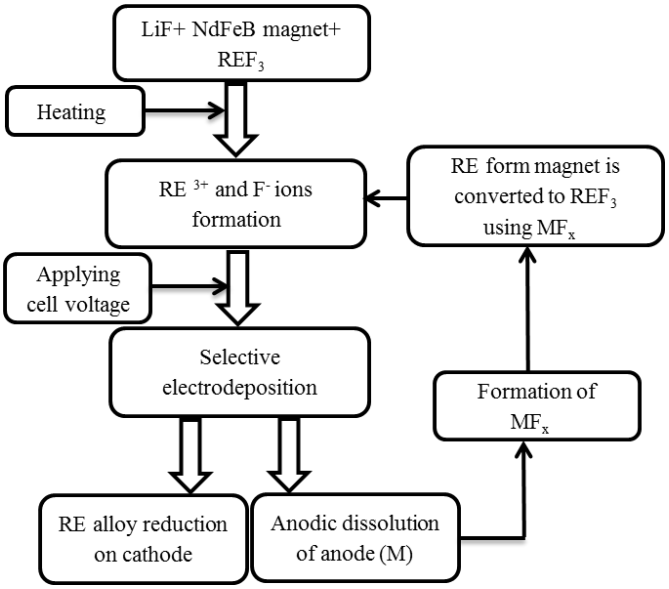

Figure 3.1 – Schematic diagram of the salt extraction process

3.3 Experiments

In this chapter the feasibility of fluorinating NdFeB magnet with aluminium fluoride, zinc fluoride, iron fluoride and cryolite is investigated. Lithium fluoride (98.5%-Alfa Aesar) is mixed in a glove box with NdFeB magnets (supplied by Magneti Ljubljana), which are ground into fine powder. The magnet composition as provided by Magneti Ljubljana is shown in Table 3.6.

Table 3.6 – Composition of the neodymium magnet supplied by Magneti Ljubljana analyzed with XRF.

Element	Nd	Dy	Al	Fe	B	Co	Pr	Cu	Ga	Total
(wt. %)	28.9	2.72	0.14	63.4	-	2.91	0.67	0.19	0.07	99.0

Either aluminium fluoride (99+%-Alfa Aesar), zinc fluoride (99%-Alfa Aesar), iron fluoride (97%-Alfa Aesar) or cryolite (99%-Alfa Aesar) powder is added to the lithium fluoride and magnet mixture. This mixture is then charged into a graphite crucible. The fluorinating agents are added in the stoichiometric amount that is needed for fluorinating the rare earth element in the magnet. The mixtures are heated up to 950 ^{o}C for 3 hours under argon atmosphere. The Ar gas is purified by passing through KOH flakes for CO_2 removal and also through silica gel and P_2O_5 to remove moisture. The gas is further purified by passing through a tube furnace containing Ti sponge which is heated to 950 ^{o}C in order to remove the traces of O_2. After 3 hours treatment, the samples are quenched in liquid nitrogen.

The samples are analysed by X-Ray Diffractometry (XRD) as well as by Electron Probe Micro Analysis (EPMA) in order to determine the phases that are formed during the experiments and their compositions. For the EPMA analyses, Wavelength Dispersive Spectrometry (WDS) point analyses and mappings are performed at either 15 kV-15 nA or 5 kV-15 nA. For the quantification, standards are used.

3.4 Results

3.4.1 AlF_3 in LiF-NdFeB system

From the XRD pattern of the LiF-NdFeB-AlF_3 sample after fluorination treatment (Figure 3.2), the peaks of NdF_3 phase are identified along with LiF, α-Fe and the Fe_3Al intermetallic phase. Because of the low concentration of B in the magnet, B-containing phases are not detected by the XRD analysis.

Figure 3.3 shows the EPMA mapping of the LiF-NdFeB-AlF_3 sample after fluorination treatment. Nd and Fe are distributed separately in the sample. This indicates that Nd is selectively extracted from the Nd magnet, whereas Fe remains in the magnet matrix. F is detected in the Nd-containing regions and Al is distributed in the Fe-containing regions. B could not be detected in the EPMA mapping due to its low atomic number and low concentration in the NdFeB magnet.

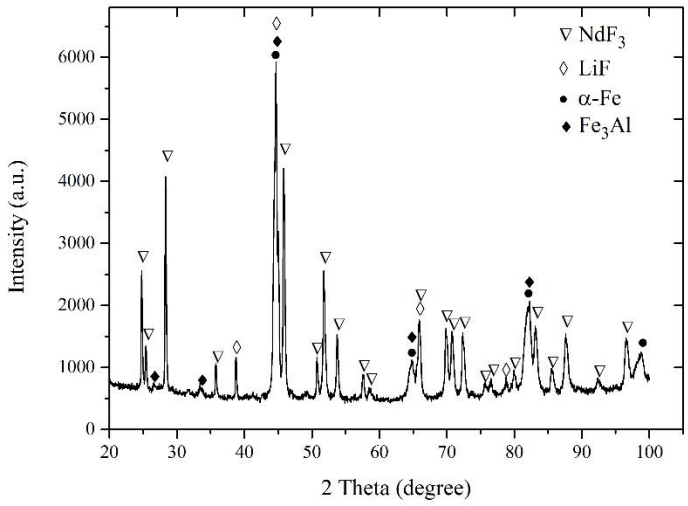

Figure 3.2– XRD pattern with phase identification of the LiF-$Nd_2Fe_{14}B$-AlF_3 sample after fluorination treatment.

The sample is also analyzed using EPMA point analysis. A BackScatter Electron (BSE) image and the measured composition of the RE-fluoride, the FeAl and the FeAlB phase are shown in Figure 3.4. The results clearly show the formation of an FeAl intermetallic phase (89 at% iron and 9 at% aluminum). Boron is quantified in the FeAlB phase with

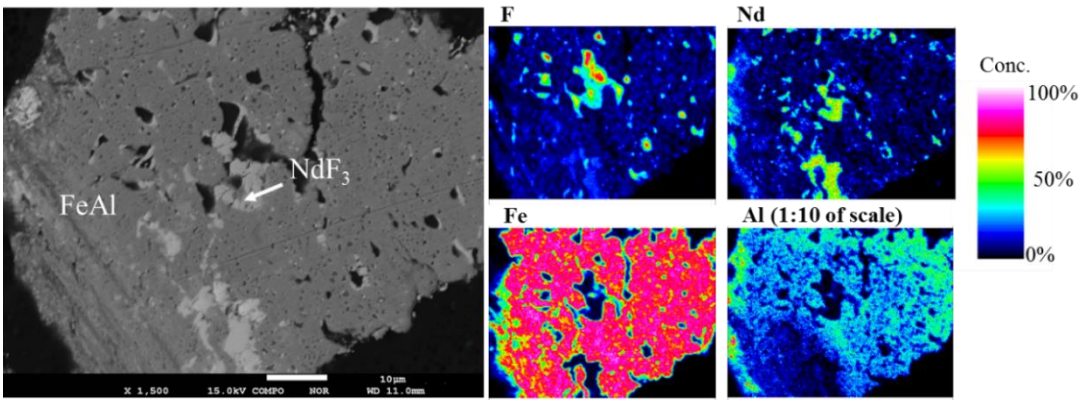

Figure 3.3– EPMA mapping of the LiF-NdFeB-AlF_3 sample after fluorination treatment showing F, Nd, Fe and Al distribution

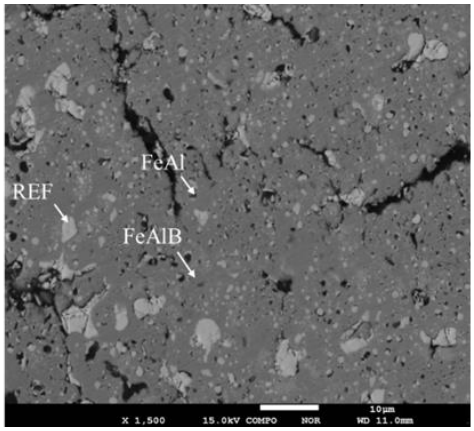

Element	REF	FeAl	FeAlB
F	72	-	-
Al	-	9	15
Nd	25	-	-
Dy	2.5	-	-
Fe	-	89	80
B	-	-	1.1

Figure 3.4– BSE image and composition of the phases (in at%) of the LiF-NdFeB-AlF_3 sample after fluorination treatment showing the presence of REF, FeAl and FeAlB phases.

concentrations of 80 at% iron, 15 at% aluminum and 1.1 at% boron. The quantification data show a fluorine concentration of 72 at% and Nd concentration of 25 at% in the REF phase. The presence of 2.5 at% dysprosium along with 25 at% neodymium is detected in the rare earth fluoride phase.

3.4.2 ZnF_2 in LiF-NdFeB system

The XRD result of the experiment of the LiF-NdFeB-ZnF_2 system after fluorination shows the formation of NdF_3 in the sample (Figure 3.5). LiF, Fe-Zn, Li_2ZnF_4 and Fe_2B are the other identified phases. Nd is thus selectively extracted by ZnF_2 as extracting agent and Fe remains unreacted. B also stays unreacted in the Fe_2B phase. Part of the Zn has formed Fe_9Zn with Fe and the rest is dissolved in the salt by forming Li_2ZnF_4.

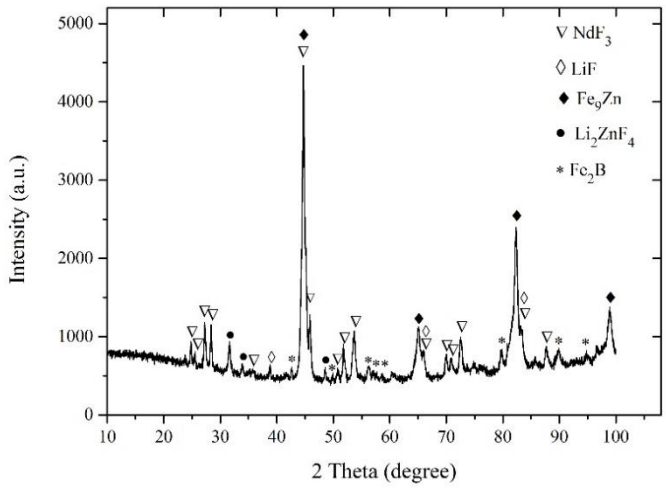

Figure 3.5 – XRD pattern with phase identification of the LiF-NdFeB-ZnF_2 sample after fluorination treatment.

The EPMA mapping of the LiF-NdFeB-ZnF_2 sample after fluorination treatment is shown in Figure 3.6. The formation of NdF_3 is confirmed by Figure 3.6(a). The areas with higher concentration of fluoride correspond to the LiF phase. Fe and Zn are distributed in the same areas and are separated from Nd and F. In order to detect B, an EPMA mapping is performed at 5 kV (Figure 3.6(b)). B is present in the areas with the highest Fe concentration. In agreement with the XRD results, this can be the Fe_2B phase. In the areas where both Fe and Zn are present, B is present in a lower concentration. This is the FeZnB phase. The areas where both Nd and F are detected correspond to the NdF_3 phase.

In Figure 3.7, the BSE image of the LiF-NdFeB-ZnF_2 sample after fluorination is shown. The light areas in this image are REF_3 phase (RE being 23 at% neodymium and 2 at% dysprosium) with 74 at% fluorine and the dark matrix is FeZnB intermetallic phase consisting of 91 at% iron, 8 at% zinc and 1 at% boron.

In Figure 3.7, the EPMA quantification results show that the dark grey grains correspond to iron boron phase with high concentration of boron (25 at% boron and 73 at% iron).

For more detailed detection of the element distribution and especially for a better detection of B, a WDS mapping is also performed at 5 kV (Figure 3.6 (b)). This mapping agrees with Figure 3.6(a), *viz.* the white phase is the NdF_3 phase dispersed in the grey matrix of Fe-Zn-B phase and the darker grains on the sample are Fe borides. A BSE image of the same area in the LiF-NdFeB-ZnF_2 sample after fluorination is shown in Figure 3.7 together with the measured phase compositions.

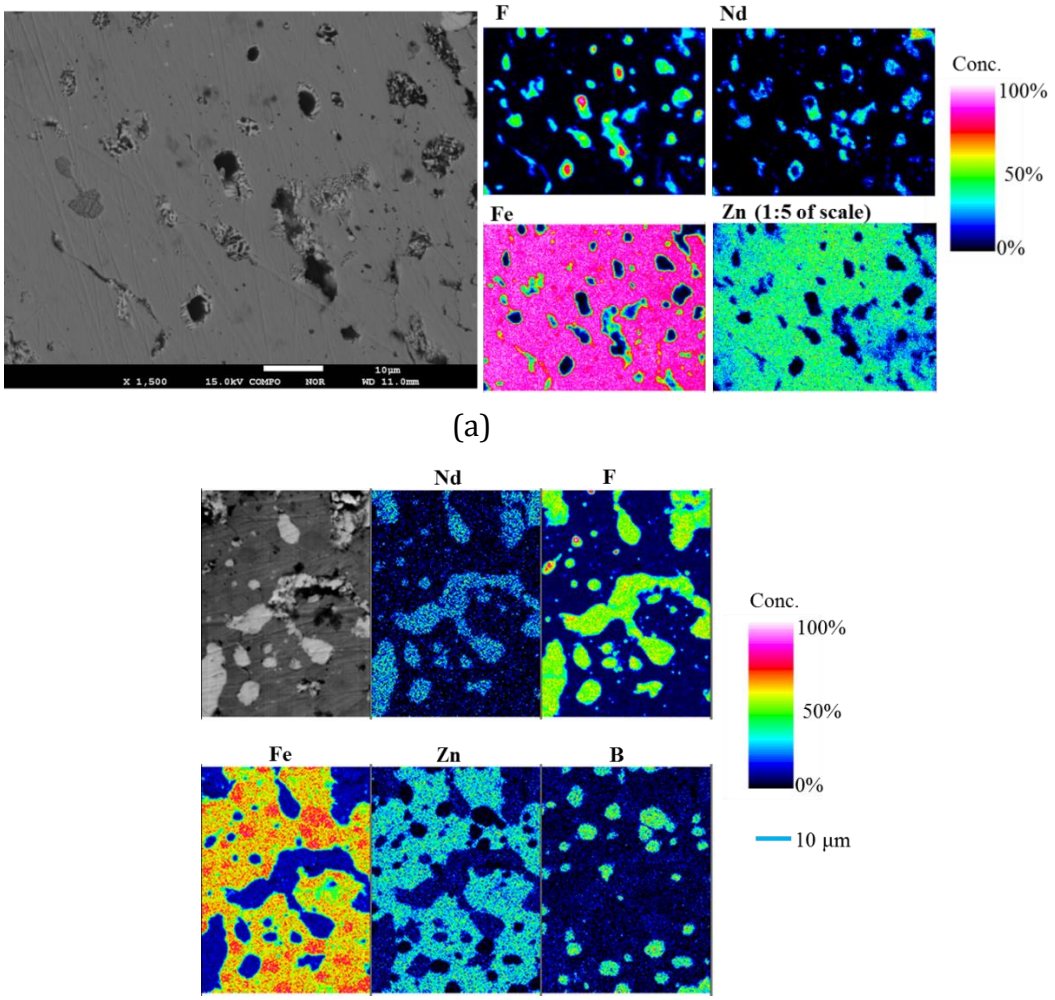

Figure 3.6– EPMA mapping of the LiF-NdFeB-ZnF_2 sample after fluorination treatment (a) at 15 kV and (b) at 5 kV.

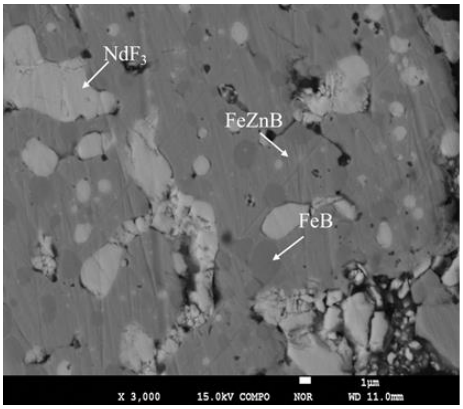

Element	$NdFe_3$	FeB	FeZnB
F	74	-	-
O	-	-	-
Nd	23	-	-
Zn	-	-	8
Fe	-	73	91
Dy	2	-	-
B	-	25	1

Figure 3.7– BSE image of the LiF-NdFeB-ZnF_2 sample in at% after fluorination treatment showing the presence of NdF_3, FeB and FeZnB.

3.4.3 FeF_3 in LiF-NdFeB system

The XRD result of the LiF-NdFeB-FeF_3 sample after fluorination treatment is shown in Figure 3.8. NdF_3 has formed from the reaction between FeF_3 and the Nd in the magnet. LiF and α-Fe are the two other identified phases. For the same reasons mentioned earlier, B-containing phases are not detected with the XRD analysis.

The elemental mappings of F, Nd, B, Fe and Co elements are shown in Figure 3.9. Nd is extracted from the Nd magnet and forms NdF_3 (the white appearing phase). Fe and Co are distributed in the same areas indicating that no FeF_3 or CoF_3 has formed during fluorination treatment. The slightly darker grains in the FeCoB matrix consist of Fe and B, indicating the presence of Fe borides. The concentration of Co in these grains is lower than in the FeCoB matrix. The EPMA mapping images show the presence of NdF_3, FeCo and FeB phases.

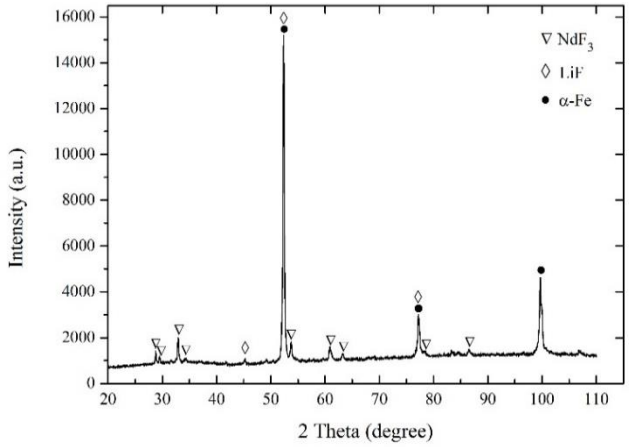

Figure 3.8– XRD pattern with phase identification of the LiF-NdFeB-FeF_3 sample after fluorination treatment.

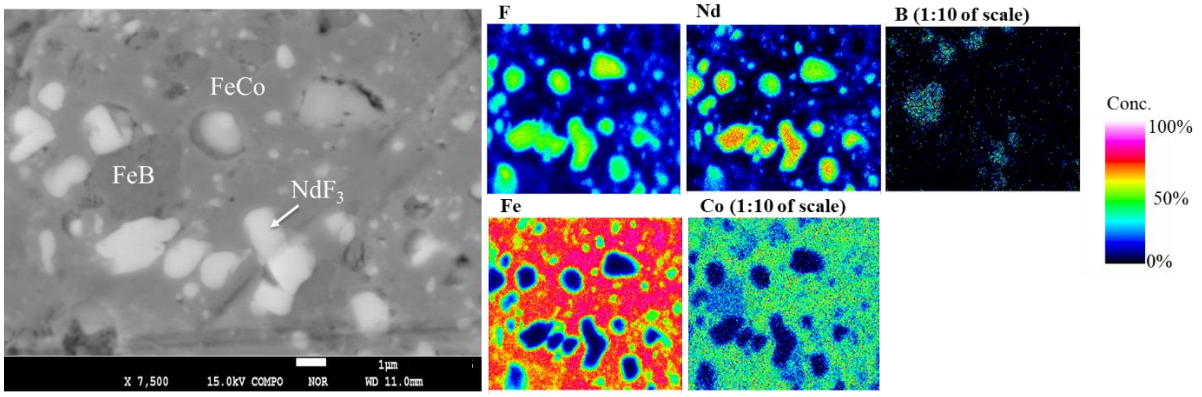

Figure 3.9– EPMA mapping of the LiF-NdFeB-FeF_3 sample after fluorination treatment.

3.4.4 Na_3AlF_6 in LiF-NdFeB system

The XRD result of the LiF-NdFeB-Na_3AlF_6 sample after fluorination treatment is shown in Figure 3.10. The formation of $Na_{1.5}Nd_{1.5}F_6$ shows that Nd in the magnet has substituted Al in the cryolite, hence Nd is extracted from the magnet. The small peaks related to cryolite show that a low concentration of this phase remained in the sample. The XRD pattern also shows peaks related to α-Fe and LiF.

The EPMA elemental mappings of the LiF-NdFeB-Na_3AlF_6 sample after fluorination are shown in Figure 3.11. Different phases in the sample are identified and are marked in Figure 3.12. Fe and Co are present in the same areas. Al is distributed in the same areas as Nd and F, but its concentration is low compared to Nd. The light appearing grey grains contain Fe and Co and are clearly separated from the dark appearing phase consisting of Nd, Dy, F and Al. The very bright appearing phases in the middle of the Fe-rich grains are the phases in which the concentrations of Nd and F are very high and Al is not present. This can be related to the $Na_{1.5}Nd_{1.5}F_6$ phase. According to the XRD results, both $Na_{1.5}Nd_{1.5}F_6$ and Na_3AlF_6 phases are present in the sample. The small black spots on the sample have high concentration of F; in these Nd and Al are absent. This can be LiF phase. Cobalt, being a minor additive to the NdFeB magnet, is difficult to detect by EPMA. This can be a reason that it could be detected in the EPMA mapping of the samples after fluorination with FeF_3 and Na_3AlF_6 and not in the samples of ZnF_2 and AlF_3.

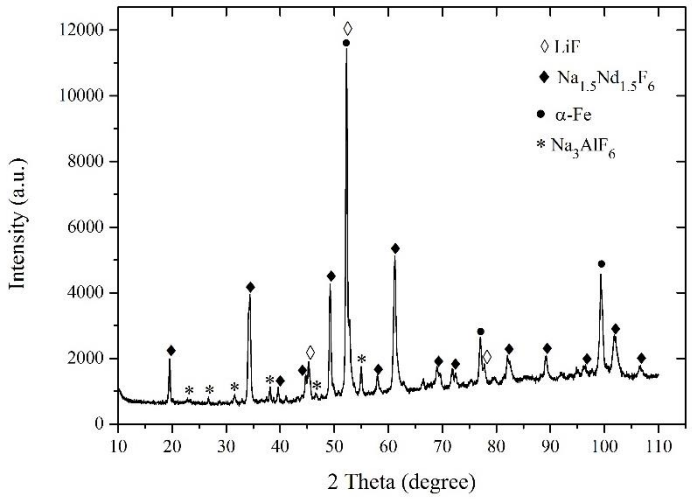

Figure 3.10– XRD pattern with phase identification of the LiF-NdFeB-Na_3AlF_6 sample after fluorination treatment.

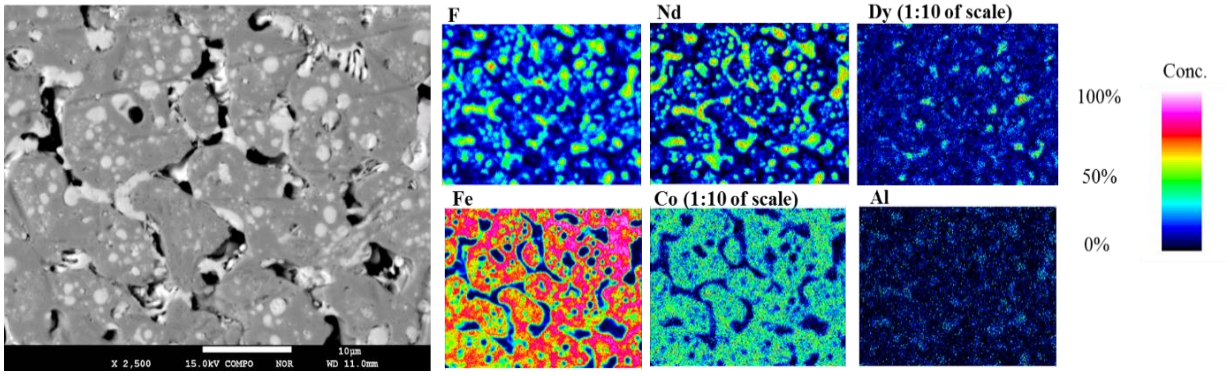

Figure 3.11– EPMA mapping analysis of LiF-NdFeB-Na_3AlF_6 sample after fluorination treatment. Note that the colour scale for Co and Dy is rescaled by a factor 10.

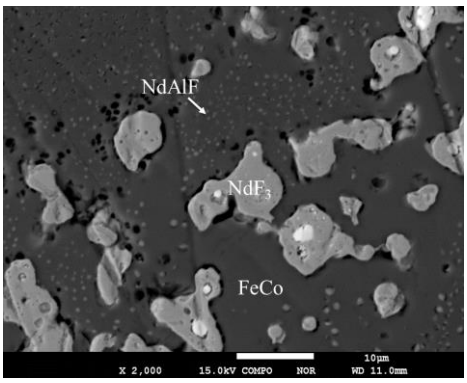

Figure 3.12– BSE image of the LiF-NdFeB-Na_3AlF_6 sample after fluorination treatment.

3.5 Discussion

In all experiments, Nd and Dy (in the case of the fluorinated samples after treatment with cryolite) are completely extracted from the NdFeB magnet and have formed rare earth fluoride. No (intermetallic) phases consisting of both rare earth elements and Fe are found by XRD and EPMA. This shows the complete extraction of the rare earth elements from the magnet. Extracted Nd is completely converted to NdF_3 after reaction with AlF_3, ZnF_2 and FeF_3. In the case of using cryolite as the fluorinating agent, $Na_{1.5}Nd_{1.5}F_6$ is formed instead of NdF_3. Dissolution of $Na_{1.5}Nd_{1.5}F_6$ in molten LiF during the electrochemical extraction process will lead to reduction of both Nd and Na on the cathode, due to the lower stability of NaF compared to NdF_3:

$$NaF \rightleftarrows Na + 1/2\ F_2 \qquad \Delta G^o(T=1223\ K)=571\ kJ/mol \qquad (3.7)$$

$$NdF_3 \rightleftarrows Nd + 3/2\ F_2 \qquad \Delta G^o(T=1223\ K)=1665\ kJ/mol \qquad (3.8)$$

The decomposition voltages of NaF and NdF_3, which are calculated from the standard Gibbs free energy of these reactions at their standard states, are –4.6 and –4.7 V for NaF

and NdF_3, respectively. Na will therefore deposit on the cathode at lower voltages compared to Nd and co-deposition of Nd and Na will occur.

Both the XRD and EPMA results of the experiments with AlF_3 show that Al replaces Nd in the magnet, forming FeAl and FeAlB phases and no Al in the form of fluoride is present in the system. The same results can be seen using FeF_3 as fluorinating agent. All FeF_3 reacts with Nd in the magnet and Fe replaces the rare earths in the magnet matrix, thereby forming FeCo and Fe boride phases.

In the experiment with ZnF_2, XRD and EPMA results show that different Zn compounds are formed. The XRD result indicates the presence of the Li_2ZnF_4 phase. It is expected that Zn from Li_2ZnF_4 phase will co-deposit together with Nd during the electrochemical extraction process of Nd from NdF_3, hence forming NdZn alloy. Besides formation of Li_2ZnF_4 phase, EPMA analysis indicates that Zn replaces Nd in the matrix, thereby forming FeZnB phase.

The results from the experiments with Na_3AlF_6 show that not all cryolite reacts with Nd, hence dissolution of the excess cryolite in LiF during the electrolysis process will lead to co-deposition of not only Na with Nd, but also Al.

Assuming that FeAl, FeB, FeZn and FeCo compounds (with varying stoichiometry) do not dissolve in the molten salt, it is expected that only rare earth deposition will occur during the electrolysis process. However, as was discussed earlier, in the case of cryolite treatment, co-deposition of Na and Al along with the rare earth elements can be expected.

Based on the thermodynamic calculations, the formation of boron fluoride is feasible using FeF_3 as the fluorinating agent. However, the experimental results analysed by EPMA mappings show that B and Fe are distributed in the same area, indicating the presence of Fe borides. The reason that boron does not react with iron fluoride can be the fact that stoichiometric amount of FeF_3 was used in the experiment and since REF_3 has higher stability than BF_3, REF_3 is formed and no excess iron fluoride is present for reaction with boron. Another reason might be related to the kinetics of the reactions.

3.6 Conclusion

This study shows that AlF_3, ZnF_2, FeF_3 and Na_3AlF_6 can act as strong fluorinating agents for extraction of Nd and Dy in the NdFeB magnet. In all treatments, Nd is separated from the Fe and B in the magnet and is converted to rare earth fluoride. Al, Zn and Fe from AlF_3 (Na_3AlF_6), ZnF_2 and FeF_3, respectively, replace the rare earth element in the magnet matrix, thereby forming intermetallic compounds with Fe which all remain as solid and are separated from the formed NdF_3 and DyF_3. In the case of cryolite, co-deposition of Al and Na along with the rare earth elements, makes cryolite as fluorinating agent unsuitable for the recovery of rare earth elements from NdFeB magnet. Based on the results, FeF_3 and ZnF_2 among all studied fluorinating agents, have the highest potential to be used as fluorinating agents for Nd in the magnet.

Once NdF_3 is formed, Nd can subsequently be reduced on the cathode by an electrolysis process in the same batch. Hence, conversion of the rare earth elements in the magnet to rare earth fluorides provides the possibility of a one-step recycling process of the rare earth elements from magnets.

3.7 References

[1] Binnemans, K., Jones, P. T., Blanpain, B., Van Gerven, T., Yang, Y., Walton, A., and Buchert, M., 2013, "Recycling of rare earths: a critical review," Journal of Cleaner Production, 51(0), pp. 1-22.

[2] Takeda, O., Okabe, T. H., and Umetsu, Y., 2006, "Recovery of neodymium from a mixture of magnet scrap and other scrap," Journal of Alloys and Compounds, 408–412(0), pp. 387-390.

[3] Bian, Y., Guo, S., Jiang, L., Liu, J., Tang, K., and Ding, W., 2016, "Recovery of Rare Earth Elements from NdFeB Magnet by VIM-HMS Method," ACS Sustainable Chemistry & Engineering, 4(3), pp. 810-818.

[4] Nohira, T., Kobayashi, S., Kobayashi, K., Hagiwara, R., Oishi, T., and Konishi, H., 2010, "Electrochemical Formation of Nd-Ni Alloys in Molten LiF-CaF_2-NdF_3," ECS Transactions, 33(7), pp. 205-212.

[5] Martinez, A. M., Kjos, O., Skybakmoen, E., Solheim, A. r., and Haarberg, G. M., 2013, "Extraction of Rare Earth Metals from Nd-based Scrap by Electrolysis from Molten Salts," ECS Transactions, 50(11), pp. 453-461.

[6] Riaño, S., and Binnemans, K., 2015, "Extraction and separation of neodymium and dysprosium from used NdFeB magnets: an application of ionic liquids in solvent extraction towards the recycling of magnets," Green Chemistry, 17(5), pp. 2931-2942.

[7] Bandara, H. D., Field, K. D., and Emmert, M. H., 2016, "Rare earth recovery from end-of-life motors employing green chemistry design principles," Green Chemistry, 18, pp. 753-759.

[8] Mishra, B., and Olson, D. L., 2005, "Molten salt applications in materials processing," Journal of Physics and Chemistry of Solids, 66(2–4), pp. 396-401.

[9] Han, W., Chen, Q., Sun, Y., Jiang, T., and Zhang, M., 2011, "Electrodeposition of Mg-Li-Al-La Alloys on Inert Cathode in Molten LiCl-KCl Eutectic Salt," Metallurgical and Materials Transactions B, 42(6), pp. 1367-1375.

[10] Castrillejo, Y., Bermejo, M. R., Díaz Arocas, P., Martínez, A. M., and Barrado, E., 2005, "Electrochemical behaviour of praseodymium (III) in molten chlorides," Journal of Electroanalytical Chemistry, 575(1), pp. 61-74.

[11] Taxil, P., Massot, L., Nourry, C., Gibilaro, M., Chamelot, P., and Cassayre, L., 2009, "Lanthanides extraction processes in molten fluoride media: Application to nuclear spent fuel reprocessing," Journal of Fluorine Chemistry, 130(1), pp. 94-101.

[12] Seetharaman, S., and Grinder, O., 2010, US patent application nr. 12/991128, ref. no.: 12057

[13] Abbasalizadeh, A., Seetharaman, S., Teng, L., Sridhar, S., Grinder, O., Izumi, Y., and Barati, M., 2013, "Highlights of the Salt Extraction Process," Journal Of Materials, 65(11), pp. 1552-1558.

[14] Okabe, T. H., and Shirayama, S., 2012, "Method and apparatus for recovery of rare earth element," Method and apparatus for recovery of rare earth element, US8323592 B2.

[15] Abbasalizadeh, A., Teng, L., Sridhar, S., and Seetharaman, S., 2015, "Neodymium extraction using salt extraction process," Mineral Processing and Extractive Metallurgy, 124(4), pp. 191-198.

[16] Uda, T., 2002, "Recovery of Rare Earths from Magnet Sludge by $FeCl_2$," Materials Transactions, 43(1), pp. 55-62.

Chapter 4 Fluorinating treatment of rare earth oxides

Abstract

In the present research on rare earth metal extraction from rare earth oxides (REOs), conversion of rare earth oxides into rare earth fluorides with fluoride fluxes is investigated in order to overcome the problem of low solubility of the rare earth oxides in the molten fluoride salts as well as the formation of oxyfluorides in the fluorination process. Based on thermodynamic calculations a series of experiments are performed for converting the rare earth oxides into rare earth fluorides using AlF_3, ZnF_2, FeF_3 and Na_3AlF_6 as fluorinating agents in a LiF-Nd_2O_3 system. The formation of neodymium fluoride as the result of the reactions between these fluxes and neodymium oxide is confirmed with nearly complete conversion. The rare earth fluoride thus formed can subsequently be processed through the electrolysis route in the same reactor and rare earth metal can be produced as the cathodic deposit as rare earth metal or rare earth alloys depending on the nature of the anode materials and the used fluorinating agents. In this concept, the REO dissolution in the molten fluorides would become unnecessary due to the complete conversion of the oxide into the fluoride, REF_3. The results of X-Ray Diffraction (XRD) and Electron Probe MicroAnalysis (EPMA) analysis of the reacted samples indicate that AlF_3, ZnF_2 and FeF_3 can act as strong fluorinating agents for the neodymium oxide giving rise to a complete conversion of neodymium oxide into neodymium fluoride.

Keywords: rare earth oxides, rare earth fluorides, recycling, fluorination

---

Chapter 4 is based on the published scientific paper:

A. Abbasalizadeh, A. Malfliet, S. Seetharaman, J. Sietsma and Y. Yang, J. Sus. Met, 2017, *3*(3)-627

4.1 Introduction

Rare earth oxides are among the most stable oxides of the elements in the periodic table. Oxygen removal from rare earth metals is therefore very difficult due to the strong affinity of these metals to oxygen.

Chen et al. [1] have developed a direct electrochemical process; FFC process for the reduction of solid metal oxides into their metals in molten salts. This method has been extensively studied in metal extraction for a number of elements including rare earth metals (RE = Gd, Tb, Dy, Er and Ce) [2-4]. The direct electrochemical reduction of oxide into metal is influenced by a number of parameters such as duration of electrolysis, temperature, applied voltage, open porosity of the oxide pellet and mode of electrolysis [5]. The efficiency of the oxygen removal by direct electrochemical reduction of oxides is mainly determined by the geometry of the samples, the surface area of the solid sample in contact with the molten salt and the initial oxygen concentrations. The FFC process has not yet been commercialized and one of the main challenges is the residual oxygen concentration in the reduced metal.

Electrowinning (molten salt electrolysis) is the dominating industrial method for rare earth metal extraction from their oxides in the salt extraction process [6-8]. It is generally considered that in an electrowinning process, it is the dissolved oxide in the electrolyte that is subjected to electrolysis [9]. Hence in fluoride systems, the solubility of the oxide in fluoride electrolytes is an important parameter. Except for cryolite, which has a high solubility for alumina (about 10 wt%), generally molten fluorides have a low oxide solubility; the solubility of neodymium oxide in molten alkali fluorides was reported to be 2-4 weight percent [10, 11]. The concentration of dissolved oxide cannot be increased by adding excess oxide into the melt at a constant temperature and fixed salt composition. Nevertheless, exposure of an excess quantity of oxide into the melt can increase the kinetics of the reactions. Besides the low solubility of rare earth oxides in molten fluorides, another problem for RE metals extraction that needs to be addressed is that these oxides can form rare earth oxyfluorides in the LiF-NdF_3 molten salt. It has been reported that neodymium oxyfluorides cannot be reduced to neodymium metal [12]. It has been confirmed that neodymium oxyfluoride participates in the anodic reaction to generate oxygen [13]. However, the role of neodymium oxyfluoride in the anodic and cathodic reactions is not very clear and needs to be clarified further in detail [12-16]. This issue has also been discussed in chapter 2 of this thesis.

Similar to the fluorinating treatment of NdFeB magnet scrap (chapter 3), in the present work, a new approach is proposed for solving the problem of low oxide solubility and oxyfluoride formation of rare earth oxides (REOs) in molten fluorides. Addition of fluorinating agents such as AlF_3, ZnF_2 and FeF_3 to the LiF-Nd_2O_3 system changes the thermodynamic equilibrium and thus allows for converting rare earth oxides into rare earth fluorides. Use of cryolite (Na_3AlF_6) as fluorinating agent is also investigated as a substitute for AlF_3, due to its availability and cost advantages. By treatment with fluorinating agents, the REO is converted into rare earth fluoride. The rare earth fluoride thus formed can subsequently be processed through the electrolysis route in the same reactor to extract rare earth metal or more likely the rare earth based alloy as

the cathodic deposit. In this concept, the REO dissolution in the molten fluorides would become redundant due to the complete conversion of the oxide into the fluoride, REF_3.

4.2 Thermodynamic evaluation of the process

The Standard Gibbs free energies (ΔG^o) of formation of the reacted fluorides and oxides at 950°C, calculated using FactSage, are given in Table 4.1. The values indicate a decreasing stability of the fluorides in the order CaF_2, LiF, NaF and KF. The decomposition voltages of rare earth fluorides and the alkali fluorides are also compared in Table 4.1. It can be seen that only CaF_2 and LiF are more stable than NdF_3 and DyF_3. Thus, after fluorination of rare earth oxide into rare earth fluorides using the fluorinating agent, the most suitable solvents among fluorides for electrochemical decomposition of the formed rare earth fluorides are CaF_2 and LiF.

Table 4.1 Standard Gibbs free energies and the decomposition voltages of different fluorides salts and REOs and REF_3 (RE=Nd, Dy).

Reaction	ΔG^o(kJ/mol)	Decomposition potential (V)	ΔG^o(kJ/mol)
	at 950 °C		at 25 °C
$CaF_2 \rightleftarrows Ca + F_2$	1020	–5.3	1173
$LiF \rightleftarrows Li + ½F_2$	497	–5.2	584
$NaF \rightleftarrows Na + ½F_2$	442	–4.6	544
$KF \rightleftarrows K + ½F_2$	433	–4.5	538
$NdF_3(s) \rightleftarrows Nd(s) + {}^3/_2F_2(g)$	1370	–4.7	1590
$DyF_3(s) \rightleftarrows Dy(s) + {}^3/_2F_2(g)$	1392	–4.8	1614
$Nd_2O_3(s) \rightleftarrows 2Nd(s) + {}^3/_2O_2(g)$	1464	–2.5	1718
$Dy_2O_3(s) \rightleftarrows 2Dy(s) + {}^3/_2O_2(g)$	1508	–2.6	1771

In the present work, AlF_3, ZnF_2, FeF_3 and Na_3AlF_6 are investigated as candidates for the fluorination of rare earth oxides prior to electrolysis in molten fluoride bath. From the calculated standard Gibbs free energies of the following reactions at 950 °C:

$$Nd_2O_3 + 2AlF_3(salt) \rightarrow 2NdF_3 + Al_2O_3 \qquad \Delta G^o = -177 \text{ kJ/mol} \quad (4.1)$$

$$Nd_2O_3 + 3ZnF_2(salt) \rightarrow 2NdF_3 + 3ZnO \qquad \Delta G^o = -274 \text{ kJ/mol} \quad (4.2)$$

$$Nd_2O_3 + 2FeF_3(salt) \rightarrow 2NdF_3 + Fe_2O_3 \qquad \Delta G^o = -222 \text{ kJ/mol} \quad (4.3)$$

$$Nd_2O_3 + Na_3AlF_6(salt) \rightarrow NdF_3 + Al_2O_3 + 3NaF \qquad \Delta G^o = -23.4 \text{ kJ/mol} \quad (4.4)$$

it is evident that these metal fluorides can react with rare earth oxides to form rare earth fluorides, and the formed NdF_3 can further be reduced at the cathode. The metal oxides Al_2O_3, ZnO and Fe_2O_3 are formed in the system during formation of NdF_3. It should be noted that in argon atmosphere and low oxygen pressure, in reaction (4.3) it is expected that instead of Fe_2O_3, FeO could be formed, which means that Fe_2O_3 will convert to FeO and O_2 under experimental conditions.

NdF_3 formed as the result of the reaction between Nd_2O_3 and MF_x (M=Al, Zn, Fe) or Na_3AlF_6 will be subjected to electrolysis. In this process, in theory, the main cathodic reaction would be:

$$Nd^{3+} + 3e^- \rightarrow Nd \quad (4.5)$$

According to reactions (4.1)-(4.4), during the Nd_2O_3 conversion into NdF_3 by AlF_3, ZnF_2, FeF_3, or Na_3AlF_6 the corresponding oxides, Al_2O_3, ZnO, FeO and Al_2O_3, respectively, are formed in the salt. Since the stability of these oxides is lower than that of the NdF_3, parts of Al_2O_3, ZnO and FeO might dissolve in the fluoride melt and can go through the electrolysis process. The solubility of alumina in the molten fluorides is 6 mol% [17]. Based on the density of the LiF containing different concentrations of NdF_3 [18], an estimation shows that the density of LiF-5mol% NdF_3 is 4.03 g/cm^3 (aluminium oxide density is 3.95 g/cm^3). This means that the critical composition in which the aluminium oxide will float is LiF-5mol% NdF_3. The floating oxide can be then removed from the top of the liquid before it substantially dissolves back into the fluoride salt. The density of the LiF-NdF_3 system can go up to 5 g/cm^3 when NdF_3 reaches 50 mol%. Yet ZnO and FeO have a higher density (5.60 and 5.74 g/cm^3, respectively), so the formed oxide will sink in the liquid and should be removed. If the newly formed oxide could be removed before electrolysis, the co-deposition could be minimised. For separation of newly formed oxide solids from the molten salt (for electrolysis), a two chamber inter-connected furnace system can be designed: NdF_3 conversion in chamber 1 and NdF_3 electrolysis in chamber 2. By arranging the connection channel in the middle or the bottom level (depending on the density of the newly formed oxide), the new oxide particles can be removed from the top or bottom, before entering the electrolysis chamber.

The decomposition voltages of these oxides as well as their corresponding fluorides are compared with neodymium fluorides as shown in Figure 4.1. These data are calculated for the pure substances at their standard states at the specified temperatures. In the real system, the activity values of the fluorides and the oxides will deviate from unity (standard state) due to the dissolution in the salt bath. Yet these data from pure substances are very useful and crucial for the comparison of the different fluorides.

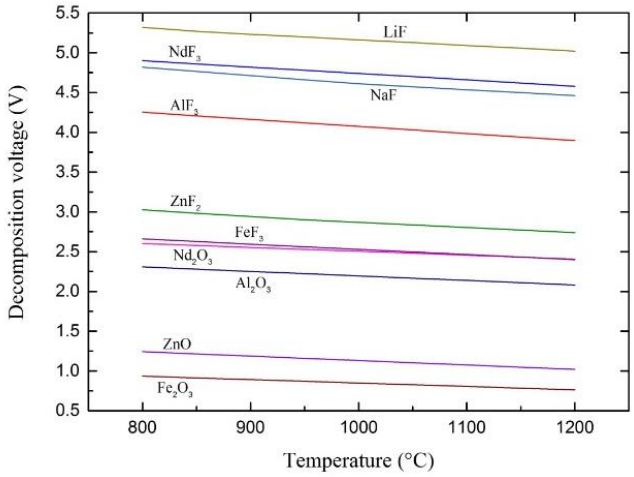

Figure 4.1– Decomposition voltages of metals oxides and fluorides calculated by FactSage

Based on the stability line of the different compounds in Figure 4.1, addition of AlF_3, ZnF_2, FeF_3 and Na_3AlF_6 to the LiF-Nd_2O_3 system and subsequent electrolysis (with a cell voltage of ~4.8 V at T=950°C, without considering the over-potential) would enable the extraction of neodymium from neodymium fluoride. It is also expected that Al, Zn and Fe will be co-deposited on the cathode, forming Nd-Al, Nd-Zn and Nd-Fe alloys if there AlF_3, ZnF_2 or FeF_3 are remaining in the salt or the formed oxides of Al_2O_3, ZnO or Fe_2O_3 are dissolved in the salt and participate in the electrochemical reactions. In the case of using cryolite, Na can also deposit. Hence, along with the reaction (4.5), one of the following reactions can take place at the cathode:

$$Al^{3+} + 3e^- \rightarrow Al \quad (4.6)$$

$$Zn^{2+} + 2e^- \rightarrow Zn \quad (4.7)$$

$$Fe^{3+} + 3e^- \rightarrow Fe \quad (4.8)$$

$$Na^+ + e^- \rightarrow Na \quad (4.9)$$

The anodic reactions will be as follows if a graphite anode is used:

$$O^{2-}(salt) + C(anode) \rightarrow CO(g) + 2e^- \quad (4.10)$$

$$2O^{2-}(salt) + C(anode) \rightarrow CO_2(g) + 4e^- \quad (4.11)$$

$$2F^-(salt) \rightarrow F_2(g) + 2e^- \quad (4.12)$$

4.3 Experiments

Lithium fluoride (98.5%-Alfa Aesar) is mixed with neodymium oxide (Rhodia) in a glove box. A fluorinating agent of aluminium fluoride (99+%-Alfa Aesar), zinc fluoride (99%-Alfa Aesar), iron fluoride (97%-Alfa Aesar) or cryolite (97%- Sigma Aldrich) is added to the mixture separately and the mixture is charged into a graphite crucible. The ratio of

neodymium fluoride to fluorinating agent are prepared based on the stoichiometry of equations (4.1)-(4.4); Nd_2O_3:$2AlF_3$, Nd_2O_3:$3ZnF_2$, Nd_2O_3:$2AlF_3$ and Nd_2O_3:Na_3AlF_6. No excessive fluorinating agents is added more than theoretical requirement. LiF concentration is determined assuming that after reaching the complete conversion of Nd_2O_3 to NdF_3, the eutectic composition of LiF-23 mol% NdF_3 [19] is formed in the system. The total amount of the mixture for all the systems is about 30 grams. The mixtures are heated at 950°C for 3 hours in a purified argon atmosphere. The Ar gas is purified by passing through KOH flakes in order to remove sulphur and also through silica gel and P_2O_5 to remove moisture. The gas is passed through a tube furnace containing Ti sponges which is held at 850°C in order to remove the traces of O_2. The samples are quenched in liquid nitrogen after the experiment.

The samples are analysed by XRD as well as Electron Probe Micro Analysis (EPMA), in order to determine the phases that are formed during the experiments. For the EPMA analyses, Wavelength Dispersive Spectrometry (WDS) point analyses or mappings are performed at either 15 kV-15 nA or at 5 kV-15 nA. For the quantification, standards are used. The EPMA quantification data are within 1% error.

4.4 Results

4.4.1 AlF_3 in LiF-Nd_2O_3 system

The XRD analysis results of the sample from the LiF-Nd_2O_3-AlF_3 mixture after the fluorination treatment, shown in Figure 4.2, indicate the formation of NdF_3, LiF, $AlNdO_3$ and Al_2O_3 phases. These results thus confirm the formation of NdF_3 based on reaction (4.1).

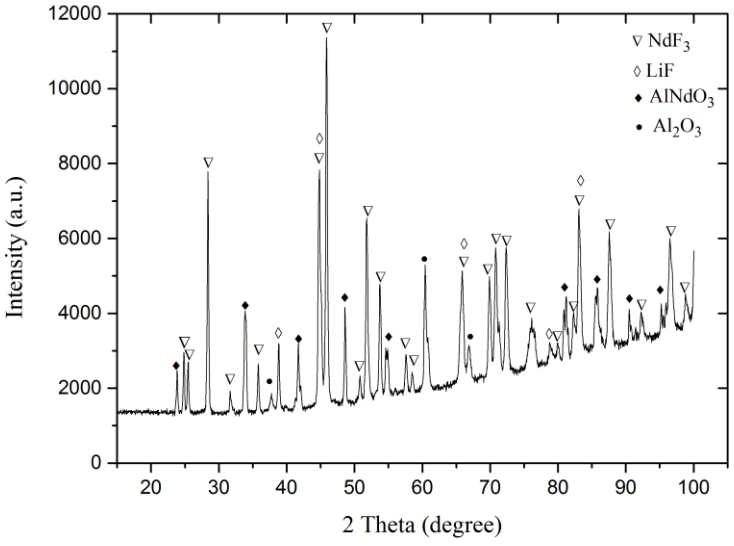

Figure 4.2– XRD pattern of LiF-Nd2O3-AlF_3 sample after fluorination treatment with identified phases.

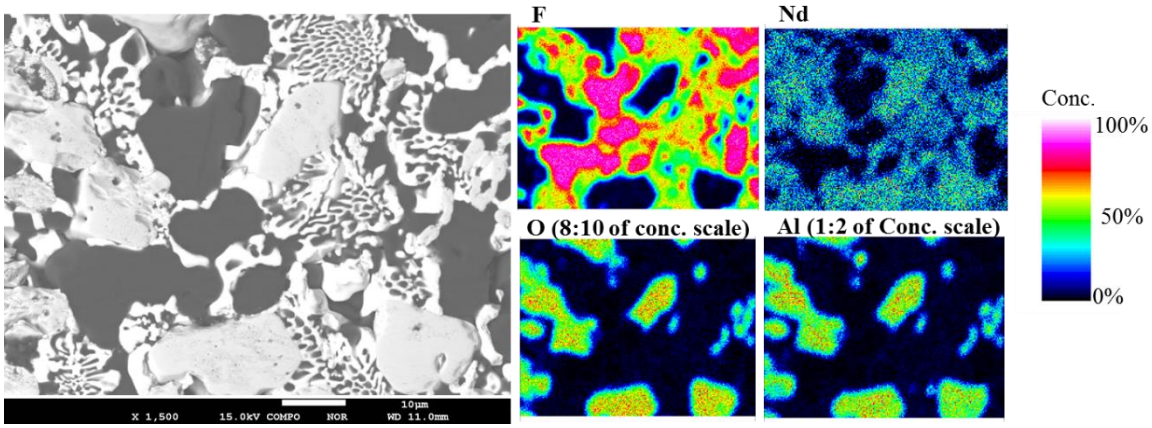

Figure 4.3– EPMA mapping images of LiF-Nd_2O_3-AlF_3 sample after fluorination treatment.

Al, Nd and oxygen distributions shown by EPMA mapping in Figure 4.3 provide further evidence for the formation of Al-Nd-O Phase, which is identified as $AlNdO_3$ in XRD results. Formation of $AlNdO_3$ could inhibit the complete conversion of Nd_2O_3 to NdF_3. Furthermore, Nd is distributed in the fluorine areas, which indicates neodymium fluoride formation. The dark phase in the sample is possibly LiF, since the fluorine concentration is very high in this area. Lithium, being a light element, could not be measured by EPMA.

The microstructure of the liquid nitrogen-quenched sample is shown in Figure 4.4. From the EPMA point analysis, different phases present in the samples are identified and are marked. The dark phase with high fluorine concentration is identified as lithium fluoride and the fibrous phase is NdF_3. Fibrous pattern of NdF_3-LiF eutectic structure can be seen in this picture. The large light grains correspond to oxides (Al_2O_3, $AlNdO_3$). Both aluminium oxide and aluminium neodymium oxide are identified by XRD. The EPMA analysis shows the distribution of neodymium, aluminium and oxygen in the same areas which can be referred to $AlNdO_3$ phase.

Point analysis of the LiF-Nd_2O_3-AlF_3 sample shows the presence of 77 at% fluorine and 19 at% neodymium, forming NdF_3 phase, a fluorine-rich phase (LiF) and $AlNdO_3$ (20 at% aluminium, 17 at% neodymium and 62 at% oxygen). Al_2O_3 is not identified in the EPMA results. This could be due to the fact that EPMA point analysis is limited to the certain areas, whereas in XRD analysis which detect the whole sample Al_2O_3 phase is identified.

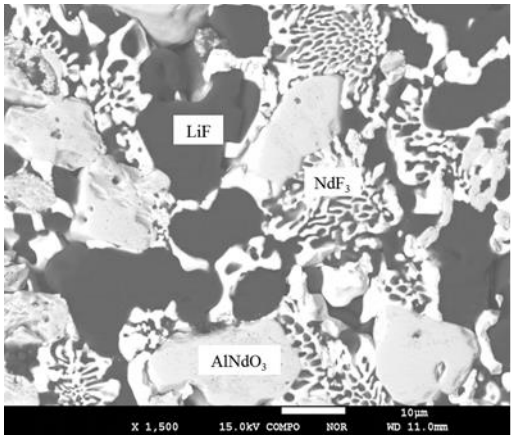

Element	NdF_3	LiF	$AlNdO_3$
F	77	99.5	-
Nd	19	-	17
O	-	-	62
Al	-	-	20

Figure 4.4– BSE image and EPMA quantification result of the LiF-Nd_2O_3-AlF_3 sample in at% after fluorination treatment, showing the presence of NdF_3 and $AlNdO_3$.

4.4.2 ZnF_2 in LiF-Nd_2O_3 system

The XRD analysis result for LiF-Nd_2O_3-ZnF_2 after fluorination is shown in Figure 4.5. The identified phases are NdF_3, LiF and ZnO. This confirms the complete conversion of Nd_2O_3 to NdF_3 based on reaction (4.2).

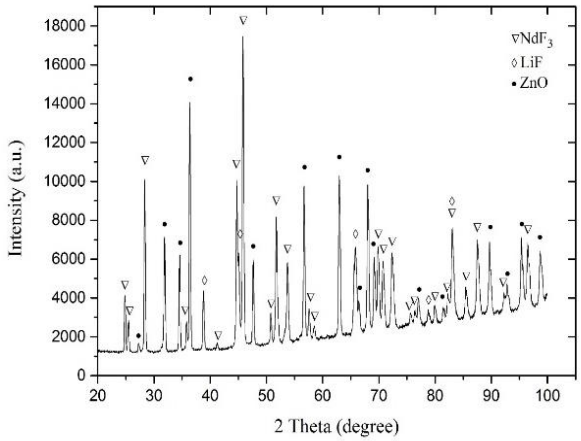

Figure 4.5 – XRD pattern of LiF-Nd_2O_3-ZnF_2 sample after fluorination treatment with identified phases.

Very strong peaks of neodymium fluoride show that the neodymium oxide is converted to neodymium fluoride after reaction with ZnF_2. Oxygen is detected only in the zinc oxide phase, and there are no peaks corresponding to the remaining neodymium oxide in the sample. Hence neodymium oxide is considered to have been completely converted to neodymium-fluoride. It should be noted that no oxyfluoride phase is detected by XRD analysis.

The EPMA mapping images in Figure 4.6 also clearly show the formation of NdF_3 and ZnO as separate phases. Mapping (a) in this figure is analysed at 15 kV voltage; in order to see more detail and distinguish between the two phases, mapping (b) is performed at the lower voltage level of 5 kV. The LiF-NdF_3 eutectic microstructure, lamellar NdF_3 phase in the LiF phase, is clearly visible in this image. In this figure, it is clearly shown that neodymium is distributed in the lamellar phase and fluorine is found in both microstructural constituents. The level of fluorine in the black phase is twice that of the lamellar phase which is a reflection of LiF presence as the basic salt constituent (solvent).

The EPMA point analysis of the LiF-Nd_2O_3-ZnF_2 sample after fluorination treatment with the elemental quantification is shown in Figure 4.7. The results show the presence of dark grey ZnO grains in a lamellar LiF-NdF_3 eutectic matrix. The quantifications show that no oxyfluoride phase is formed and that all neodymium oxide has been converted to neodymium fluoride. The lamellar light grey phase having fluorine and neodymium in a 3:1 atomic ratio indicates the formation of neodymium fluoride. NdF_3-LiF eutectic structure is clearly shown in the BSE image. The composition measurement of the NdF_x phase indicates (referring to the table under Figure 4.7) that the fluorine concentration is relatively high (9 times the Nd concentration). This data results from the area analysis with a radius of 7 µm, could contain both NdF_3 and LiF. Li cannot be detected by EPMA. The small grey grains correspond to the presence of the ZnO phase (52 at% Zn and 47 at. % O).

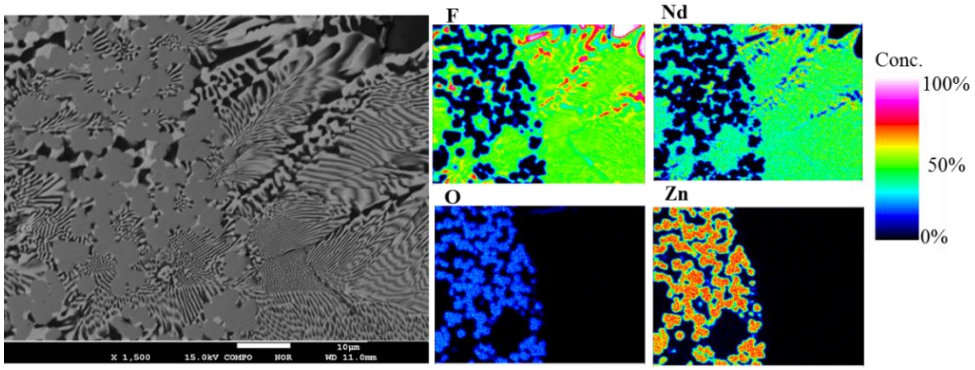

(a)

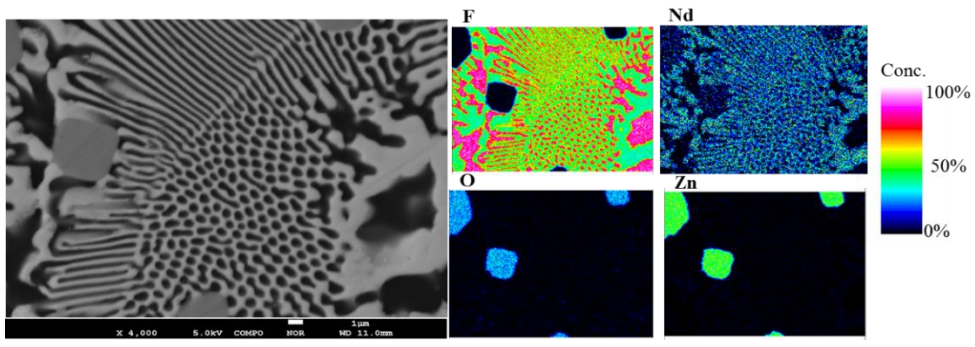

(b)

Figure 4.6– EPMA mapping images of LiF-Nd_2O_3-ZnF_2 sample after fluorination treatment, (a) analysed at 15 kV and (b) at 5 kV.

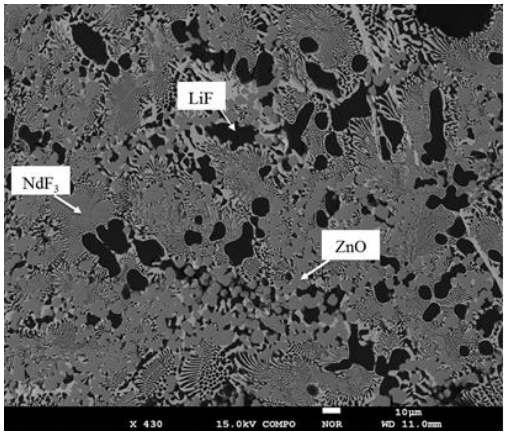

Element	NdF_3	ZnO	NdF_x
F	74	-	89
O	-	47	-
Nd	25	-	10
Zn	-	52	-

Figure 4.7– BSE image and EPMA quantification result of LiF-Nd_2O_3-ZnF_2 sample in at% after fluorination treatment showing the presence of NdF_3 and ZnO.

4.4.3 FeF_3 in LiF-Nd_2O_3 system

The result of the XRD analysis of the LiF-Nd_2O_3-FeF_3 sample is shown in Figure 4.8. The strong peaks of neodymium fluoride show the oxide to fluoride conversion. FeO is formed in the reaction of iron fluoride with neodymium oxide. As mentioned earlier, in the Ar ambient and low oxygen pressure atmosphere, hematite (Fe_2O_3) will not be formed or, depending upon the oxygen pressure prevailing, the formed Fe_2O_3 is decomposed to Fe_3O_4 and FeO. At temperatures higher than the eutectoid temperature (ca. 560°C) for FeO in equilibrium with metallic iron and Fe_3O_4, the stable oxide is wüstite (FeO). Furthermore, three peaks were detected in the XRD pattern corresponding to the presence of NdOF phase.

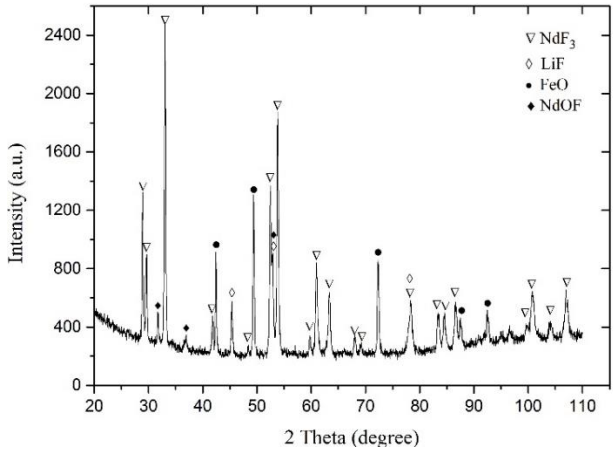

Figure 4.8 – XRD pattern of LiF-Nd_2O_3-FeF_3 sample after fluorination treatment with identified phases

In the EPMA mapping (Figure 4.9) the distribution of iron and oxygen is clearly shown. Based on the mapping images, neodymium has a high concentration around the FeO grain boundaries. Oxygen and fluorine are also present in these areas in very low concentration. Hence these areas could be neodymium oxyfluoride that is detected by XRD. Based on the mapping images, the lamellar phase is NdF_3 in the LiF, indicating LiF-NdF_3 eutectic microstructure.

The BSE images and EPMA quantification results are shown in Figure 4.10. In this figure, the presence of FeO (45 at% Fe and 54 at% O) grains is seen. This phase can be a mixture of FeO and Fe_2O_3, since concentration can also be related to magnetite phase (Fe_3O_4). From reaction (4.3), Fe_2O_3 formation is expected, but as both XRD results and EPMA results show, the oxide of iron which is formed is wüstite or non-stoichiometric FeO_x. However, oxygen measurement by EPMA at 15 kV is not precise.

In Figure 4.10, the presence of needle-shaped grains of neodymium fluoride is seen. No neodymium oxyfluoride phase is detected by EPMA for the selected area of the sample. However, in XRD results of the same sample (Figure 4.9), small peaks corresponding to

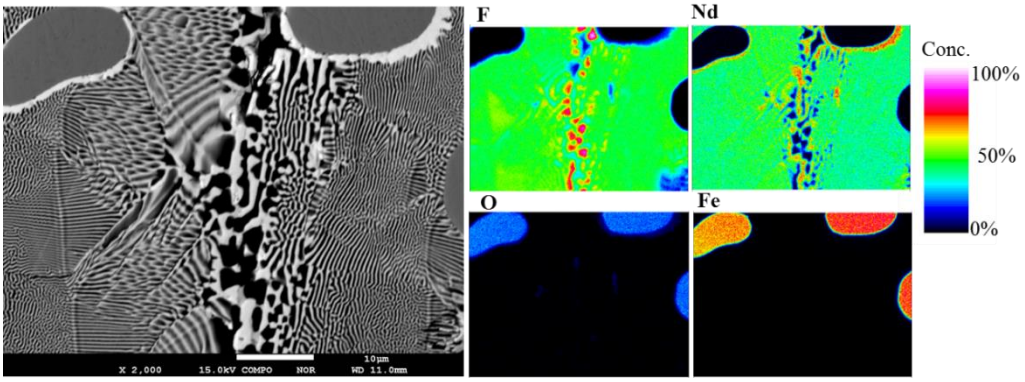

Figure 4.9– EPMA mapping of LiF-Nd_2O_3- FeF_3 sample after fluorination treatment showing the presence of NdF3 and FeO.

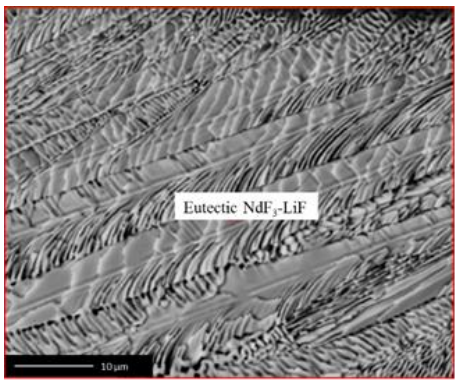

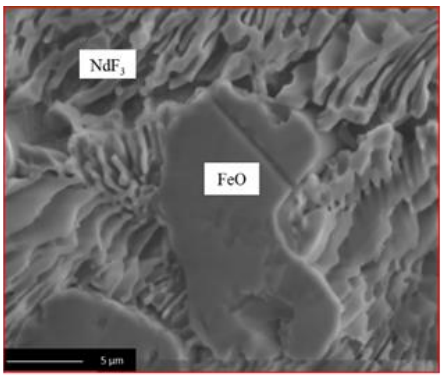

Element	NdF_3	FeO
F	72	-
O	-	54
Nd	26	-
Fe	-	45

Figure 4.10– BSE image and EPMA quantification result of LiF-Nd_2O_3-FeF_3 sample in at% after fluorination treatment showing the presence of NdF_3 and FeO.

NdOF phase are detected. Considering the fact that XRD analysis is valid for the whole sample while EPMA analysis is limited to the certain areas, it is assumed that NdOF is formed as the result of the chemical reaction. The EPMA quantitative analysis shows the presence of 26 at% Nd and 72 at% F.

4.4.4 Na_3AlF_6 in LiF-Nd_2O_3 system

Figure 4.11 shows the XRD results of the LiF-Nd_2O_3-Na_3AlF_6 system after fluorination. It can be seen that unlike the NdF_3 formation in other systems, in this system $Na_{1.5}Nd_{1.5}F_6$ compound is formed. It seems that neodymium from the neodymium oxide reacts with the cryolite and substitutes the aluminium in the cryolite. Furthermore, there are peaks corresponding to $AlNdO_3$ and also three peaks related to aluminium metal which is considered as an unexpected result. This observation is inexplicable at this stage and is not discussed further in this chapter.

The EPMA analysis results in Figure 4.12 show the distribution of fluorine and neodymium in the same areas, indicating the presence of neodymium fluoride. It can be seen that the large grains in the sample consist of aluminium, oxygen and neodymium, which shows the presence of AlNdO.

The BSE image and the EPMA quantification results of LiF-Nd_2O_3-Na_3AlF_6 sample shown in Figure 4.13, indicate the formation of $Nd_{1.5}Na_{1.5}F_6$ lamellar structure containing 18 at% Nd, 11 at% Na and 70 at% F and the AlNdO phase with 21 at% Nd, 22 at% Al and 54 at% O. These results confirm the XRD results on the same sample.

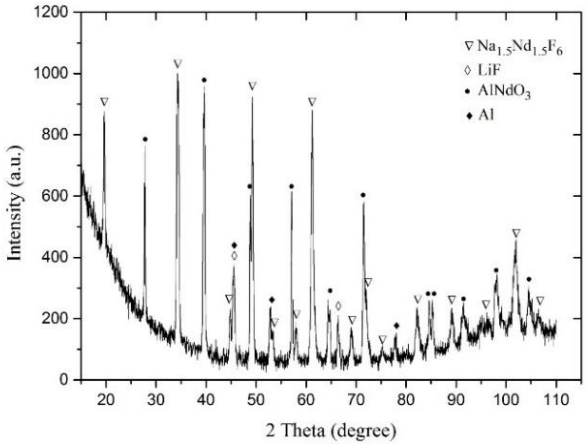

Figure 4.11– XRD pattern of LiF-Nd_2O_3-Na_3AlF_6 sample after fluorination treatment with identified phases

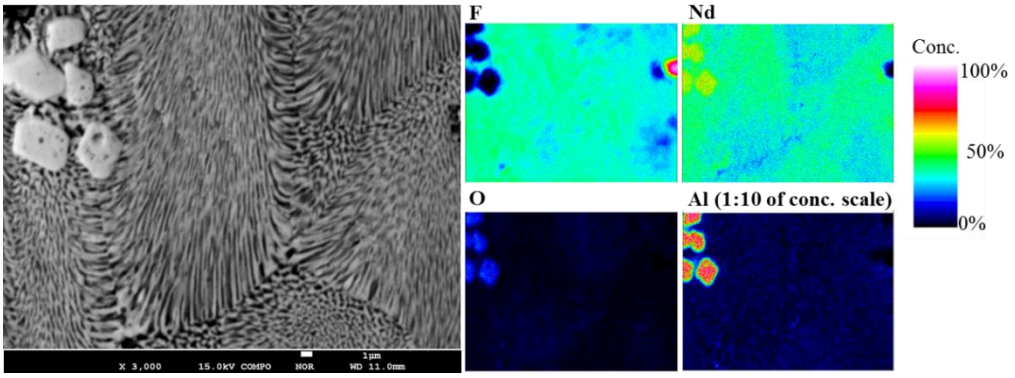

Figure 4.12– EPMA mapping of LiF-Nd_2O_3- Na_3AlF_6 sample after fluorination treatment showing the presence of NdF_3.

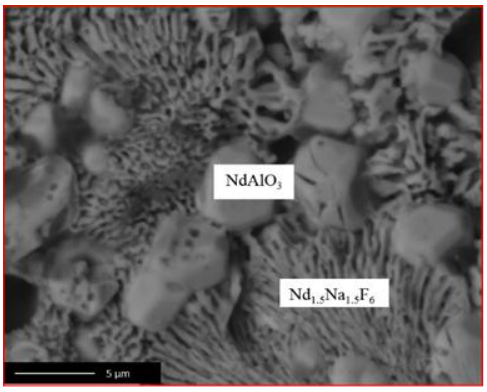

Element	$Nd_xNa_yF_z$	NdAlO
F	70	-
O	-	54
Al	-	22
Nd	18	21
Na	11	-

Figure 4.13– BSE images and EPMA quantification result of LiF-Nd_2O_3- Na_3AlF_6 sample in at% after fluorination treatment showing the presence of $Nd_{1.5}Na_{1.5}F_6$ and NdAlO.

4.5 Discussion

4.5.1. Reactions

Among the four fluorides used as fluorinating agents, the complete conversion of rare earth oxide to rare earth fluoride is observed only in the case that ZnO is used. According to the Gibbs formation free energy of reactions (4.1)-(4.4) at 950 °C, formation of NdF_3 as the result of reaction of Nd_2O_3 with ZnF_2 is the most favourable reaction since it has the lowest Gibbs energy under the standard conditions.

The reaction related to cryolite has the highest Gibbs free energy, hence the lowest tendency for the formation of NdF_3. Instead of neodymium fluoride, $Na_{1.5}Nd_{1.5}F_6$ is formed. Some of the oxide phase is also found in the form of $AlNdO_3$. In the next step of the process, which is electrochemical reduction of rare earth on cathode, neodymium

should be extracted from $Na_{1.5}Nd_{1.5}F_6$. It is expected that Na will be co-deposited with Nd on the cathode.

Results of the LiF-Nd_2O_3-AlF_3 system show that aluminium is substituted with the neodymium from neodymium oxide, resulting in the formation of neodymium fluoride. But this conversion has obviously not reached completion since some neodymium is detected in the oxide phase in $AlNdO_3$. Adding an excess amount of AlF_3 to the system can result in the complete conversion of neodymium oxide, which needs to be proven in the future research.

In the case of FeF_3, three small peaks in XRD are identified as corresponding to the neodymium oxyfluoride phase; in the EPMA mappings of this system, neodymium has the high concentration on the FeO grain boundaries, whereas oxygen and fluorine are present with very low concentrations. This leads to the conclusion that a small fraction of oxyfluoride is present in this system, however most of the neodymium oxide is converted to neodymium fluoride.

In-situ formation of REF_3 is very important since the solubility of REOs is very low in molten fluorides [20]. Furthermore, the additional advantage is that the formation of rare earth oxyfluoride is likely to be inhibited. Based on the suggested reaction by Stefanidaki *et al.* [20] for the solubility of neodymium oxide in LiF-NdF_3 eutectic melt

$$Nd_2O_3 + NdF_3 + 3(x-1)LiF \rightleftarrows 3NdOF_x^{(x-1)-} + 3(x-1)Li^+ \quad x = 4, 5 \qquad (4.12)$$

oxyfluoride compounds are formed. Taxil et al. [15] results show that the oxyfluoride is an insoluble compound. Dysinger and Murphy [21] have explained that formation of neodymium oxyfluoride could be one factor to decrease the current efficiency.

Hence, formation of rare earth oxyfluoride as an insoluble product is a significant drawback in the extraction of rare earth in molten salts, since they do not participate in the cathodic reactions and they lower the current efficiency by participating in anodic reaction [12]. However, conversion of neodymium oxide to neodymium fluoride preempts the formation of neodymium oxyfluoride, since neodymium fluoride formation is thermodynamically favorable and it is formed directly as the result of the chemical reaction between neodymium oxide and fluorinating agents.

4.5.2 Microstructure

The maximum conductivity of the electrolyte is usually at the eutectic compositions of the fluoride salts. In all experiments in this work the stoichiometry of neodymium oxide and the fluorinating agent is calculated based on theoretical values of reactions (4.1) – (4.4), assuming that if the conversion of neodymium oxide completes, the LiF-NdF_3 forms the eutectic composition. The eutectic composition of the LiF-NdF_3 system is experimentally determined to be 0.23 mole fraction of NdF_3 [19] and is calculated to be about 0.25 mole fraction of NdF_3 by Van der Meer *et al.* [22]. The LiF-NdF_3 phase diagram determined by the same researchers using the experimental data, is shown in Figure 4.14.

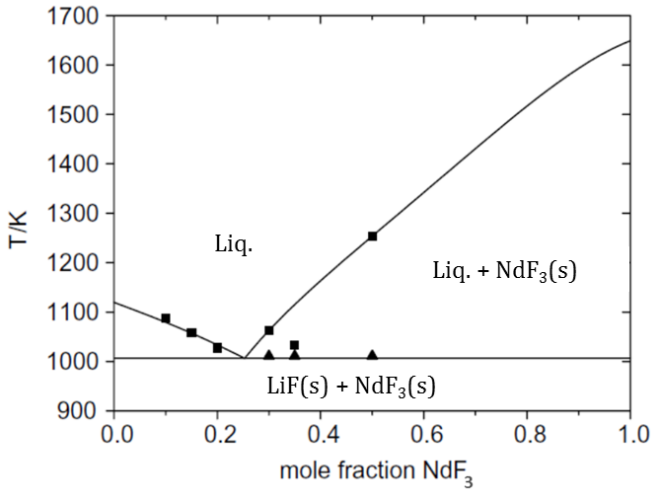

Figure 4.14– The optimized LiF–NdF_3 phase diagram: (■) experimental data liquidus; (▲) experimental data solidus [19, 22]

In many systems, the microstructure is dependent on the growth conditions; thus the cooling rate and other thermal conditions. Hence it does not directly resemble the molten state of the salt. However, the volume fraction ratio of the two eutectic phases can lead to formation of lamellar, fibrous or mixed microstructures. In general, when both phases have camparable volume fractions, a lamellar structure is formed [23].

In all four systems, due to the fast cooling using liquid nitrogen, a fine eutectic structure with fine alternations of LiF and NdF_3 lamellae is formed (Figures 4.4, 4.7, 4.10 and 4.13). In LiF-Nd_2O_3-ZnF_2 and LiF-Nd_2O_3-FeF_3 systems, XRD analysis shows that most of the neodymium oxide is converted to neodymium fluoride. Hence the composition of the LiF-NdF_3 mixture would be close to the eutectic. The lamellar microstructure of NdF_3 light phase in the LiF dark phase which can be seen in Figures 4.7, 4.9 and 4.10, shows that the volume fraction of LiF and NdF_3 is close to the eutectic composition. Also in the case of the system LiF-Nd_2O_3-$Na_2Al_3F_6$, the lamellar microstructure is observed; however in this system, $Nd_{1.5}Na_{1.5}F_6$ is formed instead of NdF_3. There is insufficient data in the literature for this system; but the microstructure observations show that LiF-$Nd_{1.5}Na_{1.5}F_6$ behaves very similarly to the eutectic composition of the LiF-NdF_3 system. In LiF-Nd_2O_3-AlF_3 system, presence of $NdAlO_3$ shows that not all the neodymium oxide is converted into neodymium fluoride. Hence the volume fraction of NdF_3 is expected to be lower than 0.25 (eutectic composition of LiF-NdF_3 system). With decrease in the volume fraction of one phase below 0.29, the microstructure forms the fibrous pattern. The fibrous microstructure in Figure 4.4 indicates that the microstructure corresponds to a non-eutectic phase. With increasing growth velocity, the dimensions of the two phases are expected to decrease [23, 24].

4.5.3 Alloy formation

The neodymium fluoride which is formed will be dissolved in the molten LiF and will be subjected to electrolysis when the appropriate voltage is applied. As shown in Figure 4.1, the voltage needed for NdF_3 electrolysis would be higher than the decomposition voltage of the other oxides which are present in the system. Hence the dissolved Al_2O_3, ZnO and FeO will also participate in the electro-decomposition process, and co-deposition of Al, Zn and Fe will occur at the cathode. The challenge would be to remove the undissolved oxides in order to minimize their side effect on cathodic deposition of Nd. A new design of a two-chamber furnace system is one way for removing the undissolved oxide. The density difference between the formed oxide and the fluoride bath could also be used to separate the oxides from the molten salt.

In the case that dissolved metal oxides (Al_2O_3, ZnO and FeO) participate in the electrochemical reactions, there is likely to be a competition between oxygen gas and fluorine gas evolution at the carbon anode. In the former case, the oxidation reactions between the carbon anode the oxygen gas lead to the CO or CO_2 gas formation (reactions (4.10) and (4.11)) and in the latter case, reaction between fluorine gas and the carbon anode would result in the formation of fluorine gas (reaction (4.12)), more specifically such as CF_4 and C_2F_6 [25]. CO and CO_2 evolutions have more negative potentials than fluorocarbon or fluorine gas evolution. According to Stefanidaki *et al.* [12], fluorocarbon generation on the anode can be inhibited by controlling the cell voltage. However, in order to avoid fluorine gas formation, the use of an alternative anode is proposed, which will be discussed in chapter 5.

Regarding the cathodic reactions, formation of Nd-Fe alloy is desirable since it can be used as master alloy for magnet production. In this regard using FeF_3 as the fluorinating agent would be a great advantage.

In general, RE-Al alloy can be applied to improve the magnetic properties of the RE magnets. Dy-Ni-Al eutectic alloy is used in grain boundary diffusion treatment in the neodymium magnets in order to improve the coercivity [26]. Alloying pure aluminium with rare earth elements is also an effective means to reduce the defect formation in the films which are used as interconnect lines in large scale integration circuits [27]. This will give support for using AlF_3 as fluorinating agent and producing Nd-Al alloy on the cathode.

In the case of using cryolite instead of AlF_3, Nd_2O_3 converts to $Na_{1.5}Nd_{1.5}F_6$ and not NdF_3. In the electrolysis step Na reduction with Nd from $Na_{1.5}Nd_{1.5}F_6$ and Al reduction from Al_2O_3 are expected. Hence Nd-Al-Na alloy is formed on the cathode. In order to avoid Na reduction, AlF_3 should be used instead on Na_3AlF_6.

Nd-Zn alloy can be used for magnesium alloying in production of novel composites. Zn is the major alloying element of the magnesium materials and it has been proven that rare earth elements are the most effective alloying elements to improve the strength and corrosion behaviour of zinc [28, 29].

4.6 Conclusion

The results of XRD and EPMA analyses show that AlF_3, ZnF_2 and FeF_3 can act as strong fluorinating agents for neodymium oxide. In all these systems, neodymium oxide is converted to neodymium fluoride. By the addition of AlF_3, ZnF_2 and FeF_3 to the LiF-Nd_2O_3 system, aluminium oxide, zinc oxide and iron oxide are formed, respectively. In the case of Na_3AlF_6, $Na_{1.5}Nd_{1.5}F_6$ is formed instead of NdF_3. Also as the result of the conversion reaction, instead of Al_2O_3, $AlNdO_3$ is formed. In general, cryolite has the least tendency for the formation of NdF_3 compared to other fluorinating agents that are studied in this research. The reaction related to cryolite has the highest Gibbs free energy, hence the lowest tendency for the formation of NdF_3.

The results show the feasibility of the conversion of the rare earth oxide to rare earth fluoride using fluorinating agents. Conversion of neodymium oxide to neodymium fluoride solves the problem of low solubility of the neodymium oxide in molten fluorides, to a large extent. Once neodymium fluoride is formed, it can subsequently be electrolysed and extracted on the cathode. One consequence of extracting rare earth metal through rare earth fluoride electro-decomposition would be formation of fluorocarbon at the anode. In order to prevent this, use of an alternative reactive anode as a substitution for conventional graphite anode is suggested which is studied in chapter 5.

4.7 References

[1] Chen, G. Z., Fray, D. J., and Farthing, T. W., 2000, "Direct electrochemical reduction of titanium dioxide to titanium in molten calcium chloride," Nature, 407, pp. 361-364.

[2] Hirota, K., Okabe, T. H., Saito, F., Waseda, Y., and Jacob, K. T., 1999, "Electrochemical deoxidation of RE–O (RE=Gd, Tb, Dy, Er) solid solutions," Journal of Alloys and Compounds, 282(1–2), pp. 101-108.

[3] Claux, B., Serp, J., and Fouletier, J., 2011, "Electrochemical reduction of cerium oxide into metal," Electrochimica Acta, 56(7), pp. 2771-2780.

[4] Wang, D., Qiu, G., Jin, X., Hu, X., and Chen, G. Z., 2006, "Electrochemical Metallization of Solid Terbium Oxide," Angewandte Chemie International Edition, 45(15), pp. 2384-2388.

[5] Sri Maha Vishnu, D., Sanil, N., Panneerselvam, G., Mahato, S. K., Soja, K. V., Mohandas, K. S., and Nagarajan, K., 2013, "Factors Influencing the Direct Electrochemical Reduction of UO_2 Pellets to Uranium Metal in $CaCl_2$-48 mol% NaCl Melt," Journal of The Electrochemical Society, 160(11), pp. D583-D592.

[6] Seetharaman, S., and Grinder, O., 2010, US patent application nr. 12/991128, ref. no.: 12057

[7] Abbasalizadeh, A., Seetharaman, S., Teng, L., Sridhar, S., Grinder, O., Izumi, Y., and Barati, M., 2013, "Highlights of the Salt Extraction Process," Journal Of Materials, 65(11), pp. 1552-1558.

[8] Abbasalizadeh, A., Teng, L., Sridhar, S., and Seetharaman, S., 2015, "Neodymium extraction using salt extraction process," Mineral Processing and Extractive Metallurgy, 124(4), pp. 191-198.

[9] Porter, B., and Brown, E. A., 1961, Determination of oxide solubility in molten fluorides, U.S. Dept. of the Interior, Bureau of Mines, Washington, DC.

[10] Morrice, E., and Henrie, T. A., 1967, Electrowinning high-purity neodymium, praseodymium, and didymium metals from their oxides, U.S. Dept. of the Interior, Bureau of Mines, Washington D.C.

[11] Murphy, J. E., Dysinger, D. K., and Chambers, M. F., "Electrowinning neodymium metal from chloride and oxide-fluoride electrolytes," Proc. Light Metals: Proceedings of Sessions, TMS Annual Meeting, Warrendale, Pennsylvania, pp. 1313-1320.

[12] Stefanidaki, E., Hasiotis, C., and Kontoyannis, C., 2001, "Electrodeposition of neodymium from LiF-NdF_3-Nd_2O_3 melts," Electrochimica Acta, 46(17), pp. 2665-2670.

[13] Kaneko, A., Yamamoto, Y., and Okada, C., 1993, "Electrochemistry of rare earth fluoride molten salts," Journal of Alloys and Compounds, 193, pp. 44-46.

[14] Thudum, R., Srivastava, A., Nandi, S., Nagaraj, A., and Shekhar, R., 2010, "Molten salt electrolysis of neodymium: electrolyte selection and deposition mechanism," Mineral Processing and Extractive Metallurgy, 119(2), pp. 88-92.

[15] Taxil, P., Massot, L., Nourry, C., Gibilaro, M., Chamelot, P., and Cassayre, L., 2009, "Lanthanides extraction processes in molten fluoride media: Application to nuclear spent fuel reprocessing," Journal of Fluorine Chemistry, 130(1), pp. 94-101.

[16] Zhu, H., 2014, "Rare Earth Metal Production by Molten Salt Electrolysis," Encyclopedia of Applied Electrochemistry, G. Kreysa, K. Ota, and R. Savinell, eds., Springer New York, pp. 1765-1772.

[17] Lacassagne, V., Bessada, C., Florian, P., Bouvet, S., Ollivier, B., Coutures, J.-P., and Massiot, D., 2002, "Structure of High-Temperature $NaF–AlF_3–Al_2O_3$ Melts: A Multinuclear NMR Study," The Journal of Physical Chemistry B, 106(8), pp. 1862-1868.

[18] Hu X., Wang Z., Gao B., Shi Z. , Liu F. , and Cao X., 2010, "Density and ionic structure of NdF3-LiF melts," Journal of Rare Earths, 28(4), pp. 587-590.

[19] Thoma, R. E., Brunton, G. D., Penneman, R. A., and Keenan, T. K., 1970, "Equilibrium relations and crystal structure of lithium fluorolanthanate phases," Inorganic Chemistry, 9(5), pp. 1096-1101.

[20] Stefanidaki, E., Photiadis, G. M., Kontoyannis, C. G., Vik, A. F., and Østvold, T., 2002, "Oxide solubility and Raman spectra of NdF_3-LiF-KF-MgF_2-Nd_2O_3 melts," Journal of the Chemical Society, Dalton Transactions(11), pp. 2302-2307.

[21] Dysinger, D. K., and Murphy, J. E., 1994, "Electrowinning of neodymium from a molten oxide-fluoride electrolyte. Report of investigations."

[22] van der Meer, J. P. M., Konings, R. J. M., Jacobs, M. H. G., and Oonk, H. A. J., 2004, "Thermodynamic modelling of LiF–LnF_3 and LiF–AnF_3 phase diagrams," Journal of Nuclear Materials, 335(3), pp. 345-352.

[23] Trnovcová, V., Fedorov, P. P., Bárta, Č., Labaš, V., Meleshina, V. A., and Sobolev, B. P., 1999, "Microstructure and physical properties of superionic eutectic composites of the LiF–RF3 (R=rare earth element) system," Solid State Ionics, 119(1–4), pp. 173-180.

[24] Trnovcová, V., Starostin, M. Y., Čička, R., Fedorov, P. P., Bárta, Č., Labaš, V., and Sobolev, B. P., 2000, "Microstructure and fast ionic conduction of inorganic fluoride and oxide eutectic composites prepared from the melt," Solid State Ionics, 136–137, pp. 11-17.

[25] Keller, R., and Larimer, K., 1997, "Rare Earths: Science, Technology and Applications III, The Minerals," Metals & Materials Society, 175.

[26] Oono, N., Sagawa, M., Kasada, R., Matsui, H., and Kimura, A., 2011, "Production of thick high-performance sintered neodymium magnets by grain boundary diffusion treatment with dysprosium–nickel–aluminum alloy," Journal of Magnetism and Magnetic Materials, 323(3–4), pp. 297-300.

[27] Sarkar, J., Saimoto, S., Mathew, B., and Gilman, P. S., 2009, "Microstructure, texture and tensile properties of aluminum–2 at.% neodymium alloy as used in flat panel displays," Journal of Alloys and Compounds, 479(1–2), pp. 719-725.

[28] Zhang, C., Luo, A. A., Peng, L., Stone, D. S., and Chang, Y. A., 2011, "Thermodynamic modeling and experimental investigation of the magnesium–neodymium–zinc alloys," Intermetallics, 19(11), pp. 1720-1726.

[29] Polmear, I. J., 1994, "Magnesium alloys and applications," Materials Science and Technology, 10(1), pp. 1-16.

Chapter 5 Use of iron reactive anode in RE extraction process

Abstract

Electrolytic production of metallic neodymium is carried out in fused neodymium fluoride salts containing neodymium oxide. Two major challenges pertaining to neodymium production in fluoride salts are a) low solubility of neodymium oxide in fluoride melt, b) possibility of anodic gas evolution (CO, CO_2, CF_4, C_2F_6). In this study we propose a two-pronged approach to address both issues. Addressing the former challenge, rare earth oxide is converted to rare earth fluoride by the use of fluorinating agent. Regarding the second challenge, iron is used as a reactive anode in the electrolysis process, promoting electrochemical dissolution of iron into the melt, thus preventing fluorocarbon gas evolution at the anode. Therefore, the fluorinating agent is constantly regenerated *in situ* which enables the continuous conversion of neodymium oxide feed. The cathodic product is Nd-Fe alloy which can be directly used as a master alloy for the production of NdFeB magnets.

Keywords: rare earth metals, electrochemical extraction, reactive anode, fluorocarbon gas, molten salts.

5.1 Introduction

Rare earth (RE) metals and their alloys have important applications in different fields of modern technology, in particular in green technologies for clean energy such as wind turbines and electric vehicles [1].

Deoxidation of rare earth metals is very difficult due to the strong affinity of these metals to oxygen. Direct electrochemical process for the reduction of solid oxides into their metals has been studied in metal extraction for a number of rare earth metals (RE = Gd, Tb, Dy, Er and Ce) [2-5]. The low efficiency of this process is the main obstacle for commercializing this process.

Traditionally, RE metals have been produced by the calciothermic reduction of REF_3. However, molten salt electrolysis is becoming the dominant industrial method for the extraction of RE metals from their oxides in the molten salt process [6-8]. Because of very negative deposition potential, RE metals cannot be electrochemically extracted in aqueous media.

Solubility of the rare earth oxide (REO) in the fluoride electrolyte is an important factor, since it is the dissolved oxide that is subjected to electrolysis. However, the solubility of rare earth oxide in molten alkali fluoride does not exceed 4 weight percent [9-11]. Moreover, neodymium oxide is likely to form neodymium oxyfluoride in molten fluoride salts. Oxyfluoride formation has been reported to effect the neodymium electrodeposition adversely [12]. However, the role of neodymium oxyfluoride in the anodic and cathodic reactions is not very clear and needs to be clarified further in detail [12-16]. Another challenge in neodymium production by fluoride electrolysis is the evolution of fluorine associated gasses on the carbon anode when the electrolysis rate exceeds the rare earth oxide feeding and dissolution rate [14].

In the framework of this research for electrochemical extraction of rare earths from their oxides in molten fluoride media, a two-fold approach is adopted in order to address the solubility issue of neodymium oxides in fluoride melts. Initially, a treatment is proposed to convert the neodymium oxide into neodymium fluoride using strong fluorinating agents such as iron(III) fluoride [17]. The results prove the feasibility of the conversion of Nd_2O_3 to NdF_3 in molten salts which solves the problem of low solubility of the neodymium oxide in molten fluorides to a large extent. Once neodymium fluoride is formed, it can subsequently be electrolyzed and deposited on the cathode, along with CO, CO_2, potentially also CF_4 or C_2F_6 evolution on the anode side. However, fluorocarbon gas generation on the graphite anode in the rare earth metal/alloy production industry is a serious drawback of this process, in common with aluminium production industry [18, 19]. The present study is aimed to address this problem. An alternative reactive anode is employed to overcome the problem of halogen or fluorocarbon gas evolution on the anode. In this situation, iron is anodically dissolved, generating the fluorinating agent FeF_2/FeF_3 *in situ* in the electrochemical reactor. The rare earth fluoride thus formed can subsequently be processed through the electrolysis route in the same reactor to extract rare earth metal as the cathodic deposit. In this concept, the REO

dissolution in the molten fluorides would become redundant due to RE oxide conversion into the fluoride as REF_3.

5.2 Thermodynamic evaluations of the process

In the present study, use of iron anode is suggested for the electrolysis process in which instead of CO/CO_2 or fluorocarbon gas formation, the anodic reaction is iron dissolution. The dissolved iron would react with the fluorine ions which are formed as the result of decomposition of added NdF_3 or FeF_3 to LiF-Nd_2O_3 mixture and subsequently FeF_2 and FeF_3 are formed *in situ* in the system as the result of anodic reactions:

$$Fe^{2+} + 2F^- \rightarrow FeF_2 \quad (5.1)$$

$$Fe^{3+} + 3F^- \rightarrow FeF_3 \quad (5.2)$$

Iron(II) fluoride is more stable than iron(III) fluoride. However, depending on the electrolysis conditions, FeF_3 is formed in the electrolyte. The anode potential indicates the concentration ratio of FeF_2/FeF_3. The generated iron fluoride will act as fluorinating agent and convert Nd_2O_3 to NdF_3. From the calculated standard Gibbs free energy (ΔG^o) of the reactions (5.3)-(5.4) at 950°C using FactSage:

$$Nd_2O_3(s) + 3FeF_2(salt) + \rightarrow 2NdF_3(salt) + 3FeO\ (s) \qquad \Delta G^o = -215\ kJ/mol \quad (5.3)$$

$$Nd_2O_3(s) + 2FeF_3(salt) \rightarrow 2NdF_3(salt) + Fe_2O_3(s) \qquad \Delta G^o = -222\ kJ/mol \quad (5.4)$$

it is evident that FeF_3 can react with Nd_2O_3 to form NdF_3, and the formed NdF_3 can further be reduced on the cathode. As the result of the fluorinating reaction, FeO/Fe_2O_3 is formed in the system. The results in chapter 3 confirm the feasibility of the conversion of neodymium oxide to neodymium fluoride using FeF_3 as fluorinating agent [17].

In Table 5.1 the standard Gibbs free energies of formation of the reacted fluorides and oxides in the system at 950°C, calculated using FactSage, are given. It is important to note that these reactions refer to the case of the reacting species at their standard state as pure substances. In the real systems, the activity of the components would be lower than unity. From Table 5.1 it is evident that iron fluoride has lower decomposition voltage than neodymium fluoride. Hence, from the thermodynamic perspective, two scenarios are possible for the formed iron fluoride generated in the system as the result of anodic dissolution. In one scenario iron fluoride acts as the fluorinating agent and converts Nd_2O_3 to NdF_3. Moreover, iron fluoride can undergo the electrolysis process and decompose along with Nd on the cathode, since NdF_3 has higher decomposition voltage. Hence the cathodic reactions would be:

$Fe^{3+} + 3e^- \rightarrow Fe$ / $Fe^{2+} + 2e^- \rightarrow Fe$ (5.5)

$Nd^{3+} + 3e^- \rightarrow Nd$ (5.6)

From Table 5.1 it can also be concluded that the dissolved neodymium oxide and iron oxide can participate in the electrochemical process resulting to Nd and Fe extraction on the cathode, respectively. Hence the solubility of these oxides plays a significant role on their participation in the electrochemical reaction process. In order to prevent the accumulation of the oxide in the LiF-Nd_2O_3 salt bath, the undissolved iron oxide should be removed from the system.

Table 5.1– Standard Gibbs free energies and the decomposition potential of different fluorides salts and REOs and REF_3

Reaction	ΔG^o(kJ/mol)	Decomposition potential (V)	ΔG^o(kJ/mol)
	at 950°C		at 25°C
$LiF \rightleftarrows Li + 1/2\ F_2(g)$	497	−5.2	584
$NdF_3 \rightleftarrows Nd(s) + 3/2F_2(g)$	1370	−4.7	1590
$FeF_3 \rightleftarrows Fe(s) + 3/2F_2(g)$	780	−2.7	972
$FeF_2 \rightleftarrows Fe(s) + F_2(g)$	538	−2.8	663
$Nd_2O_3 \rightleftarrows 2Nd + 3/2O_2(g)$	1464	−2.5	1718
$Fe_2O_3 \rightleftarrows 2Fe + 3/2O_2(g)$	508	−0.88	744

5.3 Experiments

Pure lithium fluoride (98.5%-Alfa Aesar) was used as the electrolyte bath and is mixed with neodymium oxide (Solvay) or neodymium fluoride or iron fluoride (97%-Alfa Aesar) in a glove box. A schematic of the experimental apparatus used for the electrochemical extraction of metals in molten salt [20] is shown in Figure 5.1. A graphite crucible served as the container of the mixtures. The crucible was placed in an electric furnace under the inert argon atmosphere. A water cooling system was used for both flanges at the top and bottom. All experiments were carried out at 950 °C within the limit of $\pm$ 3°C at the hot zone. A K-type thermocouple was used for the measurement of the temperature at the bottom of the graphite crucible.

5.3.1 Electrochemical behaviour of LiF-NdF_3/Nd_2O_3 systems

Cyclic voltammetry, chronopotentiometry and square wave voltammetry experiments were conducted using Parastat 4000 potentiostat (Ametek) and the data was recorded using Versastudio software. A molybdenum rod (2 mm diameter) was used as the

working electrode and the immersion depth of the Mo rod was measured after each experiment. The auxiliary electrode was an iron rod (silver steel 98% iron - Salomon metals, 3 mm diameter) or graphite. The potentials were referred to a 1 mm diameter platinum wire immersed in the molten electrolyte, acting as a quasi-reference electrode $Pt/PtO_x/O^{2-}$ [21].

5.3.2 Electrochemical extraction of Nd

Electrochemical extraction of Nd is carried out in $LiF\text{-}NdF_3$ and $LiF\text{-}Nd_2O_3$ systems. The metallic deposit on the molybdenum electrode after the experiments are analysed by Bruker D8 Advance X-Ray diffractometer (XRD) Bragg-Brentano geometry with graphite monochromator and Vantec position sensitive detector. Scanning Electron Microscopy (SEM) and Energy Dispersive Spectroscopy (EDS) are also performed to analyse the microstructure of the samples with a JEOL JSM 6500F (hot Field Emission Gun) equipped with a Thermo Noran Ultradry detector (40 mm^2 SDD crystal) using Noran System 7 data acquisition and analysis software. The electron beam is operated at 15 keV energy level with a beam current of about 1 nA. Some samples are also analysed with Wavelength Dispersive Spectroscopy (WDS) mapping (Jeol 7000F FEG-SEM).

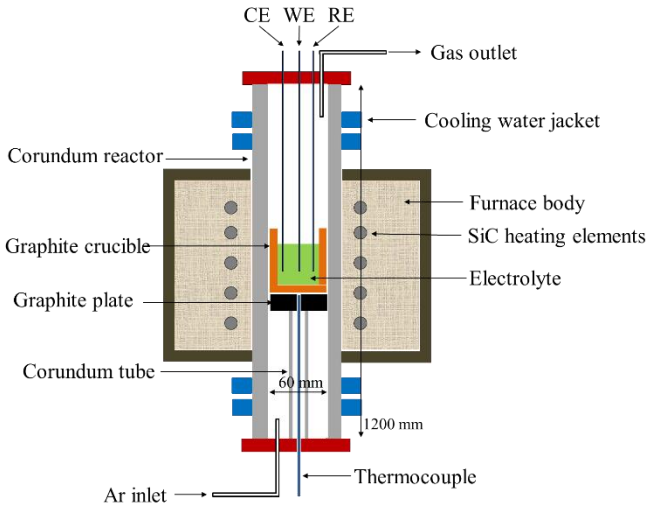

Figure 5.1– Schematic diagram of the experimental set-up for electrochemical extraction.

5.4 Results and Discussion

5.4.1 Electrochemical behaviour studies of different systems

Electrochemical dissolution of iron anode

In order to examine the use of iron as anode, it is important to investigate whether it is dissolved chemically or electrochemically in the molten salt. An iron bar is inserted in the LiF- 0.2 mol% Nd_2O_3 bath at 950 °C for 3 hours. The length and the mass of iron is not changed after 3 hours experiment, showing that iron is not chemically dissolved in the LiF molten salt. Moreover, the positive Gibbs free energies of the reactions of Fe with Nd_2O_3 and LiF in their standard states and as pure substances, shows that chemical dissolution of Fe in LiF-Nd_2O_3 is not feasible:

$3Fe + Nd_2O_3(s) \rightarrow 3FeO(s) + 2Nd$ ΔG^o [T=950 °C] = +911 kJ/mol (5.7)

$2Fe + Nd_2O_3(s) \rightarrow Fe_2O_3(s) + 2Nd$ ΔG^o [T=950 °C] = +960 kJ/mol (5.8)

$Fe + 2LiF \rightarrow FeF_2 + 2Li$ ΔG^o [T=950 °C] = +462 kJ/mol (5.9)

$Fe + 3LiF \rightarrow FeF_3 + 3Li$ ΔG^o [T=950 °C] = +763 kJ/mol (5.10)

On the contrary, when a current of 2 A is passed between the iron anode inserted 1 cm in the bath and Mo as the cathode in the molten salt electrolyte, after 840 s the cell potential suddenly decreased from -2.5 V and the electrolysis is terminated, showing that all the iron immersed in the salt is consumed (Figure 5.2). Considering the density of the iron bar, the weight of the immersed iron in the salt bath would be 0.55 g and based on Faraday's law, the iron mass dissolution in 840 s for *n=2* would be 0.48 g. This is expressed as

$$m = M\ It/(nF) \quad (5.11)$$

where m is the mass in grams, M is the molar mass in g.mol^{-1}, n is the number of exchanged electrons, F is the Faraday constant in C.mol^{-1}, I is the current in A and t is the time in s.

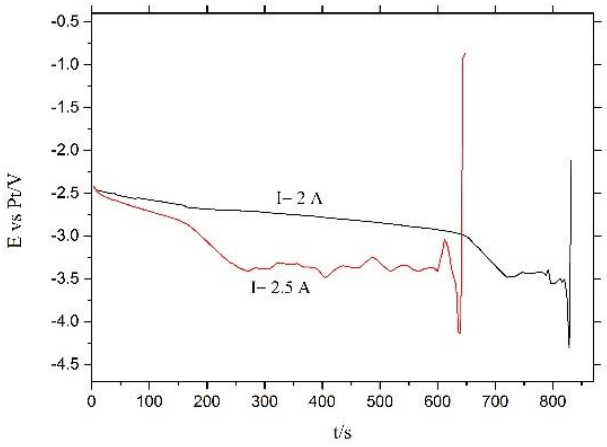

Figure 5.2– Change of cell potential with time between Fe anode (ϕ 3 mm) and Mo electrode (ϕ 2 mm) in LiF solvent at 950 °C at constant currents of 2 and 2.5 A.

LiF-NdF_3 system

Cyclic voltammetry is carried out on a molybdenum electrode in LiF–0.3mol%NdF_3 melt at 950 °C. LiF is chosen as the solvent since the deposition potential of the Li in the solvent is more cathodic than the deposition potential of Nd^{3+}. LiF is also the main solvent used in industry for the extraction of neodymium in molten fluoride process [6].

Reduction of Li^+ is the cathodic limit and oxidation of molybdenum is the anodic limit in the potential window of this system. The cyclic voltammogram of LiF-NdF_3 in Figure 5.3, recorded two peaks in the cathodic run at approximately −1.6 V and −2.3 V and two anodic peaks in the reverse run at approximately −2.2 V and −1.5 V versus the quasi-electrode $Pt/PtO_x/O^{2-}$. The cathodic peak at −1.6 V and the anodic peak at −1.5 V are associated with reduction and dissolution of neodymium, respectively. The stripping shape of the peaks is typical of deposition and dissolution of a metal. Based on this voltammogram, it is reasonable to assume that Nd^{3+} is reduced to Nd metal in a single step. It is suggested that Nd^{3+} ions are deposited from three-electron reduction of $[NdF_6]^{3-}$ in LiF salt [12]. The present observations are in agreement with the results from other researchers [22, 23] which show that the neodymium ion reduction is a single step reaction of Nd^{3+} to Nd metal. At further negative potentials to −2.3 V, an exponential increase of deposition current with no apparent peak is observed. This can be attributed to the decomposition of LiF. The corresponding anodic peak of lithium dissolution can be observed at approximately −2.2 V.

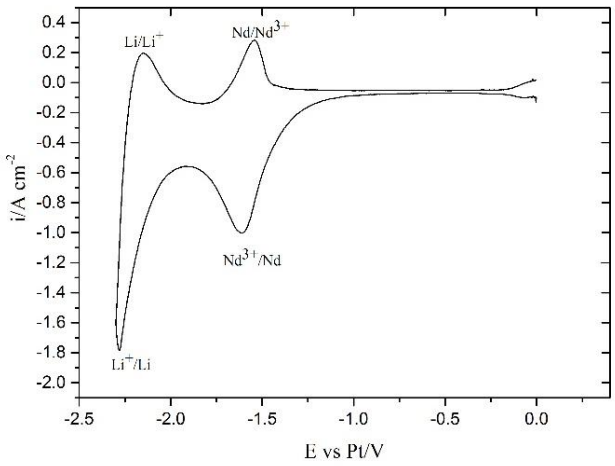

Figure 5.3– Cyclic voltammograms of LiF-0.3 mol% NdF_3 on a Mo electrode (ϕ 2 mm x 40 mm) at 950 °C, counter electrode: glassy carbon, reference electrode: Pt wire, scan rate: 100 mVs^{-1}.

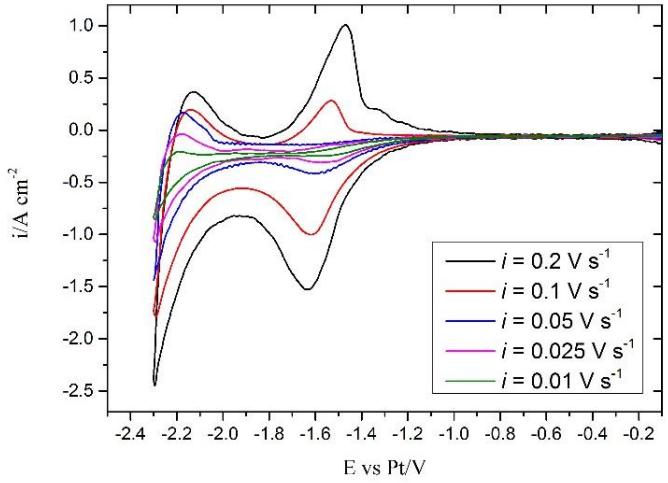

Figure 5.4– Cyclic voltammograms of LiF-0.3 mol%NdF_3 for different scan rates a Mo electrode (ϕ 2 mm x 40 mm) at 950 °C, counter electrode: glassy carbon, reference electrode: Pt wire

Figure 5.4 shows the cyclic voltammograms on the LiF-NdF_3 system at different potential scan rates (200 $mV.s^{-1}$). The intensity of the peaks is increased with increase in scan rate. The analysis of the curves in Figure 5.4 and the relationship between the peak currents and the square root of the scan rates indicates the reversibility of the system. A relationship between maximum intensity of the peak and the square root of the potential scan rate is suggested for the reversible systems [24]:

$$I_p = -0.61nFSC^o\ (nF/(RT))^{1/2}D^{1/2}v^{1/2} \quad (5.12)$$

where F is the Faraday constant (96500 C/mol), S the electrode area in cm^2, C^o the solute concentration in $mol.cm^{-3}$, n the number of exchanged electrons, D the diffusion coefficient in $cm^2\ s^{-1}$ and v the potential scanning rate in V s^{-1}. The reduction peak

current density versus square root of the potential scan rate is plotted in Figure 5.5. Based on the relationship between these two parameters, we can assume that LiF-NdF_3 system acts as a not fully reversible system but a quasi-reversible process. Hence the diffusion coefficient of Nd^{3+} ions can be calculated from the slope of the line in Figure 5.5 based on equation (5.12):

$$I_p/(S.\ v^{1/2}) = -0.61\, n\, FC^o\, (nF/(RT))^{1/2} D^{1/2} = -3.1\ \mathrm{A\ s^{1/2} V^{-1/2} cm^{-2}} \quad (5.13)$$

Assuming n=3 for Nd^{3+}/Nd reduction in one step, C^o= 5x10^{-4} mol.cm^{-3} and T=950 ^{o}C, the calculated diffusion coefficient is 4×10^{-5} cm^2 s^{-1} which is in good agreement with the result from Hamel et al. [22] being 1.3×10^{-5} cm^2 s^{-1}.

The number of exchanged electrons for a quasi-reversible system can be calculated based on

$$W_{1/2} = 3.52\, RT/(nF) \quad (5.14)$$

where $W_{1/2}$ is the width of the half peak in volts. R is the universal gas constant (8.314 J.mol^{-1}.K^{-1}), T is the temperature in K, n is the number of exchanged electrons. Using the square wave voltammetry technique, the width of the half peak is determined using OriginLab software and is shown in

Figure 5.6. Hence the number of exchanged electrons for neodymium is calculated to be 2.8, which confirms the exchange of 3 neodymium electrons in one step reduction.

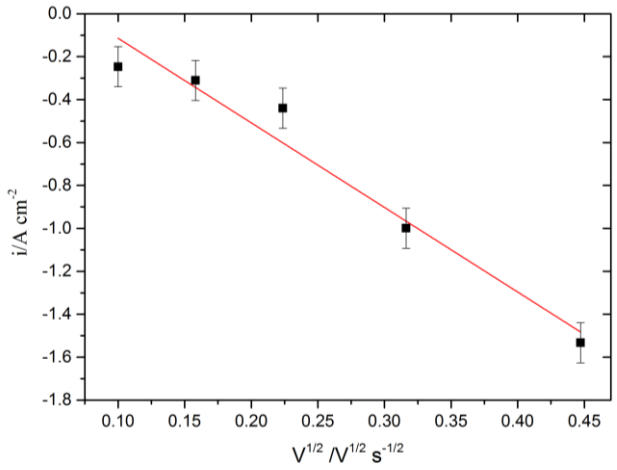

Figure 5.5– Linear relationship of Nd^{3+} reduction peak current density vs. the square root of the scanning potential rate of LiF-NdF_3 on Mo electrode (ϕ 2 mm x 40 mm); counter electrode: glassy carbon; reference electrode: Pt, T = 950 ^{o}C

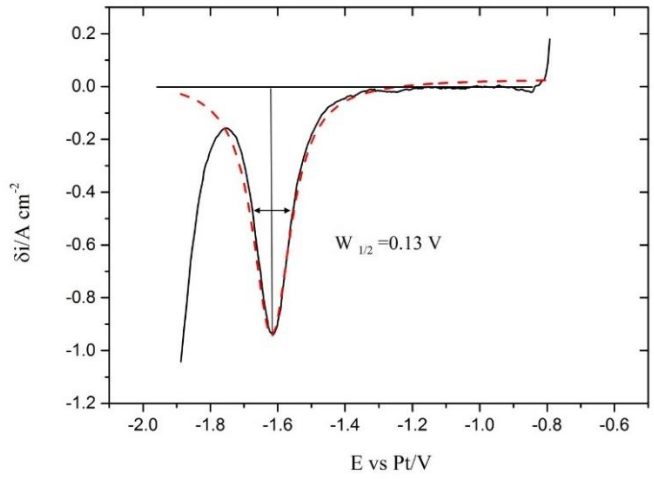

Figure 5.6– Square wave voltammogram of the LiF–0.3 mol. %NdF_3 mixture at 10 Hz. Determination of the width ($W_{1/2}$) of the half peak on Mo electrode (surface area = 0.25 cm²); counter electrode: glassy carbon; reference electrode: Pt; T = 950 °C.

The chronopotentiograms of LiF-NdF_3 system at different current densities are shown in Figure 5.7. Reduction of neodymium ions into metal starts in the same potential range as that observed on the cyclic voltammogram (−1.6 V) and the steady state is reached after 1 s. Hence the reduction of NdF_3 can be regarded a diffusion controlled process.

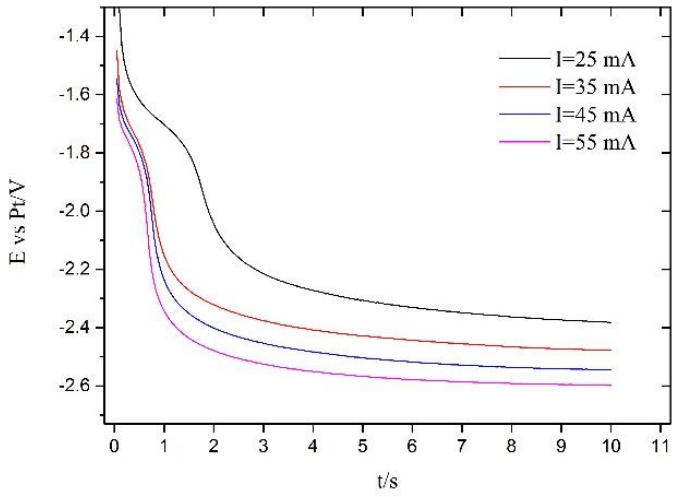

Figure 5.7– Chronopotentiograms of the system LiF–0.3 mol.% NdF_3 system on: Mo electrode (surface area = 0.25 cm²); counter electrode: glassy carbon; reference electrode: Pt; T = 950 °C.

LiF-FeF_3 system

The cyclic voltammetry is carried out on the LiF-FeF_3 system on a Mo electrode at 950 °C. The cyclic voltammogram of this system presented in Figure 5.8 shows three reduction peaks at the cathodic run at approximately –0.3 V, –0.85 V and –1.5 V, and the two dissolution peaks at the anodic run at approximately –0.7 V and –0.4 V. The first two peaks in the cathodic run and the peaks at the anodic run are associated with the reduction and dissolution of iron, respectively. It can be assumed that the reduction of Fe^{3+} to Fe is a two-step process, first from Fe^{3+} to Fe^{2+} at –0.3 V and secondly from Fe^{2+} to metallic iron at -0.85 V:

$$Fe^{3+} + e^- \rightleftarrows Fe^{2+} \quad (5.1)$$

$$Fe^{2+} + 2e^- \rightleftarrows Fe \quad (5.2)$$

The peak at -1.5 V is the Li reduction, however there is no peak related to oxidation of Li to Li^+. It is to be noted that, as mentioned earlier, the Li reduction peak in LiF-NdF_3 system was found at -2.3 V. However, in the case of LiF-FeF_3 system, Li reduction takes place at more positive potential of -1.5 V. This difference can be explained with regard to the surface layer of the reduction. In the case of LiF-NdF_3 system, Li is reduced on the Nd, while in the LiF-FeF_3, Li reduction takes place on the Fe layer which is already formed on the Mo.

The anodic peaks in the reverse run are associated to the dissolution of Fe, first to Fe^{2+} and then to Fe^{3+}. There is a small peak at approximately –0.43 V in the cathodic run which can be related to the reduction of possible contamination of the salt.

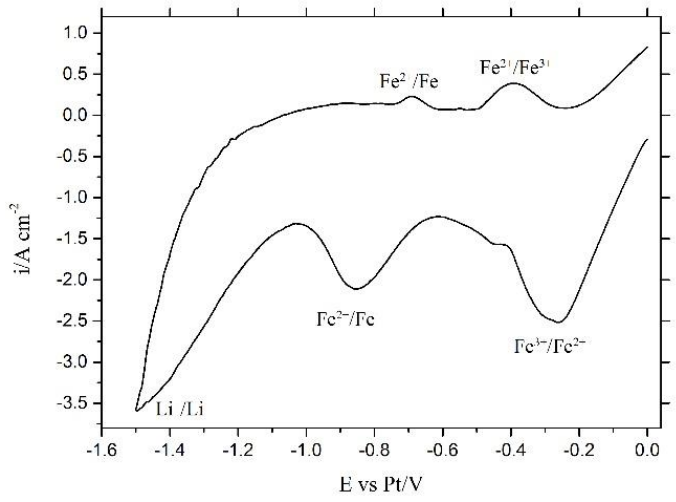

Figure 5.8– Cyclic voltammograms of LiF-0.5 mol%FeF_3 on a Mo electrode (ϕ 2 x 40 mm) at 950 °C, counter electrode: glassy carbon, reference electrode: Pt wire, scan rate: 100 mVs^{-1}

LiF-Nd_2O_3 system

Cyclic voltammetry is performed in LiF-Nd_2O_3 system at 950 °C on molybdenum working electrode using graphite as the counter electrode and $Pt/PtO_x/O^{2-}$ as quasi-reference electrode. The voltammogram is shown in Figure 5.9. The observed cathodic limit at approximately −1.5 V is assumed to be lithium fluoride and a sharp oxidation peak (approximately −1.38 V) on the anodic run are associated with the reverse reaction on molybdenum electrode. No other peak related to neodymium reduction or dissolution is present in the LiF-Nd_2O_3 voltammogram. Stefanidaki et al. [12] have claimed that the formation of neodymium oxyfluoride in the LiF-Nd_2O_3 system prohibits the neodymium reduction [25], hence Nd_2O_3 cannot be used for Nd extraction in the absence of NdF_3 in the electrolyte.

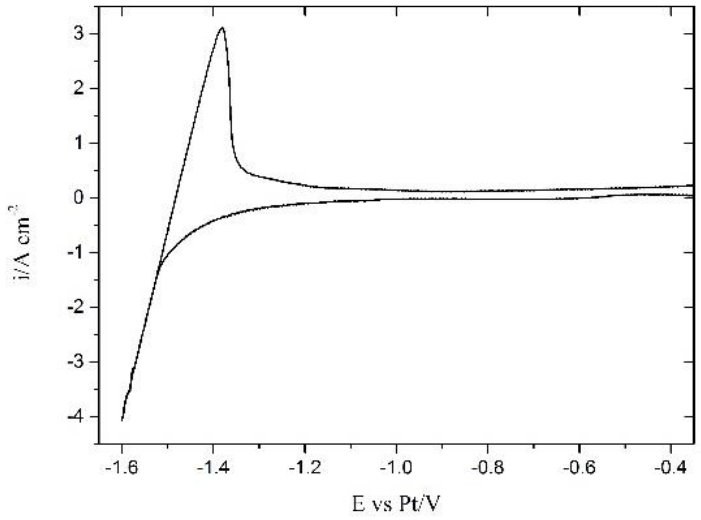

Figure 5.9– Cyclic voltammograms of LiF-Nd_2O_3 on a Mo electrode (ϕ 2 mm x 40mm) at 950 °C, counter electrode: glassy carbon, reference electrode: Pt wire, scan rate: 100 mVs^{-1}

5.4.2 Nd extraction in LiF-NdF_3 using iron anode

Nd electrochemical extraction in LiF-10 mol% NdF_3 is performed at 950 °C using Mo as cathode and Fe as anode. First cyclic voltammetry on the Mo cathode is performed to measure the decomposition voltage of NdF_3 which is found to be −1.59 V. Subsequently, electrodeposition is performed at a constant potential mode of −1.7 V. The changes of current with time is recorded and is shown in Figure 5.10. It can be seen that after about 3 hours (10 ks), the current reaches zero which shows that the iron bar inserted in the salt bath is dissolved in the bulk. The inserted graph in this figure is the cyclic voltammetry of the system, which was performed at the beginning of the experiment to obtain the decomposition voltage of the Nd extraction on the Mo working electrode.

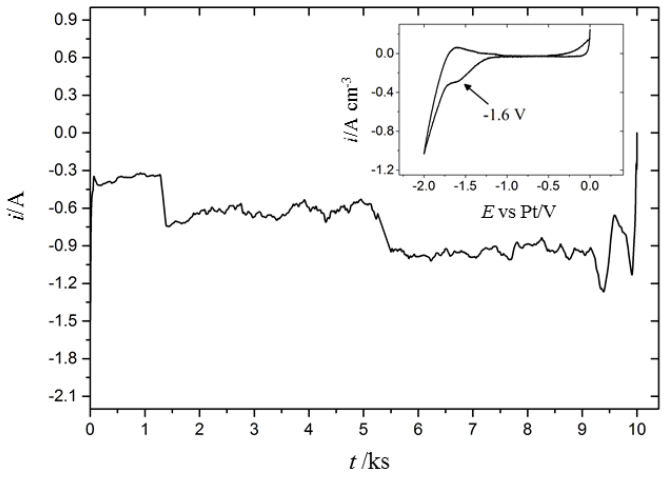

Figure 5.10– Changes of current with time in the –1.7 V constant cell potential mode of Nd electrolysis in LiF-NdF_3 using Fe as anode.

A metallic layer is seen after the experiment on the surface of the salt bath under the anode. This layer is analysed by XRD and the results are shown in Figure 5.11. The XRD results show that there is an accumulation of Fe in the form of $FeC_{0.053}$ and $Fe_{1.86}C_{0.14}$ in vicinity of the Fe anode as the result of anodic dissolution. These phases are marked as Fe(C) on the XRD graph. The peaks related to LiF and NdF_3 are marked as salt phase on the XRD graph. The formation of carbide might be due to the carbon presence in iron (silver steel that is used as iron anode contains about 0.95% carbon). The use of graphite crucible can also explain the presence of carbon in the salt bath.

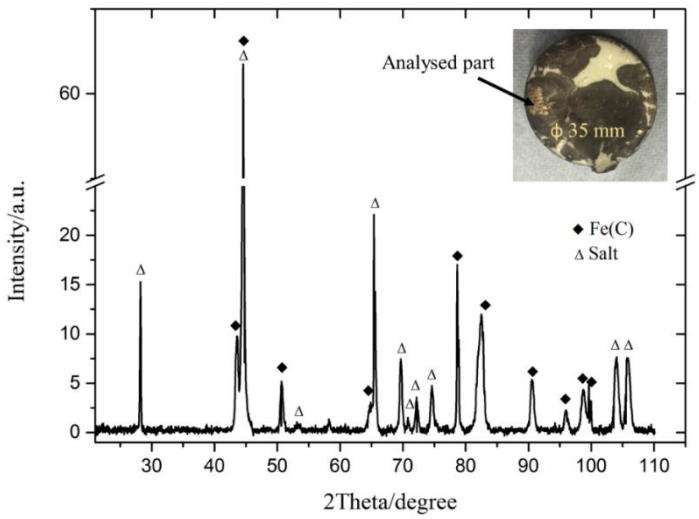

Figure 5.11– XRD result of the part of the salt under the Fe anode in LiF-NdF_3 salt bath.

The cathodic product on the Mo cathode is analysed by SEM/EDS after the experiment. The EDS analysis of the sample shows that the deposition of Nd and Fe on the Mo cathode, as is shown in Figure 5.12. In order to investigate the distribution of the Nd and Fe on the cathode, an EDS mapping is performed which is shown in Figure 5.13. It can be concluded from the EDS quantification and the mappings that an Fe rich Nd-Fe-Mo phase is formed on the cathode. From these results we can see the formation of $Fe_{15}Nd$ and $Fe_{17}Nd_2$ and $Fe_{16.2}Nd_2$ phases. However, it is noticed in Figure 5.12 that the concentration of Mo in the phases close to the cathode is high (21 at%). In the Fe-Nd binary phase diagram, which is shown in Figure 5.14, $Fe_{17}Nd_2$ and $Fe_{17}Nd_5$ are intermetallic compounds [26]. The existence of the Fe_2Nd is also indicated [27].

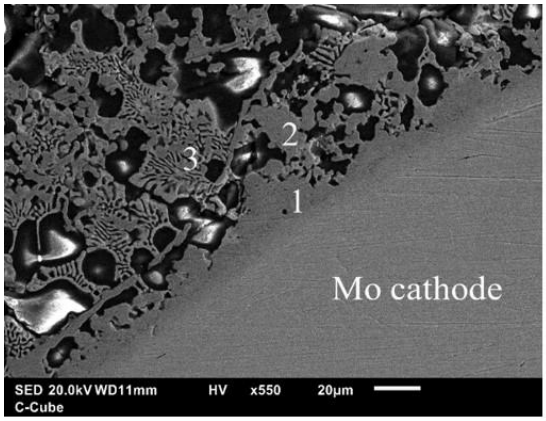

Points	Fe	Nd	Mo
1	73	5	21
2	80	10	10
3	72	9	13

Figure 5.12– SEM image and EDS quantification (in at%) of the deposit on the cathode showing the formation of Fe-Nd alloy

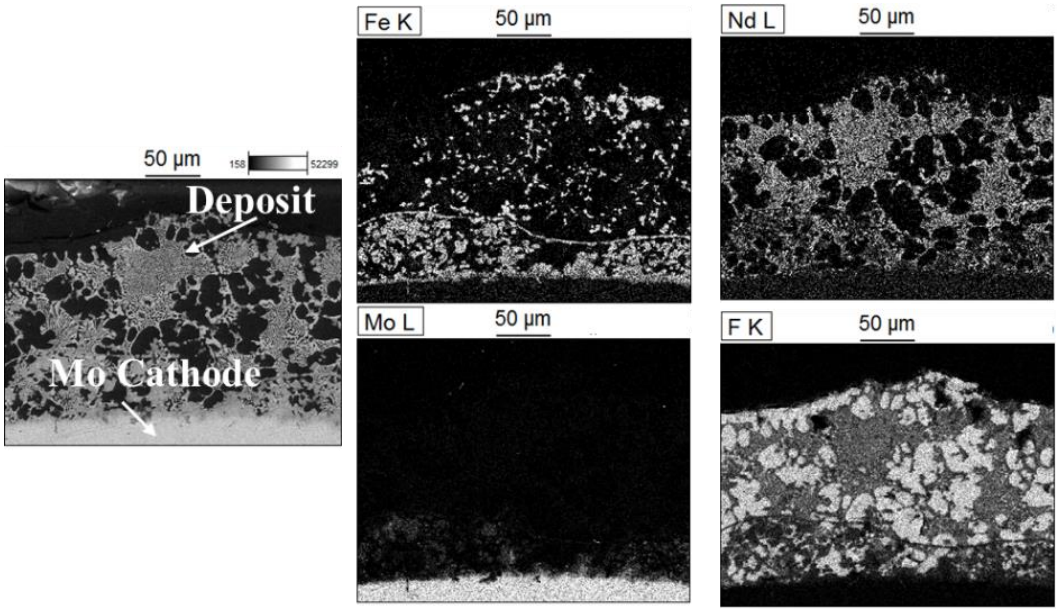

Figure 5.13– Elemental EDS mapping of the deposit on the cathode showing the distribution of Nd-Fe-F on the Mo cathode.

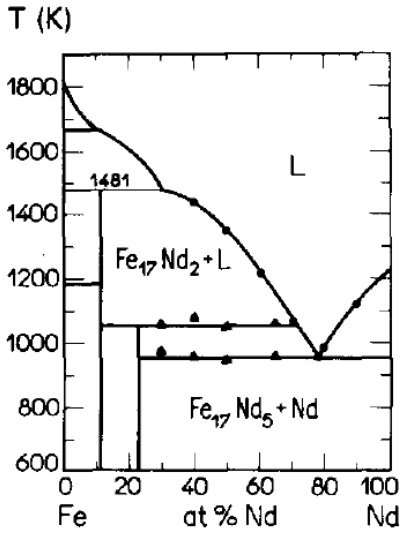

Figure 5.14– The Fe-Nd binary phase diagram [28].

5.4.3 Nd extraction in LiF-Nd_2O_3 using iron anode

The feasibility of FeF_3 formation in LiF-Nd_2O_3 system is shown based on thermodynamic calculations in section 5.2. It is shown that FeF_3 can be generated *in situ* in the system and it converts the Nd_2O_3 to NdF_3. Subsequently the formed NdF_3 will be subjected to electrolysis and Nd can be extracted on Mo cathode. The extraction of Nd from Nd_2O_3 using Fe anode is performed at 950 ^oC under argon atmosphere. The electrodeposition is performed at a constant potential mode of –1.7 V for 3 hours. A Mo bar is used as the cathode and 0.1 mol% FeF_3 is used in the LiF-Nd_2O_3 salt to initiate the fluoride ion formation in the electrolyte. The deposited material on the Mo electrode and the composition of the bulk are analysed by XRD and WDS and are shown in Figure 5.15 and Figure 5.16, respectively.

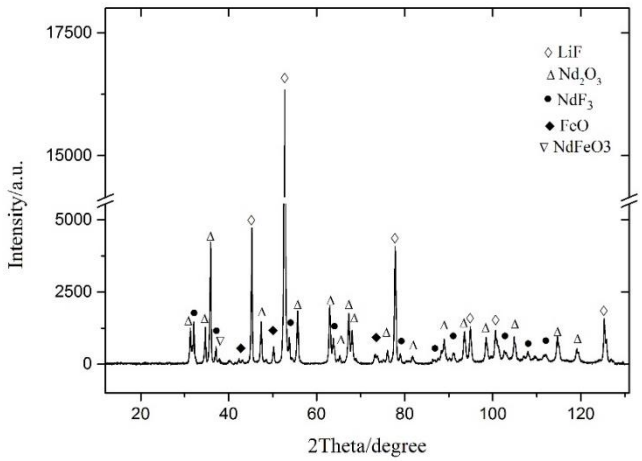

Figure 5.15– XRD result of the sample of LiF-Nd_2O_3-FeF_3 electrolyte after electrolysis with iron anode and Mo cathode.

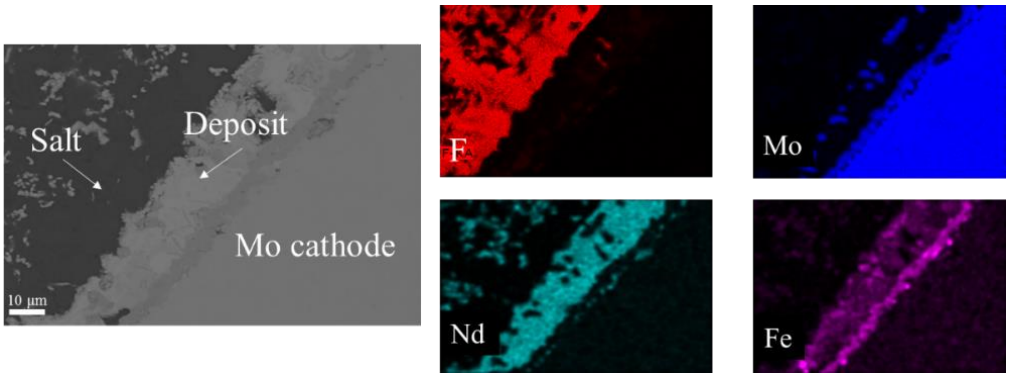

Figure 5.16– WDS mapping of the deposit on the cathode in of LiF-Nd_2O_3-0.1 mol%FeF_3 using Fe as anode.

Once the electrolysis starts, FeF_3 decomposes and metallic Fe is reduced on the Mo cathode as the result of cathodic reaction (5.5) and anodic dissolution of iron is initiated in the anodic part, leading to the formation of FeF_2 and FeF_3 based on reactions (5.1)-(5.2). The WDS mapping in Figure 5.16 also clearly shows the formation of Fe layer as the first deposited layer on the Mo cathode. Once FeF_2 and FeF_3 are formed in the system, they participate in the fluorination process of Nd_2O_3 based on reactions (5.3)-(5.4).

From this reaction, the formation of FeO and Fe_2O_3 would be expected. The XRD results in Figure 5.15 show the presence of Fe in the form of FeO (wüstite) and also $NdFeO_3$ phase in the samples from molten salt. Presence of NdF_3 shows that fluorination reaction of Fe has taken place.

In the WDS mapping in Figure 5.16 Nd and Fe co-deposition can be seen on the Fe layer. Decomposition of NdF_3 might occur at more positive potentials since Nd-Fe alloy is

reduced in a potential range between the deposition of pure Nd and Fe. This phenomenon has been studied on the Ti-B, Zr-B, Ta-B, Sm-Co, Ti-Nb and Nd-Al alloy formation by different research groups [29-33]. In all above-mentioned systems, the electrodeposition voltammogram peak of these compounds is identified in a potential between their corresponding pure metals.

Iron fluoride that is formed in the system as the result of anodic dissolution can either be decomposed through the electrochemical reaction or convert the Nd_2O_3 to NdF_3 through the chemical reaction. The applied cell potential for decomposition of NdF_3 would be enough for both FeF_2 and FeF_3 decomposition since they have more positive decomposition voltage. The negative Gibbs free energy of the reaction at 950 ^oC shows the feasibility of the Nd_2O_3 to NdF_3 conversion by FeF_3 which is also experimentally investigated as a part of this project in our group [17, 34, 35]. The Nd-Fe alloy formation from WDS results in LiF-Nd_2O_3 system shows that Fe participates in the electrochemical process. It is to be noted that, while the present results identify the electrochemical reactions involved in the deposition of Nd as well as Fe-Nd alloys, the parallel chemical reactions (5.3)-(5.4) cannot be ruled out. The presence of FeO and NdF_3 shown in the XRD results shows that the conversion has taken place. Further experiments need to be conducted to investigate the impact of the chemical reactions on the overall process. Moreover, design of a set-up in which the accumulated iron oxide is removed from the salt bath is of great importance for the continuity of the process.

5.5 Conclusion

During the extraction of neodymium by electrolytic deposition, problems associated with the choice of the suitable halide, generation of CO, CO_2 and fluorocarbon gases and the low solubility of the neodymium oxide in molten fluorides are solved by fluorinating the oxide to fluoride and the use of reactive anode. In this study, a novel method is adopted in which iron is used as anode, promoting electrochemical dissolution of iron into the melt, thus preventing CO, CO_2 and fluorocarbon gas evolution at the anode. Thus, the fluorinating agent is constantly regenerated *in situ*, which enables the continuous conversion of neodymium oxide feed to the corresponding fluoride. Once neodymium fluoride is formed, it is possible to electrolyze and deposit Nd on the cathode. The cathodic product is Nd-Fe alloy which can be directly used as a master alloy for the production of NdFeB magnets. Furthermore, more research is needed to investigate the parallel chemical reactions of fluorination by FeF_3 on the overall process and the chemical composition of the cathode product.

5.6 References

[1] Yang, Y., Walton, A., Sheridan, R., Güth, K., Gauß, R., Gutfleisch, O., Buchert, M., Steenari, B.-M., Van Gerven, T., Jones, P. T., and Binnemans, K., 2017, "REE Recovery from End-of-Life NdFeB Permanent Magnet Scrap: A Critical Review," Journal of Sustainable Metallurgy, 3(1), pp. 122-149.

[2] Hirota, K., Okabe, T. H., Saito, F., Waseda, Y., and Jacob, K. T., 1999, "Electrochemical deoxidation of RE–O (RE=Gd, Tb, Dy, Er) solid solutions," Journal of Alloys and Compounds, 282(1–2), pp. 101-108.

[3] Claux, B., Serp, J., and Fouletier, J., 2011, "Electrochemical reduction of cerium oxide into metal," Electrochimica Acta, 56(7), pp. 2771-2780.

[4] Wang, D., Qiu, G., Jin, X., Hu, X., and Chen, G. Z., 2006, "Electrochemical Metallization of Solid Terbium Oxide," Angewandte Chemie International Edition, 45(15), pp. 2384-2388.

[5] Chen, G. Z., Fray, D. J., and Farthing, T. W., 2000, "Direct electrochemical reduction of titanium dioxide to titanium in molten calcium chloride," Nature, 407, pp. 361-364.

[6] Siming, P., Shihong, Y., Zongan, L., Dehon, C., Liha, X., and Bin, Z., 2011, "Development on Molten Salt Electrolytic Methods and Technology for Preparing Rare Earth Metals and Alloys in China," Chinese Journal of Rare Metals, 35(3), pp. 440-450.

[7] Seetharaman, S., and Grinder, O., 2010, US patent application nr. 12/991128, ref. no.: 12057

[8] Abbasalizadeh, A., Seetharaman, S., Teng, L., Sridhar, S., Grinder, O., Izumi, Y., and Barati, M., 2013, "Highlights of the Salt Extraction Process," Journal Of Materials, 65(11), pp. 1552-1558.

[9] Morrice, E., and Henrie, T. A., 1967, Electrowinning high-purity neodymium, praseodymium, and didymium metals from their oxides, U.S. Dept. of the Interior, Bureau of Mines, Washington D.C.

[10] Murphy, J. E., Dysinger, D. K., and Chambers, M. F., "Electrowinning neodymium metal from chloride and oxide-fluoride electrolytes," Proc. Light Metals: Proceedings of Sessions, TMS Annual Meeting, Warrendale, Pennsylvania, pp. 1313-1320.

[11] Porter, B., and Brown, E. A., 1961, Determination of oxide solubility in molten fluorides, U.S. Dept. of the Interior, Bureau of Mines, Washington, DC.

[12] Stefanidaki, E., Hasiotis, C., and Kontoyannis, C., 2001, "Electrodeposition of neodymium from LiF-NdF_3-Nd_2O_3 melts," Electrochimica Acta, 46(17), pp. 2665-2670.

[13] Thudum, R., Srivastava, A., Nandi, S., Nagaraj, A., and Shekhar, R., 2010, "Molten salt electrolysis of neodymium: electrolyte selection and deposition mechanism," Mineral Processing and Extractive Metallurgy, 119(2), pp. 88-92.

[14] Kaneko, A., Yamamoto, Y., and Okada, C., 1993, "Electrochemistry of rare earth fluoride molten salts," Journal of Alloys and Compounds, 193, pp. 44-46.

[15] Taxil, P., Massot, L., Nourry, C., Gibilaro, M., Chamelot, P., and Cassayre, L., 2009, "Lanthanides extraction processes in molten fluoride media: Application to nuclear spent fuel reprocessing," Journal of Fluorine Chemistry, 130(1), pp. 94-101.

[16] Zhu, H., 2014, "Rare Earth Metal Production by Molten Salt Electrolysis," Encyclopedia of Applied Electrochemistry, G. Kreysa, K. Ota, and R. Savinell, eds., Springer New York, pp. 1765-1772.

[17] Abbasalizadeh, A., Malfliet, A., Seetharaman, S., Sietsma, J., and Yang, Y., 2017, "Electrochemical Extraction of Rare Earth Metals in Molten Fluorides: Conversion of Rare Earth Oxides into Rare Earth Fluorides Using Fluoride Additives," Journal of Sustainable Metallurgy, 3(3), pp. 627-637.

[18] Haarberg, T., Solheim, A., Johansen, S. T., and Solli, P. A., 1998, "Effect of anodic gas release on current efficiency in Hall-Héroult cells," Light Metals pp. 475-482.

[19] Haupin, W. E., 1983, "Electrochemistry of the Hall-Heroult process for aluminum smelting," Journal of Chemical Education, 60(4), p. 279.

[20] Xu, L., 2016, "Electrochemical behavior of zirconium in molten LiF-KF-ZrF_4 at 600° C," RSC Advances, 6(87), p. 84472.

[21] Berghoute, Y., Salmi, A., and Lantelme, F., 1994, "Internal reference systems for fused electrolytes," Journal of Electroanalytical Chemistry, 365(1), pp. 171-177.

[22] Hamel, C., Chamelot, P., and Taxil, P., 2004, "Neodymium(III) cathodic processes in molten fluorides," Electrochimica Acta, 49(25), pp. 4467-4476.

[23] Nohira, T., Kobayashi, S., Kobayashi, K., Hagiwara, R., Oishi, T., and Konishi, H., 2010, "Electrochemical Formation of Nd-Ni Alloys in Molten LiF-CaF_2-NdF_3," ECS Transactions, 33(7), pp. 205-212.

[24] Store, T., 1999, "PhD Thesis," Norwegian University of Science and Technology, Department of Electrochemistry, p. 22.

[25] Stefanidaki, E., Photiadis, G. M., Kontoyannis, C. G., Vik, A. F., and Østvold, T., 2002, "Oxide solubility and Raman spectra of NdF_3-LiF-KF-MgF_2-Nd_2O_3 melts," Journal of the Chemical Society, Dalton Transactions(11), pp. 2302-2307.

[26] Chen, T. L., Wang, J., Rong, M. H., Rao, G. H., and Zhou, H. Y., 2016, "Experimental investigation and thermodynamic assessment of the Fe-Pr and Fe-Nd binary systems," Calphad, 55, pp. 270-280.

[27] Santos, I. A., and Gama, S., 1999, "Evidence for the stable existence of the Fe2Nd phase in the Fe-Nd system," Journal of Applied Physics, 86(4), pp. 2334-2336.

[28] Landgraf, F. J. G., Schneider, G. S., Villas-Boas, V., and Missell, F. P., 1990, "Solidification and solid state transformations in Fe-Nd: A revised phase diagram," Journal of the Less Common Metals, 163(1), pp. 209-218.

[29] Wendt, H., Reuhl, K., and Schwarz, V., 1992, "Cathodic deposition of refractory intermetallic compounds from flinak-melts—I. Voltammetric investigation of Ti, Zr, B, TiB_2 and ZrB_2," Electrochimica Acta, 37(2), pp. 237-244.

[30] Makarova, O., Polyakova, L., Polyakov, E., Shevyryov, A., & Arakcheeva, A., 2003, "Phase composition of cathodic deposits synthesized in FLINAK-K_2TaF_7-KBF_4 melt," Journal of Mining and Metallurgy B: Metallurgy, 39(1-2), pp. 261-267.

[31] Iida, T., Nohira, T., and Ito, Y., 2003, "Electrochemical formation of Sm–Co alloys by codeposition of Sm and Co in a molten LiCl–KCl–$SmCl_3$–$CoCl_2$ system," Electrochimica Acta, 48(17), pp. 2517-2521.

[32] Polyakova, L. P., Taxil, P., and Polyakov, E. G., 2003, "Electrochemical behaviour and codeposition of titanium and niobium in chloride–fluoride melts," Journal of Alloys and Compounds, 359(1), pp. 244-255.

[33] Gibilaro, M., Massot, L., Chamelot, P., and Taxil, P., 2008, "Study of neodymium extraction in molten fluorides by electrochemical co-reduction with aluminium," Journal of Nuclear Materials, 382(1), pp. 39-45.

[34] Aida Abbasalizadeh , A. M., Seshadri Seetharaman, Jilt Sietsma, Yongxiang Yang, 2017, "Electrochemical recovery of rare earth elements from magnets: conversion of rare earth based metals into rare earth fluorides in molten salts," Materials transactions, 48(7).

[35] Abbasalizadeh, A., Teng, L., Seetharaman, S., Sietsma, J., and Yang, Y., 2015, "Rare earth extraction from NdFeB magnets and rare earth oxides using aluminium chlorie/fluoride molten salts," Rare Earths Industry: Technological, Economic, and Environmental Implications, D. Lima, I. Borges, and W. Leal Filho, eds., Elsevier, p. 357.

Chapter 6 Thermodynamic modelling of LiF-NdF_3-DyF_3 system

Abstract

Electrolysis of molten fluorides is one of the promising methods for the recovery and recycling of rare earth metals from used magnets. Due to the dearth of phase equilibria data for molten fluoride systems, thermodynamic modelling of LiF-DyF_3-NdF_3 system using the CALPHAD approach is carried out. Gibbs energy modelling for LiF-NdF_3 and LiF-DyF_3 systems is performed using the constitutional data from literature. Ab initio calculations are used to obtain enthalpy of formation of $LiDyF_4$, an intermediate phase that is found to exist in the LiF-DyF_3 system. Differential thermal analysis is carried out for selected compositions in the NdF_3-DyF_3 system, in order to determine liquidus and solidus temperatures. The Gibbs energy parameters for the limiting binary phase diagrams determined in this work is used for modelling the Gibbs energy functions of equilibrium phases in the ternary system. Selected compositions of LiF-NdF_3-DyF_3 are investigated by Differential Thermal Analysis (DTA) in order to validate the calculated phase temperatures involving melt.

Keywords: Calphad, phase equilibria, LiF-DyF_3, DyF_3-NdF_3, LiF-NdF_3, LiF-DyF_3-NdF_3, DTA

Chapter 6 is based on the published scientific paper:

A. Abbasalizadeh, S. Sridar, Z. Chen, M. Sluiter, Y. Yang, J. Sietsma, S. Seetharaman and K.C. Hari Kumar, Journal of Alloys and compounds, 2018, (753), 388

6.1 Introduction

Rare earth elements are essential in the green and low-carbon economy due to their superior magnetic properties. They play a key role in hybrid and electric vehicle industries as well as in wind turbines and many other high-tech applications [1]. Neodymium along with dysprosium are expected to dominate the future of magnetic material industry, increasing their demand over the next 25 years by 700 and 2600%, respectively [2-4]. Due to the uneven distribution of the resources and recent issues in the supply and demand of the rare earth metals, demand for recovery of these metals from waste products is strongly rising.

Molten salt electrolysis process is the dominant industrial method for extraction of rare earth elements [5]. Electrolysis of molten fluorides has been the subject of many studies on the recovery of rare earth metals [6-8]. Evolution of fluorine associated gasses (fluorocarbons), low solubility of the rare earth oxide in the fluoride electrolytes and formation of oxyfluoride complexes are the challenges of the recovery of the rare earth elements which were discussed in the previous chapters.

In order to optimally design such processes, knowledge of phase equilibria and thermodynamics of molten fluorides system is crucial. However, there is a dearth of such information in the literature. In this chapter, we report thermodynamic modelling of the LiF-DyF_3-NdF_3 system using the CALPHAD approach.

6.2 Experiments

In order to investigate the phase transformation temperatures for NdF_3-DyF_3 binary and LiF-NdF_3-DyF_3 ternary system, differential thermal analysis (DTA) is carried out. Anhydrous LiF (99.98% - Alfa Aesar, USA), DyF_3 (99.9% - Alfa Aesar, USA) and NdF_3 (99.9% - Alfa Aesar, USA) are used for preparing the samples for thermal analysis. Various compositions investigated in the NdF_3-DyF_3 and LiF-DyF_3-NdF_3 systems are listed in Table 6.1 and Table 6.2, respectively. The samples are prepared by mixing the chemicals in a glove box and heating the mixture to a temperature above the melting point under Ar atmosphere and subsequently quenching the molten mixture using liquid nitrogen.

DTA is carried out using Netzsch STA 409C apparatus with DTA/TG sample carrier. The instrument is calibrated by measuring the melting point of high purity metals such as Al, Ag, Au, Ni and Sn [9]. The signal related to temperature difference between the sample and the reference measured by DTA is converted into heat flux difference by means of appropriate calibration. Hence the DTA results are reported as heat flux change with temperature. Each sample (weighing between 60 and 90 mg) is loaded in a platinum cup with a lid because of the corrosive character of fluoride salts. The platinum cup is positioned inside an alumina crucible. An empty alumina crucible serves as the reference material. For each experiment, three cooling and heating runs are carried out. Heating rate is fixed at 10 K min^{-1}, based on the instability of the fluoride salts. All

experiments are carried out under high purity nitrogen atmosphere with a flow rate of 40 $ml.min^{-1}$.

6.3 Experimental results

6.3.1 Thermal analysis

The extrapolated onset temperature is less affected by heating rate and other experimental factors in comparison with offset temperature [10]. Hence, the DTA peaks are analysed using the onset technique [11] in order to determine the phase transformation temperatures. Liquidus and solidus temperatures thus calculated from the heating and cooling curves, respectively, have an uncertainty of ± 8 K. The uncertainty is high due to the instability of the fluoride system and the difference between the second and third heating/cooling cycles.

DTA curves of NdF_3-DyF_3 samples (Figure 6.1(a)) do not show any solid state transformation, which could be due to the small enthalpy of the orthorhombic to hexagonal transformation in DyF_3 [12]. The results from DTA analysis for the NdF_3-DyF_3 mixtures indicate complete solubility of NdF_3 and DyF_3 and provide no evidence for any solid state phase transformation. All samples show only one peak in the heating curve corresponding to the solidus. Results are given in Table 6.1. The maximum weight loss of the samples measured by thermogravimetric analysis (TGA), is 1.43%.

The phase transformation temperature for the LiF-DyF_3-NdF_3 system is also obtained using the DTA. In Figure 6.1(b), the DTA curves corresponding to LiF-30 mol% NdF_3-30 mol% DyF_3 composition show two peaks. The transformation temperatures are measured to be 955 and 1053 K, respectively. Except for LiF-30 mol%NdF_3-30 mol%DyF_3, all DTA results for the ternary compositions show one peak while three thermal events are expected for each composition. High heating rate and mass loss in the samples can be two of the possible reasons that these transitions are not captured by DTA. Because of the high evaporation of salts, especially LiF, which results in the mass loss of the samples, reliable measurement of the transformation temperatures of LiF-DyF_3-NdF_3 system using DTA is difficult. The mass loss of the samples increases with the increase in the amount of LiF in the samples. For the sample LiF-10 mol% NdF_3-10 mol% DyF_3, the mass loss is measured to be about 34%. Moreover, in ternary

Table 6.1– Solidus and liquidus of NdF_3-DyF_3 measured by DTA and calculated by Calphad.

Composition (mol% DyF_3)	Solidus (K) experimental / modelled	Liquidus (K) experimental / modelled
20	1569 / 1603	1646 / 1640
40	1519 /1491	1606 / 1612
60	1449 /1444	1549 / 1560
80	1418 /1429	1492 / 1465

Table 6.2– Experimental (DTA) and calculated temperatures of phase transformations for LiF-NdF_3-DyF_3.

Composition		Temperature (K)		
(mol% DyF_3)	(mol% LiF)	Experimental	Calculated	Phase transformation
10	80	982	981	L+Cub⇄L+Cub+Hex
20	60	948	955	L⇄Cub+Hex+LiDyF4
40	40	1063	1063	L+Hex⇄L+Hex+LiDyF4
30	40	1053	1045	L+Hex⇄L+Hex+LiDy4
20	20	1038	1037	L+Hex⇄L+Hex+LiDyF4

systems some of the compositions go through four-phase as well as three-phase regions in addition to the two-phase region before melting is completed. Some of these events are not necessarily captured in a DTA experiment. Hence, the DTA results are only used for comparing with the calculated results. The liquidus temperature determined by DTA results for all ternary compositions are listed in Table 6.2.

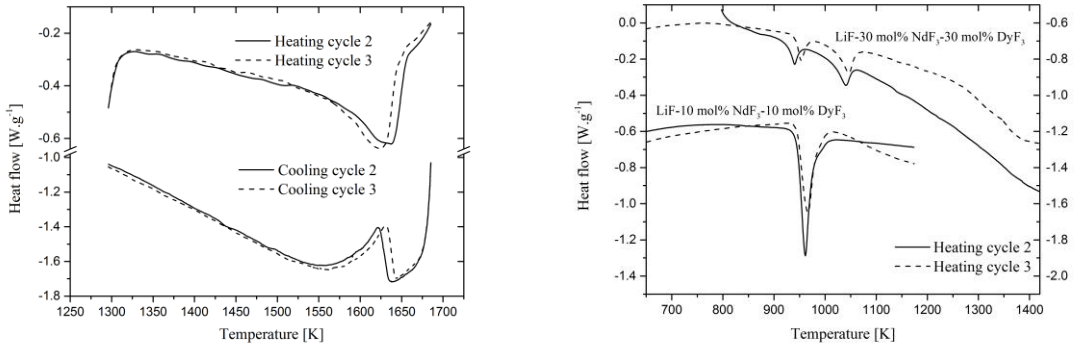

(a) NdF_3-20 mol% DyF_3 (b) LiF-DyF_3-NdF_3

Figure 6.1– DTA thermograms of representative compositions.

6.3.2 Microstructure analysis

In order to investigate the solubility of the solid phase at high temperatures in the NdF_3-DyF_3 system, the samples are heated below the liquidus temperature and quenched in liquid nitrogen. The quenched samples are investigated by SEM/EDS to determine the phases present at various compositions of NdF_3-DyF_3. The results (Figure 6.2) show the presence of a single phase in all investigated samples, proving extended solid solubility just below their solidus. No evidence of phase separation could be detected in any of the samples.

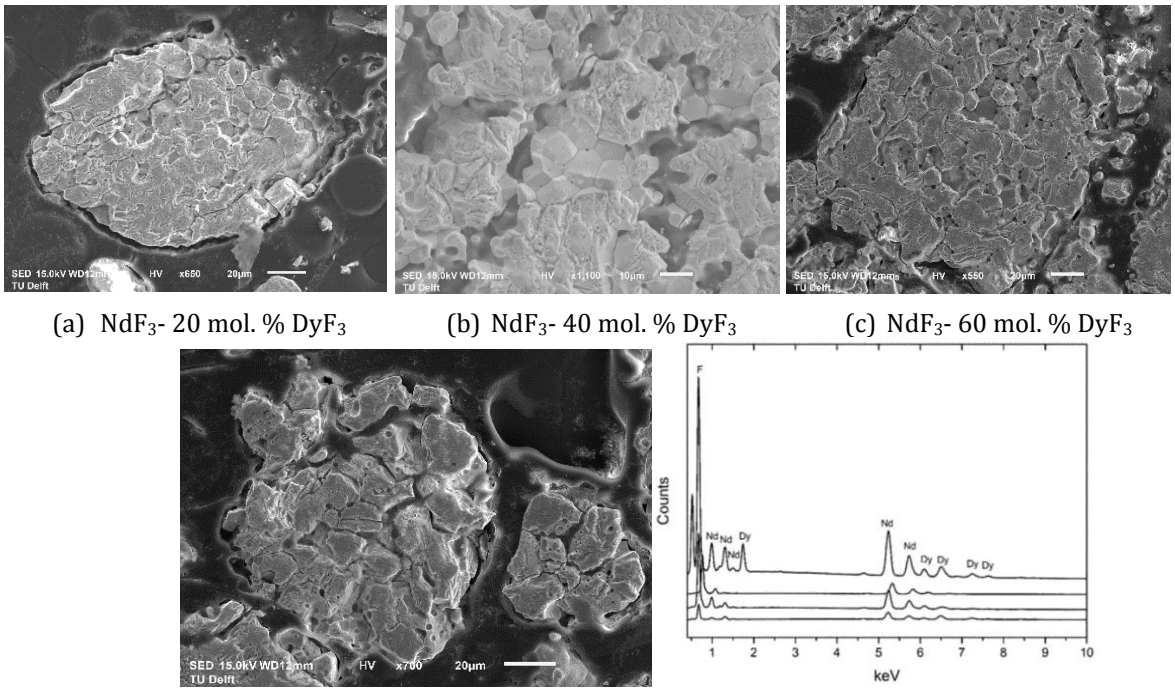

(a) NdF_3- 20 mol. % DyF_3 (b) NdF_3- 40 mol. % DyF_3 (c) NdF_3- 60 mol. % DyF_3

(d) NdF_3- 80 mol. % DyF_3 (e) EDS spectra of NdF_3-DyF_3

Figure 6.2– BSE image and EDS spectra of selected compositions.

6.4 *Ab initio* calculations

Due to lack of experimental thermochemical information for the compound $LiDyF_4$ forming in LiF-DyF_3 system, *ab initio* calculations are performed to estimate its enthalpy of formation. The Vienna *Ab initio* Simulation Package (VASP) [13, 14] is used. The input parameters used for relaxing the structures are listed in Table 6.3. The enthalpies of formation of $LiDyF_4$ in tetragonal (tI24,$I4_1/a$) and orthorhombic (oP24,Pbcn) are estimated. It is found that tetragonal $LiDyF_4$ is more stable in comparison with orthorhombic $LiDyF_4$. The formation enthalpy $\Delta_r H^0_{298}$ is calculated by

$$\Delta_r H^o_{298}(LiDyF_4) \approx E_0(LiDyF_4) - E_0(LiF) - E_0(DyF_3) \quad (6.1)$$

In order to validate the calculated $\Delta_r H^o_{298}$ for $LiDyF_4$, the enthalpies of formation of LiF and DyF_3 are calculated with the same input parameters as in Table 6.3 using VASP. The values of $\Delta_f H^o_{298}$ for these compounds are calculated using Equation (6.1).

The enthalpy of the reaction LiF+DyF_3 ⇄ $LiDyF_4$ is calculated according to:

$$\Delta_f H^o_{298}(AF_y) \approx E_0(AF_y) - E_0(A) - (y/2)\, E_0(F_2) \quad (6.2)$$

in which A represents Dy or Li.

The enthalpy of formation of LiF is calculated with respect to Li (bcc) and F_2 (gas) and DyF_3 is calculated with respect to Dy (dhcp) and F_2 (gas). The total energy of F_2 (gas) is calculated using the same procedure as in [15] for calculating the total energy of N_2

(gas). The difference in total energies of DyF_3 with hexagonal ($P\bar{3}c1$) and orthorhombic (Pnma) structures is also calculated. The calculated enthalpies from the present work and the comparison with experimental data from literature are listed in Table 6.4.

Table 6.3– VASP input parameters.

Potential	PAW [16]
Exchange-correlation functional	GGA-PBE [17]
Energy cut-off	600 eV
k-point mesh spacing	$\leq$0.8Å^{-1}
Force convergence	1×10^{-3} eV/Å
Stress convergence	0.1 kB
SCF convergence	1×10^{-4} eV
Integration scheme	Tetrahedron method with Blöchl correction [18]

Table 6.4– Calculated enthalpies using *ab initio* calculations

Phase	$\Delta_r H^o_{298}/\Delta_f H^o_{298}$ (kJ/mol)	
	Ab initio	Experiment
$LiDyF_4$	–19.156	–
LiF	–574.626	–594.581 [19]
DyF_3	–1606.664	–1665.23 [20]
		–1692 [21]

Table 6.5– Crystallographic data for solid phases

Phase	Space group	Stability range (K)
Cub (LiF)	$Fm\bar{3}m$	$\leq$1121
Ort (DyF_3)	Pnma	$\leq$1300
Hex (DyF_3)	$P6_3/mmc$	1300-1430
Hex (NdF_3)	$P6_3/mmc$	$\leq$1650
$LiDyF_4$	$I4_1/a$	$\leq$1093

6.5 Thermodynamic models

There are five equilibrium phases in the LiF-DyF_3 system: Liquid, Cubic (Cub), Orthorhombic (Ort), Hexagonal (Hex) and $LiDyF_4$. The crystallographic information for the solid phases of the system is listed in Table 6.5.

The liquid phase is modelled using the two-sublattice model for ionic melts [22, 23]. This is based on Temkin's model[24] assuming that cations and anions occupy separate sublattices (indicated in parentheses in Table 6.6) and mix randomly within each sublattice. The mixing model for liquid phase is thus $(Dy^{3+},Li^{+},Nd^{3+})_p$: $(F^{-},LiDyF_4)_q$.

Initially, the liquid phase is modelled without a neutral species in the anion sublattice. It is found that several model parameters are required to obtain the best fit to experimental data. Hence, $LiDyF_4$ (corresponding to the stoichiometry of the most stable compound in the system) is added as a fictitious neutral species to account for the short range ordering in LiF-DyF_3 melt. In order to keep the electroneutrality, the number of sites on each sublattice, p and q, must satisfy the following constraints:

$$p = y_{F^-} \tag{6.3}$$

$$q = 3y_{Dy^{3+}} + y_{Li^{+}} + 3y_{Nd^{3+}} \tag{6.4}$$

Cubic, orthorhombic and $LiDyF_4$ phases are modelled as stoichiometric phases. Hexagonal phase is modelled as solid solution based on the compound energy formalism [25, 26]. According to this approach, the structure of a phase is represented by two or more sublattices and constituent species mix randomly within the sublattices. Table 6.6 summarizes the sublattice formulations used in the Gibbs free energy modelling of various phases. The Gibbs free energy expressions for LiF (cubic and liquid), NdF_3 (hexagonal and liquid) and DyF_3 (hexagonal and liquid) are from the SGTE substance database (version 5.1) [27]. The Gibbs free energy expression for DyF_3 (orthorhombic) is estimated using enthalpy and temperature DyF_3 (orthorhombic) to DyF_3 (hexagonal) transformation. This is explained in Section 6.7.1.

Table 6.6– Sublattice formulations for the phases.

Phase	Sublattice formulation
Liquid	$(Dy^{3+},Li^{+},Nd^{3+})_p : (F^{-},LiDyF_4)_q$
Cub	$(Li^{+})_1 : (F^{-})_1$
Hex	$(Dy^{3+},Nd^{3+})_1 : (F^{-})_3$
Ort	$(Dy^{3+})_1 : (F^{-})_3$
$LiDyF_4$	$(Dy^{3+})_1 : (Li^{+})_1 : (F^{-})_3$

6.6 Optimization

The Gibbs free energy parameter optimization is carried out using the PARROT module [28] of the Thermo-Calc database system [29] using relevant constitutional and thermochemical data as input. The method involves minimizing reduced sum of squares of errors in an iterative manner, starting with estimated values for all optimizing variables. The optimized Gibbs free energy description thus obtained is eventually used for calculating phase diagrams and thermochemical properties at any desired temperature and composition regime in which the functions are valid. The sources of input data used in the optimization are shown in Table 6.7. Optimization is initiated by providing estimated values for the parameters. The start values are refined iteratively by minimizing the sum of the squares of deviation between input data and the corresponding model calculated values. Finally the model parameters are rounded off according to the method suggested by Hari Kumar et al. [30]. The Gibbs free energy parameters of LiF-NdF_3, LiF-DyF_3 and NdF_3-DyF_3 are optimised based on this method. No optimisation is performed for the ternary system.

Table 6.7– Data sources used for the optimisation.

	Method	Reference
	LiF- NdF3	
Liquidus	DTA	[31]
	LiF- DyF3	
Liquidus	DTA	[31]
$\Delta_r H^o_{298}$	DFT	Present work
	NdF3-DyF3	
Liquidus/Solidus	DTA	Present work

6.7 Results

6.7.1 Binary Systems

The optimised thermodynamic parameters for LiF-NdF_3, LiF-DyF_3 and DyF_3-NdF_3 systems obtained in this work are listed in Table 6.8.

The phase diagram of LiF-NdF_3 calculated using the model parameters obtained in this work is shown in Figure 6.3 along with the experimental data from [31]. The phase diagram of LiF-NdF_3 is a simple eutectic phase diagram without any significant solid solubility in cubic and hexagonal phases. The optimized eutectic composition and temperature for this system are 22 mol% NdF_3 and 1007 K, respectively.

LiF-DyF_3 phase diagram is optimised using the experimental data by Thoma et al. [31] along with the enthalpy of formation of $LiDyF_4$ obtained from *ab initio* calculation. The calculated phase diagram is shown in Figure 6.4. Here also the terminal solid phases have zero solubility.

Zalkin and Tempelton [32] were the first to recognize the dimorphism among the rare earth trifluorides. They observed hexagonal structure for LaF_3 to NdF_3 and orthorhombic structure for GdF_3 to LuF_3, while SmF_3, EuF_3, HoF_3 and TmF_3 could have both hexagonal and orthorhombic structure. Thoma and Brunton [20] also studied the dimorphism of lanthanide trifluorides systematically. They observed tysonite-type hexagonal structure for the LaF_3 to NdF_3 group. However, they have found that all lanthanide trifluorides with the orthorhombic structure transform to hexagonal crystal structure on heating. They have demonstrated that SmF_3, EuF_3, TbF_3 and DyF_3 form tysonite-type hexagonal structure, while ErF_3 to LuF_3 form α-YF_3 type structure. Spedding et al. [33, 34] confirmed the orthorhombic to hexagonal transformation for TbF_3 and DyF_3 by high temperature XRD. However, the enthalpy of the transformation for these two fluorides was not large enough to be detected by drop calorimetry. Greis and Cader [12] have not observed any first-order solid state transformation for TbF_3, DyF_3 and HoF_3.

Sobolev et al. found that presence of oxygen can influence the structure of lanthanide trifluoride, which can be a source of discrepancy [35, 36]. Meanwhile, Garashina et al. [37] have observed that the transformation of orthorhombic to hexagonal structure takes place as a result of a deformational mechanism and over a broad temperature range. Stankus et al. [38] have proposed that orthorhombic to hexagonal transformation in lanthanide trifluorides proceeds in two stages: first a continuous transformation up to the transformation temperature (T_t) and then a sharp change of lattice parameters at T_t.

The enthalpy of the orthorhombic to hexagonal transformation in DyF_3 was measured by drop calorimetry by Lyaponov et al. [39]. They reported that the transformation takes place at 1300 K and the corresponding enthalpy change is $+2400 \pm 1700$ J.mol^{-1}. Since there is large uncertainty in the reported enthalpy value, we prefer using the corresponding DFT calculated value (+3383 J.mol^{-1}) along with the measured temperature of transformation (1300 K) to describe the Gibbs free energy of DyF_3 (orthorhombic).

The solidus-liquidus data obtained by DTA in the current work are used for optimization of Gibbs energy model parameters in the NdF_3-DyF_3 system. The calculated phase diagram along with experimental data from the present work is shown in Figure 6.5. The phase diagram shows extended solubility in the hexagonal phase in the high temperature region. As was discussed earlier in this chapter, both the DTA measurements and microstructure analysis indicate the complete solubility of NdF_3 and DyF_3.

Table 6.8– Gibbs free energy parameters for DyF_3-LiF-NdF_3 system (in J/mol, with the temperature T in K).

GHSERDF = -1722267.41+512.670134T-92.91541$T\ln(T)$-0.01096079T^2-2.12147× $10^{-10}T^3$ +235586.75T^{-1}
(298.15 < T < 1430)
-1791020.92+1010.0659T-156.9$T\ln(T)$ (1430 < T < 6000)
GHSERLF = -634621.638+305.64556T-50.30632$T\ln(T)$+0.0012289475T^2-2.30170167× $10^{-6}T^3$
+399408.8T^{-1} (298.15 < T < 700)
-633813.702+278.759762T-45.75246$T\ln(T)$-0.006033035T^2-4.40324167× $10^{-7}T^3$ +433813.85T^{-1}
(700 < T < 1121)
-644878.626+411.074928T-64.18256$T\ln(T)$ (1121 < T < 3000)
GHSERNF = -1710301.85+510.665061T-92.69601$T\ln(T)$-0.01171485T^2-1.08333333× $10^{-10}T^3$ +322770T^{-1}
(298.15 < T < 1650)
-1809836.14+1142.45411T-172.4$T\ln(T)$-1.133510$^{-4}T^2$ (1650 < T < 6000)
Liquid $(Dy^{3+},Li^+,Nd^{3+})_p$: $(F^-,LiDyF_4)_q$
${}^oG^{Liquid}_{Dy^{+3}:F^-}$= +GHSERDF+58576-40.9622387T
${}^oG^{Liquid}_{Li^+:F^-}$ = +GHSERLF+27087.2-24.1569607T
${}^oG^{Liquid}_{Dy^{+3}:F^-}$= +GHSERNF+54810-33.2181818T
${}^oG^{Liquid}_{LiDyF_4}$ = GHSERLF+GHSERDF+85663.2-65.1191994T
${}^0G^{Liquid}_{Dy^{+3},Li^+:F^-}$ = -46814
${}^1G^{Liquid}_{Dy^{+3},Li^+:F^-}$ = +10509
${}^2G^{Liquid}_{Dy^{+3},Li^+:F^-}$ = +18849
${}^0G^{Liquid}_{Li^+,Nd^{+3}:F^-}$ = +27447-41.475T
${}^0G^{Liquid}_{Dy^{+3},Nd^{+3}:F^-}$ = +9956
${}^1G^{Liquid}_{Dy^{+3},Nd^{+3}:F^-}$ = -3863
${}^0G^{Liquid}_{Dy^{+3},Li^+:LiDyF_4}$ = +178255
Cub $(Li^+)_1$: $(F^-)_1$

${}^{o}G^{Cub}_{Li^{+}:F^{-}}$= +GHSERLF
Hex $(Dy^{3+},Nd^{3+})_1:(F^{-})_3$
${}^{o}G^{Hex}_{Dy^{+3}:F^{-}}$= +GHSERDF
${}^{o}G^{Liquid}_{Nd^{+3}:F^{-}}$= +GHSERNF
${}^{0}L^{Hex}_{Dy^{+3},Nd^{+3}:F^{-}}$ = +10316
${}^{1}L^{Hex}_{Dy^{+3},Nd^{+3}:F^{-}}$ = +8164
Ort $(Dy^{3+})_1:(F^{-})_3$
${}^{o}G^{Ort}_{Dy^{+3}:F^{-}}$= +GHSERDF-13532+10.409$T$
$LiDyF_4$ $(Dy^{3+})_1:(Li^{+})_1:(F^{-})_3$
${}^{0}G^{LiDyF_4}_{Dy^{+3}:Li^{+}:F^{-}}$= +GHSERDF+GHSERLF-51636+28.9T

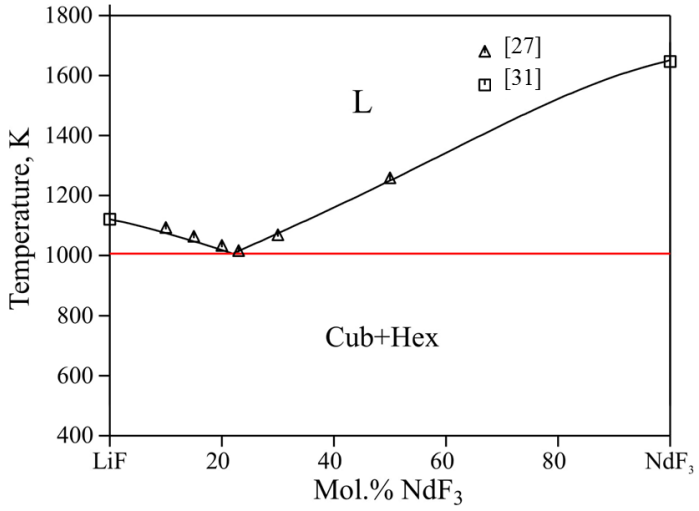

Figure 6.3– Calculated LiF-NdF_3 phase diagram and comparison with the experimental data from [27, 31].

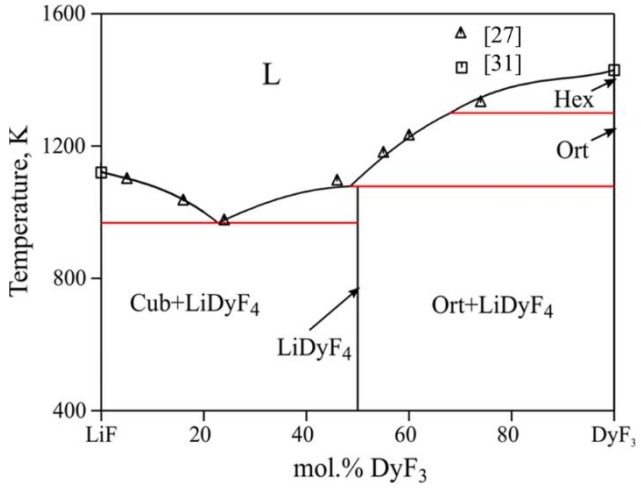

Figure 6.4– Calculated LiF-DyF_3 phase diagram and comparison with the experimental data from [27, 31].

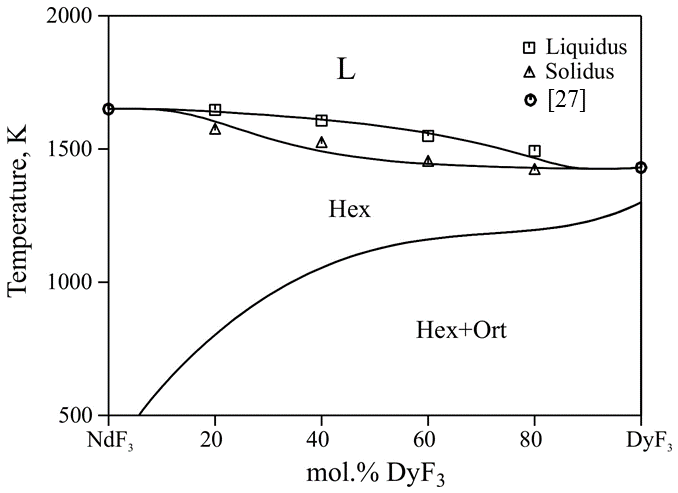

Figure 6.5– Calculated NdF_3-DyF_3 phase diagram and comparison with the experimental data from present work [27].

6.7.2 DyF_3-LiF-NdF_3

The liquidus projection along with the isotherms is shown in Figure 6.6. It is calculated using the Gibbs free energy parameters of binary systems alone. The projection shows two ternary invariant reactions, whose co-ordinates are also listed in Table 6.9. This table gives a comparison of DTA results with calculated phase transformation temperatures and the corresponding phase reactions. The corresponding Scheil reaction scheme is shown in Figure 6.7.

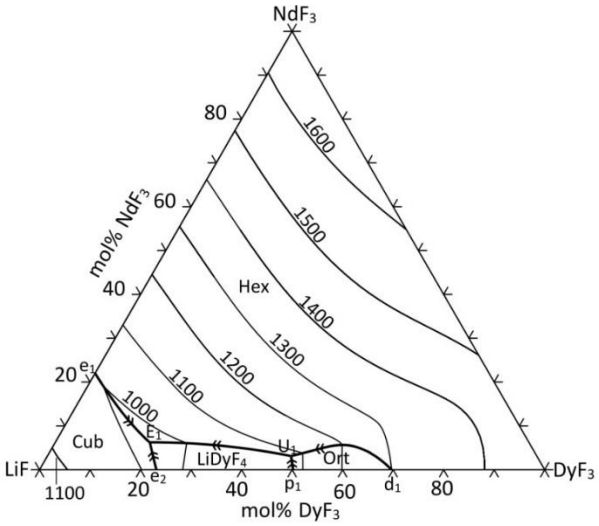

Figure 6.6– Calculated liquidus projection for the LiF-DyF_3-NdF_3 system (temperature in K).

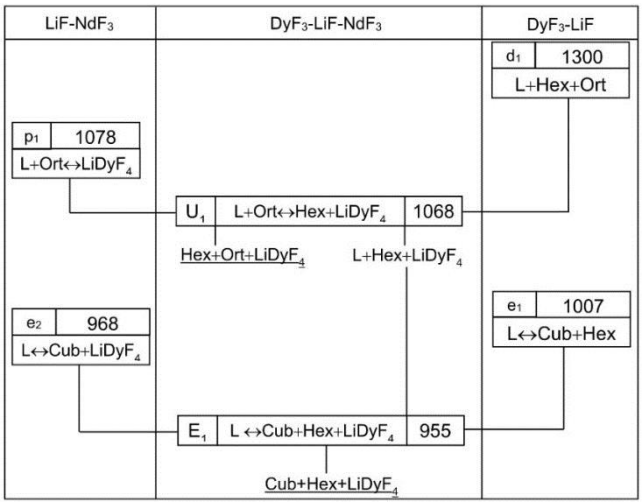

Figure 6.7– Reaction scheme for the DyF_3-LiF-NdF_3 system.

6.8 Conclusions

The Gibbs energy parameters for LiF-DyF_3 and LiF-NdF_3 systems are optimised with experimental data from literature. *Ab initio* calculations are used to obtain the enthalpy of formation for $LiDyF_4$, which is a stable phase in the LiF-DyF_3 system. NdF_3-DyF_3 system optimization is performed with the experimental data obtained from DTA analysis in this work. The phase diagram of DyF_3-LiF-NdF_3 system is computed based on the Gibbs free energy parameters of the three limiting binary systems and compared with the phase diagram data obtained by DTA experiments. All calculated phase diagrams are in good agreement with the experimental data.

Table 6.9– Details of phase reactions in LiF-NdF_3-DyF_3 system.

Reaction	Liquid composition (mol%)		Temperature (K)	Reference
	LiF	DyF_3		
		LiF-NdF_3		
L ⇄ Cub+Hex (e_1)	78	0	1007	This work
	77	0	1011	[31]
	74.7	0	1006.5	[40]
		LiF-DyF_3		
L ⇄ Cub+$LiDyF_4$ (e_2)	77.2	22.8	968	This work
	76	24	973	[31]
L + Ort ⇄ $LiDyF_4$ (p_1)	51.4	48.6	1078	This work
	54	46	1093	[31]
L + Hex + Ort (d_1)	31.9	68.1	1300	This work
		DyF_3-LiF-NdF_3		
L + Ort ⇄ Hex+$LiDyF_4$ (U_1)	48.64	48.25	1068	This work
L + Ort ⇄ Hex+$LiDyF_4$ (U_1)	75.05	18.77	955	This work

6.9 References

[1] Binnemans, K., Jones, P. T., Blanpain, B., Van Gerven, T., Yang, Y., Walton, A., and Buchert, M., 2013, "Recycling of rare earths: a critical review," Journal of Cleaner Production, 51(0), pp. 1-22.

[2] Rampin, I., Bisaglia, F., and Dabalà, M., 2010, "Corrosion Properties of NdFeB Magnets Coated by a Ni/Cu/Ni Layer in Chloride and Sulfide Environments," Journal of Materials Engineering and Performance, 19(7), pp. 970-975.

[3] Coey, J. M. D., 2002, "Permanent magnet applications," Journal of Magnetism and Magnetic Materials, 248(3), pp. 441-456.

[4] Alonso, E., Sherman, A. M., Wallington, T. J., Everson, M. P., Field, F. R., Roth, R., and Kirchain, R. E., 2012, "Evaluating Rare Earth Element Availability: A Case with Revolutionary Demand from Clean Technologies," Environmental Science & Technology, 46(6), pp. 3406-3414.

[5] Siming, P., Shihong, Y., Zongan, L., Dehon, C., Liha, X., and Bin, Z., 2011, "Development on Molten Salt Electrolytic Methods and Technology for Preparing Rare Earth Metals and Alloys in China," Chinese Journal of Rare Metals, 35(3), pp. 440-450.

[6] Lodermeyer, J., Multerer, M., Zistler, M., Jordan, S., Gores, H. J., Kipferl, W., Diaconu, E., Sperl, M., and Bayreuther, G., 2006, "Electroplating of Dysprosium, Electrochemical Investigations, and Study of Magnetic Properties," Journal of The Electrochemical Society, 153(4), pp. 242-248.

[7] Abbasalizadeh, A., Teng, L., Sridhar, S., and Seetharaman, S., 2015, "Neodymium extraction using salt extraction process," Mineral Processing and Extractive Metallurgy, 124(4), pp. 191-198.

[8] Abbasalizadeh, A., Malfliet, A., Seetharaman, S., Sietsma, J., and Yang, Y., 2017, "Electrochemical Extraction of Rare Earth Metals in Molten Fluorides: Conversion of Rare Earth Oxides into Rare Earth Fluorides Using Fluoride Additives," Journal of Sustainable Metallurgy, 3(3), pp. 627-637.

[9] Höhne, G. W. H., Cammenga, H. K., Eysel, W., Gmelin, E., and Hemminger, W., 1990, "The temperature calibration of scanning calorimeters," Thermochimica Acta, 160(1), pp. 1-12.

[10] Pope, M. I., and Judd, M., 1977, Differential Thermal Analysis-A Guide to Technique and its Applications, Heyden London.

[11] Lombardi, G., 1980, "For Better Thermal Analysis, Special Edn. of the Intern," Confederation for Thermal Analysis, University of Rome.

[12] Greis, O., and Cader, M. S. R., 1985, "Polymorphism of high-purity rare earth trifluorides," Thermochimica Acta, 87, pp. 145-150.

[13] Kresse, G., and Furthmüller, J., 1996, "Efficiency of ab-initio total energy calculations for metals and semiconductors using a plane-wave basis set," Computational Materials Science, 6(1), pp. 15-50.

[14] Kresse, G., and Furthmüller, J., 1996, "Efficient iterative schemes for ab initio total-energy calculations using a plane-wave basis set," Physical Review B, 54(16), pp. 11169-11186.

[15] Zoroddu, A., Bernardini, F., Ruggerone, P., and Fiorentini, V., 2001, "First-principles prediction of structure, energetics, formation enthalpy, elastic constants, polarization, and piezoelectric constants of AlN, GaN, and InN: Comparison of local and gradient-corrected density-functional theory," Physical Review B, 64(4), p. 045208.

[16] Blöchl, P. E., 1994, "Projector augmented-wave method," Physical Review B, 50(24), pp. 17953-17979.

[17] Perdew, J. P., Burke, K., and Ernzerhof, M., 1996, "Generalized Gradient Approximation Made Simple," Physical Review Letters, 77(18), pp. 3865-3868.

[18] Blöchl, P. E., Jepsen, O., and Andersen, O. K., 1994, "Improved tetrahedron method for Brillouin-zone integrations," Physical Review B, 49(23), pp. 16223-16233.

[19] dos Santos, I. A., Klimm, D., Baldochi, S. L., and Ranieri, I. M., 2012, "Thermodynamic modeling of the LiF–YF3 phase diagram," Journal of Crystal Growth, 360, pp. 172-175.

[20] Thoma, R. E., and Brunton, G. D., 1966, "Equilibrium Dimorphism of the Lanthanide Trifluorides," Inorganic Chemistry, 5(11), pp. 1937-1939.

[21] Konings, R. J. M., and Kovács, A., 2003, "Thermodynamic properties of the lanthanide(III) halides," Handbook on the Physics and Chemistry of Rare Earths, J. C. G. B. K.A. Gschneidner, and V. K. Pecharsky, eds., Elsevier, pp. 147-247.

[22] Hillert, M., Jansson, B., Sundman, B., and ågren, J., 1985, "A two-sublattice model for molten solutions with different tendency for ionization," Metallurgical Transactions A, 16(1), pp. 261-266.

[23] Sundman, B., 1991, "Modification of the two-sublattice model for liquids," Calphad, 15(2), pp. 109-119.

[24] Temkin, M., 1945, "Mixtures of fused salts as ionic solutions," Acta Phys. Chem., USSR, 20, p. 411.

[25] Andersson, J. O., Guillermet, A. F., Hillert, M., Jansson, B., and Sundman, B., 1986, "A compound-energy model of ordering in a phase with sites of different coordination numbers," Acta Metallurgica, 34(3), pp. 437-445.

[26] Hillert, M., 2001, "The compound energy formalism," Journal of Alloys and Compounds, 320(2), pp. 161-176.

[27] SGTE, T., 1977, "Scientific Group Thermodata Europe, substance database," Grenoble, France, http://www.sgte.Org.

[28] Jansson, B., 1984, "Computer operated methods for equilibrium calculations and evaluation of thermodynamic model parameters," Ph.D., Royal Institute of Technology, Stockholm, Sweden.

[29] Sundman, B., Jansson, B., and Andersson, J.-O., 1985, "The Thermo-Calc databank system," Calphad, 9(2), pp. 153-190.

[30] Hari Kumar, K. C., and Wollants, P., 2001, "Some guidelines for thermodynamic optimisation of phase diagrams," Journal of Alloys and Compounds, 320(2), pp. 189-198.

[31] Thoma, R. E., Brunton, G. D., Penneman, R. A., and Keenan, T. K., 1970, "Equilibrium relations and crystal structure of lithium fluorolanthanate phases," Inorganic Chemistry, 9(5), pp. 1096-1101.

[32] Zalkin, A., and Templeton, D., 1953, "The crystal structures of YF_3 and related compounds," Journal of the American Chemical Society, 75(10), pp. 2453-2458.

[33] Spedding, F., and Henderson, D., 1971, "High-Temperature Heat Contents and Related Thermodynamic Functions of Seven Trifluorides of the Rare Earths: Y, La, Pr, Nd, Gd, Ho, and Lu," The Journal of Chemical Physics, 54(6), pp. 2476-2483.

[34] Spedding, F. H., Beaudry, B. J., Henderson, D. C., and Moorman, J., 1974, "High temperature enthalpies and related thermodynamic functions of the trifluorides of Sc, Ce, Sm, Eu, Gd, Tb, Dy, Er, Tm, and Yb," The Journal of Chemical Physics, 60(4), pp. 1578-1588.

[35] Sobolev, B. P., Fedorov, P. P., Shteynberg, D. B., Sinitsyn, B. V., and Shakhkalamian, G. S., 1976, "On the problem of polymorphism and fusion of lanthanide trifluorides. I. The influence of oxygen on phase transition temperatures," Journal of Solid State Chemistry, 17(1), pp. 191-199.

[36] Sobolev, B. P., Fedorov, P. P., Seiranian, K. B., and Tkachenko, N. L., 1976, "On the problem of polymorphism and fusion of lanthanide trifluorides. II. Interaction of LnF_3 with MF2 (M = Ca, Sr, Ba), change in structural type in the LnF_3 series, and thermal characteristics," Journal of Solid State Chemistry, 17(1), pp. 201-212.

[37] Garashina, L., Sobolev, B., Aleksandrov, V., and Vishnyakov, Y. S., 1980, "On crystallochemistry of rare earth fluorides," Kristallografiya, 25(2), pp. 294-300.

[38] Stankus, S. V., Khairulin, R. A., and Lyapunov, K. M., 1999, "Phase transitions and thermal properties of gadolinium trifluoride," Journal of Alloys and Compounds, 290(1–2), pp. 30-33.

[39] Lyapunov, K. M., Baginskii, A. V., and Stankus, S. V., 2000, "The calorific properties of LiYF4 : Nd in the solid and liquid states," High Temperature, 38(1), pp. 146-148.

[40] van der Meer, J. P. M., Konings, R. J. M., Jacobs, M. H. G., and Oonk, H. A. J., 2004, "Thermodynamic modelling of LiF–LnF_3 and LiF–AnF_3 phase diagrams," Journal of Nuclear Materials, 335(3), pp. 345-352.

Chapter 7 Conclusions and future research

The objective of this research is to investigate new methods on the direct electrochemical reduction of Rare Earth (RE) Oxides and RE magnets into RE metals or RE alloys in the chloride/fluoride-based molten salts. The primary focus is on the low solubility of the RE oxides in the molten fluorides, which limits the RE metal extraction yield from RE oxides. Conversion treatment is proposed to convert RE oxides and RE magnet (NdFeB magnet) into RE fluorides using effective fluorinating agents. Hence the RE metal is extracted from RE fluorides through the electrochemical extraction route. Another objective is to employ a reactive anode as the substitute for the conventional graphite anode to prevent CO, CO_2, halogen or fluorocarbon gas generation accompanying the RE metal production from RE oxide and RE magnet in molten salt electrolysis process.

7.1 Conclusions

The main contributions of this research are categorized and summarised as following conclusions:

1- Chlorination and fluorination of NdFeB magnet

- Feasibility of the neodymium and dysprosium extraction from $Nd_2Fe_{14}B$ magnets containing 6% dysprosium is proven using a combined method of molten salt extraction and electrolysis. Aluminium chloride in LiCl-NaCl-KCl electrolyte is shown to be an effective chlorinating agent which reacts with neodymium and dysprosium in the magnet which leads to $NdCl_3$ and $DyCl_3$ formation. As the result of this approach, neodymium and dysprosium recovery from magnetic scrap is enabled by a direct separation of these metals from iron, eliminating the oxide or halide conversion steps. Subsequent electrolysis of $NdCl_3$ and $DyCl_3$ leads to the formation of Nd and Nd/Dy metal as the cathode product.
- The same approach is used for the Nd extraction from RE magnet in fluorides salts using AlF_3, ZnF_2, FeF_3 and Na_3AlF_6 as fluorinating agents. Al, Zn and Fe from AlF_3, Na_3AlF_6, ZnF_2 and FeF_3, respectively, replaced the rare earth in the magnet matrix, thereby forming intermetallic compounds with Fe in the magnet. In all conversion treatments, Nd is separated from the Fe and B in the magnet and is converted to rare earth fluoride which could be electro-chemically deposited on the cathode, hence providing the possibility of a one-step recycling process of the rare earths from

magnets. However, in the case of using ZnF_2 and FeF_3, the results show complete conversion of Nd (in the magnet) to NdF_3. Hence ZnF_2 and FeF_3 are better fluorinating agents compared to AlF_3 and Na_3AlF_6 for Nd extraction.

2- Fluorination of Nd_2O_3

- The feasibility of the conversion of the RE oxide to RE fluoride using AlF_3, ZnF_2, FeF_3 and Na_3AlF_6 as fluorinating agents is proven. Conversion of neodymium oxide to neodymium fluoride solves the problem of low solubility of the neodymium oxide in molten fluorides to a large extent. Once neodymium fluoride is formed, it can subsequently be electrolysed for Nd production on the cathode. The formed solid oxides of aluminium and zinc need to be removed from the electrolytes using e.g. high temperature filtration to generate clean fluoride electrolytes. The design of the reactor should be modified in a way that formed oxide can be collected and removed from the top of the salt or at the bottom of the cell depending on the oxide density.

3- Use of reactive anode for Nd_2O_3 electrolysis

- A novel approach is developed in which iron anode is used as a substitute for conventional graphite anode, promoting electrochemical dissolution of iron into the melt, thus preventing CO, CO_2, CF_4 and C_2F_6 gas evolution at the anode.
- A new electrochemical set-up with the iron anode is used for the extraction of Nd from Nd_2O_3 in LiF electrolyte. With dissolution of iron in the salt electrolyte as the result of anodic reaction, fluorinating agent (FeF_3) is constantly generated *in situ* which enables the continuous conversion of neodymium oxide feed to the corresponding fluoride. Once neodymium fluoride is formed, Nd and Fe are simultaneously deposited on the cathode. Finally Nd-Fe is collected as the cathodic product. The formed solid Fe_2O_3 (or FeO_x) should be removed from the bottom of the electrolytic cell.
- Nd-Fe alloy formation would increase the rare earth extraction efficiency due to lower activity of the metal in the alloy, which decreases the reduction potential of the rare earth. Nd-Fe alloy can be directly used as a master alloy for the production of NdFeB magnets. The distribution of dissolved Fe between cathode deposition and fluorination of Nd_2O_3 could be altered based on electrolysis conditions such as applied current density.

4- Electrochemical reduction mechanisms

- Studies of the electrochemical behaviour of NdF_3 in LiF electrolyte by the means of cyclic voltammetry prove that the neodymium ion reduction is a single step reaction of Nd^{3+} to Nd metal in the fluoride salt. From the chronopotentiograms of LiF-NdF_3 system it is concluded that the reduction of NdF_3 is a diffusion-controlled process. From the linear relationship between the reduction peak current density and square root of the potential scan rate, we assume that LiF-NdF_3 system acts as a quasi-

reversible system. Based on this assumption, the diffusion coefficient of Nd^{3+} ions is calculated to be 4×10^{-9} m^2 s^{-1}.

- From the cyclic voltammetry analysis of LiF-FeF_3 system, it is concluded that the reduction of Fe^{3+} to Fe is a two-step process, first from Fe^{3+} to Fe^{2+} and then Fe^{2+} to metallic iron.
- No peak related to neodymium reduction or dissolution is found in the LiF-Nd_2O_3 cyclic voltammogram. It was suggested that neodymium oxyfluoride formation in the LiF-Nd_2O_3 system prohibit the neodymium reduction, hence Nd_2O_3 cannot be used for Nd extraction in LiF electrolyte (in the absence of NdF_3).

5- Thermodynamic modelling of LiF-NdF_3-DyF_3 system

- DyF_3-NdF_3 phase diagram is optimised with the experimental data obtained from DTA analysis. DTA measurements together with microstructure analysis indicate complete solubility of NdF_3 and DyF_3.
- DyF_3-LiF-NdF_3 ternary phase diagram optimisation is performed based on the Gibbs free energy parameters of LiF-NdF_3, DyF_3-LiF and DyF_3-NdF_3 binaries and the phase diagram data obtained by DTA experiments. *Ab initio* calculations are used to obtain the enthalpy of formation for $LiDyF_4$, which is present in DyF_3-LiF system.

7.2 Recommendations for future research

The work presented in this thesis provides experimental analysis based on the thermodynamic calculations for the electrochemical recovery of RE from RE oxides and RE magnet in molten salt. The following recommendations for future work will provide possible improvement in the subject towards the industrial applications.

- Conversion of RE oxide to RE fluoride using fluorinating agents solves the problem of low solubility of the neodymium oxide in molten fluorides to a large extent. However, studies on the formation and the influence of oxyfluoride in the LiF-Nd_2O_3 system will provide insight for better control on the system which can result in higher yield of the extraction. This analysis can be performed by the means of Raman spectroscopy.
- Based on the thermodynamic calculations, the dissolved Fe from Fe anode in LiF-Nd_2O_3 system can participate in parallel in both the electrochemical process and the chemical reaction with Nd_2O_3. The Nd-Fe alloy formation identifies that Fe is involved in electrochemical reactions. Hence, the parallel electro-chemical reactions cannot be ruled out. However, the presence of FeO and NdF_3 proves that the conversion has taken place. Further experiments should be conducted to investigate the impact of the chemical reactions on the overall process. The study on the kinetics of the reactions can also give a great insight into the subject. The distribution of dissolved iron from anode between fluorination and direct cathodic reduction will be a key.

- In the current research, in-situ formation of FeF_3 is performed with the use of iron anode in the LiF-Nd_2O_3 system. Considering the physical properties, the ability to act as the fluoridising agent and the possibility of alloy formation on the cathode, other reactive anodes can be investigated.

Summary

Electrochemical metal extraction in molten salts is the dominant industrial method for production of Rare Earth (RE) metals from their oxides. Two major challenges pertaining to RE metals extraction using this technology are *a) low solubility of RE oxides in molten salts and b) carbon monoxide or carbon dioxide generation and possibility of fluorocarbon gas generation.* The primary objective of this thesis is to find new methods to overcome the problem of low solubility of RE oxides in molten fluorides in order to increase the RE metal extraction yield from RE oxides. Another objective is to study novel routes in order to prevent CO, CO_2 and halogen gas generation in the RE metal production from RE oxide and RE magnet scrap in molten salt electrolysis process.

In view of this, a treatment route is suggested for the conversion of RE oxide to RE chloride/fluoride using strong chemical agents. Chapters 2, 3 and 4 investigate the conversion routes for RE oxides as well as RE magnet scrap in both chlorides and fluorides molten salts. Chapter 5 investigates the electrolysis step in which iron as a reactive anode is used, preventing generation of fluorocarbon, CO and CO_2 gas in the extraction process. In Chapter 6 a thermodynamic modelling of the fluoride salt using CALPHAD approach is carried out. The phase equilibria and thermodynamics of molten fluorides system can be used for optimal design of RE extraction processes.

Chapter 2 of this thesis gives an overview of the previous studies on electrochemical extraction of rare earth oxides and NdFeB magnets containing dysprosium both in molten chlorides and fluorides. In this chapter the conversion of RE in the magnet into RE chloride using $AlCl_3$ in LiCl-NaCl-KCl electrolyte is studied. Subsequently the electrochemical extraction of RE from RE chloride in this system is investigated.

The concept of chlorination for the RE in the magnet is used for fluoride salts. In chapter 3 conversion of RE oxide to RE fluorides using fluorinating agents is studied. Zinc fluoride (ZnF_2), aluminium fluoride (AlF_3), iron fluoride (FeF_3) and cryolite (Na_3AlF_6) are used as fluorinating agents. The feasibility of this conversion is investigated from thermodynamic point of view using FactSage software as well as with experiments. Conversion of RE oxide to RE fluoride in the LiF electrolyte solves the problem of the low solubility of RE oxide in LiF to a large extent. After the conversion, RE can be reduced on cathode from RE fluoride instead of RE oxide.

In Chapter 4 we investigate the conversion method for NdFeB magnet using the same fluorinating agents that was used for RE oxides in chapter 3. Al, Zn and Fe, from AlF_3, Na_3AlF_6, ZnF_2 and FeF_3, respectively, replace the rare earth element in the magnet matrix, thereby forming compounds with Fe in the magnet and RE fluorides are formed. Nd fluoride formation provides the possibility of a one-step recycling process of the rare

earth elements from magnets. Based on the results, ZnF_2 and FeF_3 are the strongest fluorinating agents among the other agents investigated in these experiments.

Chapter 5 studies the use of a novel reacting electrode as a substitute for the graphite anode which is used in the industrial processes. In the electrolysis process, iron is used as a reactive anode, promoting electrochemical dissolution of iron into the melt, thus preventing carbon monoxide, carbon dioxide and fluorine or fluorocarbon gas evolution at the anode during RE fluoride electrolysis. Therefore, the fluorinating agent is constantly regenerated *in situ*, which enables the continuous conversion of neodymium oxide feed. The final cathodic product is Nd-Fe alloy which can be collected from Mo cathode. Iron dissolved from the anode will be distributed between FeF_3 and cathode product Fe-Nd alloy. Regarding this process, the proportion of Nd and Fe in the cathode alloy needs to be further studied. The design of the reactor should be also modified in a way that formed undissolved metal oxides can be collected and removed from the salt.

In this chapter the electrochemical behaviour of different fluoride salt systems is also studied using cyclic voltammetry, chronopotentiometry and square wave voltammetry techniques. The cyclic voltammogram of LiF-NdF_3 system shows that neodymium ion reduction is a single step reaction of Nd^{3+} to Nd metal. The same study on the LiF-FeF_3 system shows that the reduction of Fe^{3+} to Fe is a two-step process, first from Fe^{3+} to Fe^{2+} and then from Fe^{2+} to metallic iron. In the cyclic voltammetry study of the LiF-Nd_2O_3 system, no peak related to Nd reduction is observed. This result confirms that Nd_2O_3 cannot be used for Nd extraction in the absence of NdF_3 in the electrolyte.

Chapter 6 studies the thermodynamic modelling of LiF-DyF_3-NdF_3 system. Gibbs energies of LiF-NdF_3 and LiF-DyF_3 systems are modelled using the constitutional data from literature. Moreover, *ab initio* calculations are carried out to obtain enthalpy of formation of $LiDyF_4$, an intermediate phase that is found to exist in the LiF-DyF_3 system. Differential thermal analysis (DTA) is performed for the optimization of NdF_3-DyF_3 system. The obtained Gibbs free energy functions for limiting binary phase diagrams determined in this work along with DTA analysis for LiF-NdF_3-DyF_3 system are used for modelling Gibbs free energy functions of equilibrium phases in the ternary system.

Samenvatting

Elektrochemische extractie in gesmolten zout is de meestgebruikte methode in de industrie voor de extractie van zeldzame-aardmetalen (ZA) (Engels: Rare Earth metals, RE) uit hun oxides. De ZA-metaal-extractie met deze techniek heeft twee grote uitdagingen: a) de lage oplosbaarheid van de ZA oxides en b) de mogelijkheid van de ontwikkeling van anodisch halogeengas of de productie van koolstofdioxide en koolstofmonoxide. Het hoofddoel van dit proefschrift is het vinden van nieuwe methoden om het probleem van de lage oplosbaarheid van ZA oxide in gesmolten fluoriden te overkomen om zo het rendement van de extractie van ZA metalen uit hun oxides te verhogen. Een tweede doel is onderzoek aan nieuwe routes om de evolutie van CO, CO_2 en halogeengassen te voorkomen in de productie van ZA metaal vanuit ZA oxide en ZA-gebaseerde magneten in het gesmolten-zout elektrolyseproces. Het gaat bij deze laatste categorie vooral om NdFeB magneten.

Met dit in gedachten is een behandelingsroute voorgesteld voor de conversie van ZA oxide tot ZA chloride/fluoride die gebruik maakt van sterke chemische reactanten. Hoofdstuk 2, 3 en 4 onderzoeken de conversieroute van ZA oxiden en ook ZA-gebaseerde magneten in gesmolten chloride- en fluoride-zouten. Hoofdstuk 5 onderzoekt de elektrolysestap waarbij ijzer als reactieve anode wordt gebruikt, om zo de ontwikkeling van halogeengas en CO, CO_2 te voorkomen tijdens het extractieproces. In hoofdstuk 6 wordt een thermodynamische modelering van het fluoride-zout met de CALPHAD methode uitgevoerd.

Hoofdstuk 2 van dit proefschrift geeft een overzicht van de vorige studies aan elektrochemische extractie van zeldzame-aardoxiden en dysprosium bevattende NdFeB magneten in gesmolten chloride- en fluoride-zouten. In dit hoofdstuk wordt de conversie, gebruik makend van $AlCl_3$ in een LiCl-NaCl-KCl elektrolyt, van ZA in de magneet tot ZA chloride bestudeerd. Daarna wordt ook de elektrochemische extractie van ZA metalen uit ZA chloride in het systeem behandeld.

Het concept van chlorinatie van de ZA in de magneet wordt gebruikt in het fluoride-zout. In hoofdstuk 3 wordt de conversie van ZA oxide tot ZA fluoride bestudeerd. Zink fluoride (ZnF_2), aluminium fluoride (AlF_3), ijzer fluoride (FeF_3) en kryoliet (Na_3AlF_6) worden gebruikt als fluoreringsreagentia. De haalbaarheid van deze conversie wordt onderzocht via experimenten en ook vanuit thermodynamisch standpunt met de FACTSage software. De conversie van ZA oxide tot ZA fluoride in het LiF elektrolyt lost het probleem van de lage oplosbaarheid van ZA oxide in LiF grotendeels op.

In hoofdstuk 4 onderzoeken we de conversiemethode voor NdFeB magneten met dezelfde fluoreringsreagens. Al, Zn en Fe, respectievelijk afkomstig van AlF_3 / Na_3AlF_6,

ZnF_2 en FeF_3, vervangen de zeldzame-aardmetalen in de magneetmatrix, en vormen zo verbindingen met Fe in de magneet. De vorming van Nd fluoride voorziet in de mogelijkheid voor een één-staps-recycling proces voor zeldzame-aardmetalen uit magneten.

Hoofdstuk 5 onderzoekt het gebruik van een nieuwe anode-elektrode als vervanging van de grafietelektrode die gebruikt wordt in de industrie. In het elektrolyseproces wordt ijzer gebruikt als reactieve anode. Deze bevordert de elektrochemische oplossing van ijzer in het gesmolten zout, om zo de ontwikkeling van fluorgas aan de anode te voorkomen. Hierdoor wordt de fluoreringsreagens constant *in situ* geregenereerd, hetgeen de continue conversie van de Nd oxide voeding mogelijk maakt. Het uiteindelijke kathodische product is een Nd-Fe legering die verzameld kan worden aan een Mo kathode.

In dit hoofdstuk wordt ook het elektrochemisch gedrag van de verschillende fluoride-zoutsystemen onderzocht, gebruik makend van cyclische voltametrie, chronopotentiometrie en *square wave voltammetry*. Het cyclische voltammogram van LiF-NdF_3 toont aan dat de reductie van het neodymiumion een één-staps-proces is, namelijk Nd^{3+} tot Nd metaal. Dezelfde studie op het LiF-FeF_3 systeem toont aan dat de reductie van Fe^{3+} tot Fe een twee-staps-proces is, van Fe^{3+} naar Fe^{2+} en dan van Fe^{2+} naar metallisch ijzer. In de cyclische-voltametrie studie van het LiF-Nd_2O_3 systeem werden geen pieken gerelateerd aan de reductie van Nd waargenomen.

Hoofdstuk 6 bestudeert de thermodynamische modelering van het LiF-DyF_3-NdF_3 systeem. De Gibbs vrije energieën van de LiF-NdF_3 en LiF-DyF_3 systemen zijn gemodelleerd door gebruik te maken van de constitutionele data in de literatuur. Bovendien werden *ab initio* berekeningen uitgevoerd om de vormingsenthalpie van $LiDyF_4$, een intermediaire fase in het LiF-DyF_3 systeem, te bepalen. Differentiële thermische analyse (DTA) werd uitgevoerd om het NdF_3-DyF_3 systeem te optimaliseren. De verkregen Gibbs vrije energie functies, bepaald via het limiteren van de binaire systemen, samen met de DTA analyse van het LiF-NdF_3-DyF_3 systeem, werden gebruikt om de Gibbs vrije energie functies van de evenwichtsfasen in het ternaire systeem te modelleren.

چکیده

روش صنعتی غالب برای تولید عناصر خاکی کمیاب از اکسید آن ها، استخراج الکتروشیمیایی در نمک مذاب است. دو چالش عمده ی این روش برای استخراج این عناصر1) انحلالِ کم اکسید عناصر خاکی در نمک مذاب و 2)امکان تولید گازهای سمی (مونوکسید کربن و فلوروکربن ها) هستند. هدف اولیه ی این پایان نامه یافتن روش هایی برای فائق آمدن بر مشکل انحلال پذیریِ کم اکسید عناصر خاکی در نمک های فلوریدی برای بالا بردن راندمان استخراج این عناصر است. هدف دیگرطراحی روش های نوین به منظور جلوگیری از تولید مونوکسید کربن و فلوروکربن ها در پروسه ی الکتروشیمیایی تولید عناصر خاکی کمیاب از اکسید یا قراضه های مگنت نئودیمیومی است.

روش استحاله ی شیمیایی اکسید عناصر خاکی به فلورید یا کلورید عناصر خاکی توسط عوامل شیمیایی راه حل مطالعه شده برای حل مشکل انحلال پذیریِ کم اکسید عناصر خاکی در نمک های فلوریدی و کلوریدی است. نتیجه ی مطالعه بر روی چهار عامل شیمیایی؛ نشان داد که با استحاله ی اکسید عناصر خاکی و همچنین نئودیمیوم موجود در مگنت به فلورید یا کلورید عناصر خاکی انحلالِ اکسید در نمک های فلوریدی و کلوریدی ضرورتی ندارد. در نهایت عناصر خاکی در پروسه ی الکتروشیمیایی از ترکیب فلوریدی یا کلوریدی استخراج می شوند.

راه حل نوین دیگر استفاده ازآند مصرف شونده (آهن) به جای آند گرافیتی برای جلوگیری از تولید مونوکسید کربن و فلوروکربن ها در پروسه ی الکترولیز است. در این روش با انحلال الکتروشیمیایی آهن در نمک فلوریدی در واکنش آندی به جای تولید مونوکسید کربن یا فلوروکربن (بر حسب شرایط الکترولیز) فلورید آهن تولید می شود. فلورید آهن تولید شده در حین پروسه ی الکترولیز در طول فرآیندی شیمیایی اکسید عنصر خاکی را به فلورید عنصر خاکی تبدیل می کند. در واکنش کاتدی آلیاژ فلزی عنصر خاکی- آهن ازکاهش فلورید عنصر خاکی کمیاب و فلورید آهن بر روی کاتد شکل میگیرد.

محاسبات ترمودینامیکی و آزمایش های انجام شده بر روی این روش اثبات کرده که این روش نه تنها راه حلی برای حل همزمان دو چالش عمده ی استخراج عناصر خاکی کمیاب در پروسه ی الکترولیزدر نمک های فلوریدی و کلوریدی است بلکه با تولید فلورید آهن در حین پروسه، میزان مصرف مواد اولیه (فلورید آهن و فلورید نئودیمیوم) را کاهش می دهد.

Acknowledgment

I would like to thank EREAN (European Rare Earth Magnet Recycling Network) group for their financial support during my Ph.D. work. This research was funded by the European Community's Seventh Framework Programme (FP7) grant agreement.

I express my gratitude to my mentor in my MSc./Licentiate study at KTH; Prof. Seshadri Seetharaman, for being extremely supportive and inspiring during my continued research at TU Delft. I would like to thank him for the invaluable scientific guidance and the contribution to the new ideas in this work. He has encouraged me in playing down my worries and insecurities and I treasure the most this personal growth as a great achievement of my Ph.D. years.

I would like to thank my supervisors, Dr. Yongxiang Yang and Prof. Jilt Sietsma for their commitment and great support during all these years. This work would have not achieved significant progress without their supervision.

I would also like to express my sincere gratitude to Prof. Hari Kumar and his group for their scientific guidance, supports and hospitality during my stay in Indian Institute of Technology Madras.

I have been blessed with knowing my best friend and colleague Prakash Venkatesan who has made the challenges easier and the work place more joyous. Being with him in the same office and sharing great political views in extremely interesting conversations was indeed one of the reasons that drove me to move forward. I am forever thankful for that Dr. Venkatesan.

I would like to thank all my friends, colleagues and support staff at Materials Science and Engineering Department of Delft University of Technology for their crucial support. I would like to particularly thank Sander Van Asperen for all the interesting conversations we had during coffee and lunch breaks. I am also grateful to my manager and colleagues at TATA steel IJmuiden for their support during the completion of my thesis.

Last, but not certainly least, I would like to thank my parents and my brother who have been always the source of support and love in spite of living far away and my companion Farhad for his constant encouragement that ultimately made it possible to see this project through the end. I am grateful to them for every step I have made.

The Netherlands, Autumn 2018

Aida

List of publications

Journal papers:

1. A. Abbasalizadeh, S. Sridar, Z. Chen, M. Sluiter, Y. Yang, J. Sietsma, S. Seetharaman, K.C. Hari Kumar. Experimental investigation and thermodynamic modelling of LiF-NdF_3-DyF_3 system. **Journal of Alloys and compounds,** vol. 753, pp 388-394, 2018.

2. A. Abbasalizadeh, S. Seetharaman, P. Venkatesan, J. Sietsma, and Y. Yang. Use of iron reactive anode in electrochemical extraction of rare earth metals from rare earth oxides, **Submitted to Electrochimica Acta.**

3. A. Abbasalizadeh, A. Malfliet, S. Seetharaman, J. Sietsma, Y. Yang, Electrochemical extraction of rare earth metals in molten fluorides: conversion of rare earth oxides into rare earth fluorides using fluoride additives, **Journal of Sustainable Metallurgy,** vol. 3, pp 627-637, 2017.

4. A. Abbasalizadeh, A. Malfliet, S. Seetharaman, J. Sietsma, Y. Yang, Electrochemical recovery of rare earth elements from magnets: conversion of rare earth based metals into rare earth fluorides in molten salts. **Materials Transactions,** vol. 58, pp. 400-405, 2017.

5. A. Abbasalizadeh, L. Teng, S. Seetharaman, J. Sietsma, Y. Yang, Rare earth extraction from NdFeB magnets and rare earth oxides using aluminum chloride/fluoride molten salts, D. Lima, I. Borges and W. L. Filho, **Rare Earths Industry: Technological, Economic, and Environmental Implications,** Elsevier, pp. 357-373, 2015.

6. R. Schulze, A. Abbasalizadeh, W. Bulach, L. Schebek and M. Buchert, An ex-ante LCA study of rare earth extraction from Nd-Fe-B magnet scrap using molten salt electrolysis. **Accepted in Journal of Sustainable Metallurgy.** 2018

7. A. Abbasalizadeh, L. Teng, S. Sridhar, S. Seetharaman. Neodymium extraction using salt extraction process. **Mineral Processing and Extractive Metallurgy**, vol. 124, pp. 191-198, 2015.

8. A. Abbasalizadeh, S. Seetharaman, L. Teng, S. Sridhar, O. Grinder, Y. Izumi and M. Barati. Highlights of the salt extraction process. **Journal of Materials**, vol. 65, pp. 1552-1558, 2013

Conference presentation and proceedings:

1. A. Abbasalizadeh, S. Seetharaman, P. Venkatesan, E. Haccuria, J. Sietsma, and Y. Yang. Novel reactive anode for electrochemical extraction of rare earth metals from rare earth oxides. **TMS 2017**. San Diego, USA, Feb. 2017.

2. A. Abbasalizadeh, S. Seetharaman, E. Haccuria, J. Sietsma, and Y. Yang. Electrochemical extraction of rare earth metals from rare earth oxides using a novel reactive anode. **European Rare Earth Resources Conference (ERES),** Santorini, Greece, 28-31 May 2017.

3. A. Abbasalizadeh, E. Haccuria, and Y. Yang. Production of Nd alloys from Nd-Fe-B magnet scrap by electrolysis in molten salts. **The 24th International Workshop on Rare-Earth and Future Permanent Magnets and their Applications (REPM),** Darmstadt, Germany, 28 August to 1 September 2016.

4. A. Abbasalizadeh, S. Seetharaman, J. Sietsma, and Y. Yang. Electrochemical extraction of rare earth metals from their oxides through conversion of REOs into REF_3 using fluoride additives. **5th International Round Table on Titanium Production in Molten Salts (Ti-RT),** Hokkaido, Japan, 10-14 July 2016.

5. A. Abbasalizadeh, S. Seetharaman, J. Sietsma, and Y. Yang. Rare earth extraction from NdFeB magnet and rare earth oxides using molten salt processes. **Proceeding of 1st European Rare Earth Resources Conference (ERES),** Milos, Greece, 4-7 September 2014.

6. A. Abbasalizadeh, L. Muhmood, A. Danaei, Y.D. Yang, M. Barati, A. McLean and S. Seetharaman. A Sessile Droplet Study of Iron-Carbon-Sulphur Alloys on an Alumina Substrate, **The 9th international conference on molten slags, fluxes and salts,** Beijing, China, 27-30 May 2012.

7. A. Abbasalizadeh, L. Teng and S. Seetharaman. Neodymium extraction using salt extraction process. **5th congress in ionic liquids,** Algarve, Portugal, 21-25 April 2013.

About the author

Aida was born on 1st August 1985 in Tehran, Iran. After graduating with the high school diploma in mathematics and physics in 2004, she attended Sharif University of Technology where she received her bachelor's degree in Materials Science and Engineering in 2008. Subsequently she obtained a master's degree in materials Science and Engineering, from Royal Institute of Technology (KTH), Stockholm, Sweden in 2012. Her M.Sc. research work was on surface tension studies using sessile droplet measurement which was performed in University of Toronto, Canada in 2010. She further expanded her experience with a research internship on wetting improvement of Ag films on MgO substrate at Jessieu, Pierre and Marie Curie University, Paris, France in 2011. She was awarded a scholarship from KTH, Sweden to pursue a licentiate thesis on recovering rare earth elements from electronic waste using molten salt electrolysis. In 2014, Aida received the prestigious Marie Curie scholarship to continue her research in molten salt electrolysis at TU Delft. The title of the Ph.D. project was "Electrochemical recovery of rare earth metals in molten salts". She has published several manuscripts in peer review journals and conference proceedings.